NATIONAL TECHNICAL UNIVERSITY OF ATHENS

School of Mechanical Engineering
***I**nterdisciplinary **P**ostgraduate **S**pecialization **P**rogramme*
"AUTOMATION SYSTEMS"

Direction A: Manufacturing and Production Systems

Master Thesis

Smoothing of a non-interconnected island's power system load curve, with the use of a predictive BESS controller

SPYRIDON CHAPALOGLOU

Supervisor: Professor Ioannis Antoniadis, NTUA

Athens, July 2018

Acknowledgements

With the accomplishment of the present Master Thesis, I would like to thank my supervisor Professor Ioannis Antoniadis from the School of Mechanical Engineering of National Technical University of Athens (*NTUA*), for his consideration, giving me the opportunity to get involved with a research topic of my interest with great flexibility, while showing confidence to my skills. I would also like to thank Mr. Christos Yiakopoulos, member of the Dynamics and Structures Laboratory of Machine Design and Control Systems Section of NTUA, for all the assistance, the encouragement and the guidance he provided me with, during the realization of the present thesis. Furthermore, I would also like to deeply thank Dr. Kostis Atsonios and Dr. Nikolaos Nikolopoulos, from the Centre for Research and Technology of Hellas (*CERTH*), for the capability they gave me to undertake the present thesis under the scope of the European Research project "**SM**art **I**s**L**and **E**nergy systems" - *SMILE* and their trust to myself in order to present the results of this work at the *31st International Conference* ***ECOS 2018***, 17-22 June, Guimaraes, Portugal. Moreover, I would like to express my profound appreciation and gratitude to Mr. Athanasios Nessiadis from *CERTH*, for all the technical support he provided, especially to the *APROS* software and to the correction and amendment of the present document. Subsequently, I would like to express my greatest gratitude and appreciation to my parents who supported my decision for this Master courses in every possible aspect. Last but not least, I would like to dedicate the present thesis to my brother and sister and their families, for they have been always by my side at any emotional or practical level, giving me insight of my possibilities at each instance, guidance for my alternative options and support to my final choices.

Abstract

In this study, a novel smart algorithm for the management of the power flows of an islandic power system was developed and integrated into the dynamic simulation of the system's model. The system under investigation is composed of Diesel Generators and a PV farm while a Battery Energy Storage System (BESS) is proposed, in order to support the developed algorithm's implementation. In particular, a predictive energy management (EMS) algorithm was developed, capable of load smoothing and peak shaving of the maximum demand values, simultaneously. In this way, the maximum demand of the island's system, was covered from stored renewable energy, while the operation of the diesel engines remained stable, diminishing the ramp up and the steep gradients before the night hours' peak demand. Additionally, considering the system's ability for energy storage as a result of the BESS installation, a portion of the PV energy produced in daylight time period could be shifted for later use and therefore the diesel engines could avoid abrupt load changes. The prediction ability of the algorithm was based on a developed feedforward artificial neural network, which was capable of short-term load forecasting. Through this, it was possible to estimate an hourly based trajectory for the diesel generators operation and acquire the BESS setpoints which would result in the desired peak shaving and smoothing level. Subsequently, the islandic power system was modeled in APROS software and the algorithm was integrated into the system dynamic simulation. In order to better represent the storage capacity and the degradation effects, a nonlinear detailed model was employed for the battery operation, including charge and discharge control loops, while the rest of the power system was modelled in the energy flow level. A rule-based strategy was also developed in APROS software through basic modules, which was tasked with the implementation of the setpoints obtained from the developed management algorithm. The simulation results proved that from the application of the proposed algorithm, a smoother diesel generator operation and peak shaving is achievable. Under this scope, the diesel engines could be rated at lower maximum capacity while the renewable energy penetration to the grid was increased.

Εκτενής Περίληψη

Στην παρούσα διπλωματική εργασία, μελετήθηκε η επίδραση της ενσωμάτωσης ενός 'έξυπνου' αλγορίθμου διαχείρισης συστήματος αποθήκευσης ηλεκτρικής ενέργειας, στη λειτουργία ενός μη-διασυνδεδεμένου νησιωτικού ηλεκτρικού δικτύου. Το τελευταίο αποτελείται από σύστημα αποθήκευσης ενέργειας με συστοιχίες μπαταριών (BESS), Diesel ηλεκτροπαραγωγά ζεύγη και ένα φωτοβολταϊκό πάρκο (PV). Συγκεκριμένα, αναπτύχθηκε προβλεπτικός αλγόριθμος διαχείρισης του συστήματος αποθήκευσης, ο οποίος είχε ως κύριο σκοπό την εξομάλυνση της λειτουργίας των Diesel μηχανών, την μεγιστοποίηση της διείσδυσης ανανεώσιμης ενέργειας στο δίκτυο και την μείωση του μέγιστου φορτίου που καλούνται να καλύψουν οι μηχανές. Σχετικά με την ικανότητα πρόβλεψης του αλγορίθμου, σχεδιάστηκε ένα νευρωνικό δίκτυο (ANN), με το οποίο επιτεύχθηκε η πρόβλεψη της καμπύλης φορτίου του επόμενου 24-ώρου σε ωριαία βάση. Για την ανάπτυξη του νευρωνικού, χρησιμοποιηθήκαν τα ωριαία δεδομένα θερμοκρασίας και φορτίου του νησιωτικού συστήματος των τελευταίων 3 ετών (2014, 2015, 2016). Τα πρώτα δύο έτη χρησιμοποιήθηκαν για την διαδικασία εκπαίδευσης του δικτύου ενώ το τελευταίο έτος χρησιμοποιήθηκε για την εκτίμηση της αποτελεσματικότητας της πρόβλεψης. Για το τελευταίο έτος, το νευρωνικό δίκτυο κατάφερε να επιτύχει μέσο απόλυτο σχετικό σφάλμα (MAPE) ως προς την πραγματική ετήσια χρονοσειρά φορτίου 1.751%. Στη συνέχεια, με βάση την πρόβλεψη, έγινε η εκτίμηση της τροχιάς των σημείων λειτουργίας των συμβατικών ηλεκτροπαραγωγών μηχανών (Diesel) του νησιού, για κάθε ώρα της ημέρας, έτσι ώστε να ικανοποιούνται οι απαιτήσεις για i) περικοπή των κορυφών της καμπύλης φορτίου και ii) εξομάλυνση της καμπύλης. Συγκεκριμένα, αναπτύχθηκε αλγόριθμος ο οποίος έπαιρνε σαν δεδομένα εισόδου την πρόβλεψη του φορτίου, όπως αυτή προκύπτει από το νευρωνικό δίκτυο, την παραγωγή των PV της επόμενης ημέρας και την τιμή περικοπής της κορυφής. Με βάση τα προηγούμενα δεδομένα εισόδου και κατόπιν συγκεκριμένης διαδικασίας, έβγαζε σαν έξοδο την πορεία λειτουργίας των συμβατικών μονάδων παραγωγής καθώς και τις τιμές ισχύος που θα έπρεπε να αποθηκευτούν στο σύστημα μπαταριών (BESS) κάθε ώρα της ημέρας. Κατά την αρχικοποίησή του αλγορίθμου αυτού, ο οποίος εκτελείται για κάθε ημέρα του έτους, θεωρείται ένα επίπεδο ισχύος (που ονομάστηκε offset), πάνω στο οποίο προστίθεται η συνολική παραγωγή των PV, ενώ ταυτόχρονα περικόπτονται οι αιχμές λειτουργίας των μηχανών. Το επίπεδο offset, μεταβάλεται (αυξάνεται σταδιακά) κατά την επαναληπτική διαδικασία του αλγορίθμου και ταυτόχρονα συμπαρασύρει μαζί του την καμπύλη παραγωγής των PV, δημιουργώντας έτσι μια νέα «συνθετική» καμπύλη συνολικής παραγωγής ενέργειας, η οποία κάποια στιγμή εμφανίζει σημεία τομής με την καμπύλη του φορτίου της ίδιας ημέρας. Η διαδικασία αυτή συνεχίζεται περεταίρω με τον ίδιο τρόπο, μέχρις ότου να δημιουργηθεί μια «τεχνητή» περίσσεια ενέργειας, η οποία αποθηκεύεται στο σύστημα μπαταριών και προσεγγίζει με την ελάχιστη θετική διαφορά, το ποσό ενέργειας που θα χρειαστεί για να καλυφθεί η αιχμή του φορτίου που θα ακολουθήσει αργότερα την ίδια ημέρα. Η εκτίμηση της επίδρασης του αλγορίθμου στη λειτουργία του συστήματος, έγινε μέσω

της μοντελοποίησης του νησιωτικού δικτύου και της εκτέλεσης δυναμικής προσομοίωσης της λειτουργίας του, στο λογισμικό Advanced Process Simulator (APROS). Για την καλύτερη δυνατή προσομοίωση της λειτουργίας και της δυναμικής συμπεριφοράς του συστήματος αποθήκευσης ενέργειας, χρησιμοποιήθηκε αναλυτικό μη-γραμμικό ηλεκτρικό μοντέλο, ενώ το υπόλοιπο δίκτυο μοντελοποιήθηκε σε επίπεδο ενεργειακών ροών. Επίσης, στο δυναμικό μοντέλο του νησιωτικού συστήματος, ενσωματώθηκε ένα εποπτικό σύστημα διαχείρισης των ροών ισχύος και των κατάλληλων βρόγχων ελέγχου (Energy Management System - EMS), με βάση το οποίο ορίστηκε και ρυθμίστηκε η λειτουργία των διαφόρων υποσυστημάτων, κατά τη διάρκεια της δυναμικής προσομοίωσης. Τα αποτελέσματα των προσομοιώσεων έδειξαν ότι με την εφαρμογή της προτεινόμενης μεθοδολογίας, είναι δυνατή η επίτευξη ομαλότερης λειτουργίας των Diesel μηχανών καθώς ακόμη και η αντικατάστασή τους από μηχανές μικρότερης ισχύος, ενώ ταυτόχρονα βελτιώθηκε η αξιοποίηση της παραγόμενης ηλεκτρικής ενέργειας από το φωτοβολταϊκό πάρκο, επιτρέποντας μεγαλύτερη διείσδυση τις νυχτερινές ώρες αιχμής. Εν κατακλείδι, σύμφωνα με την διαδικασία που ακολουθήθηκε στην παρούσα εργασία, προτείνεται ένα ενοποιημένο πλαίσιο ανάπτυξης και δοκιμής προβλεπτικών διαχειριστικών αλγορίθμων, με εφαρμογή σε ενεργειακά συστήματα, στο οποίο ενσωματώνεται η δυναμική προσομοίωση και οι αντίστοιχες διατάξεις ελέγχου και αυτοματισμού. Με τον τρόπο αυτό επιτυγχάνεται η καλύτερη διακρίβωση της επίδρασης τέτοιων αλγορίθμων στη λειτουργία ενός ενεργειακού συστήματος, υπό μεταβαλλόμενες συνθήκες.

Table of contents

List of Figures 8
1 Introduction 10
1.1 Background Information 10
1.2 An overview of Smart Grids 11
1.3 Aim of this study 12
2 Literature Review 14
2.1 Load Forecasting Techniques 14
2.2 Energy Management System (EMS) Algorithms 15
2.2.1 Residential EMS 15
2.2.2 Power grid level EMS 16
3 Artificial Neural Network forecasting module 18
3.1 General Overview 18
3.1.1 Basic ANN structure 18
3.1.2 Training Process and Learning methods 21
3.2 Levenberg-Marquardt training algorithm 22
3.3 Developed ANN model structure and training 27
3.3.1 The island under investigation 27
3.3.2 Data preprocessing 28
3.3.3 Network Training 30
3.3.4 Network achieved results 33
4 Optimization algorithm for peak shaving and load smoothing 36
4.1 Algorithm Description 36
4.1.1 Problem Description 36
4.1.2 Synthetic Power Curve 38
4.1.3 The "elevator" concept 39
4.2 Acquired diesel engines setpoints 43
4.2.1 Algorithm outputs for different time periods 43
5 Modelling of the island's power system 52
5.1 General System Configuration 52
5.2 Photovoltaic power production modelling 53
5.3 Battery Energy Storage Modelling 58
5.3.1 Electrical model of the battery system 58
5.3.2 Control configuration of the BESS 63

6 Power system model dynamic simulations 68
6.1 Apros model description 68
6.1.1 Apros modules description 68
6.1.2 Signal based EMS algorithm in Apros 72
6.2 Dynamic simulation results 75
6.2.1 System operation results for short time periods 75
6.2.2 System operation result for the whole year 78
7 Diesel and BESS operation under the proposed EMS 82
7.1 Diesel Engine Operation 82
7.2 Battery Storage System Operation 87
8 Conclusions and Future work 90
8.1 Basic conclusions 90
8.2 Future work 92

List of Figures

Figure 1: Smart grid basic topology [3] 12
Figure 2: Structure of a hierarchical approximator variant with different ANN sub models combined together for a single hour power load forecast [8] 14
Figure 3:ANFIS network model for load forecasting, combining ANN structure with fuzzy rules [10] 15
Figure 4: BESS connection to the distribution grid system topology [22] 16
Figure 5:Target and achieved state of charge trajectories for the BESS operation [22] 16
Figure 6: Commonly used activation functions [38] 20
Figure 7: Basic feedforward ANN configuration with neuron's interconnections and activation functions 21
Figure 8: Summer load profile pattern of Astypalaia's system compared to Madeira's system 28
Figure 9: The "synthetic" island generation and the corresponding grid points of the Numerical Weather Model (NWM) for the temperature data 28
Figure 10: Yearly time period load curve correlation with temperature, for the test case system 29
Figure 11: Developed network structure and data flow 30
Figure 12: Training termination criteria and gradient vs epochs 30
Figure 13: Mean squared error vs epochs for the re-training of the network 31
Figure 14: Parametric investigation of the neurons number in the hidden layer 32
Figure 15: Test dataset achieved results metrics a) error histogram distribution, b) correlation coefficient 33
Figure 16: Error residual signals for the test and the train datasets 33
Figure 17: Training, test and validation data vs model output 34
Figure 18: Actual vs forecasted load data for the test set (year 2016) 34
Figure 19: Actual vs forecasted load data for a typical winter week of the test set 35
Figure 20: Ensemble of the load curves of the island for a complete year (2016) 36
Figure 21: The "duck" net load curve, illustrating steep ramp needs and overgeneration risk [46] 37
Figure 22: Peak reduction level and the corresponding area between t_1 and t_2 39
Figure 23: The elevator concept with the corresponding cross points 40
Figure 24: The equivalent areas generated by the "elevator" technique and the equilibrium pursuit 41
Figure 25: Numerical discretization and integration of the interval that corresponds to the surplus energy generation 42
Figure 26: Developed algorithm flowchart 42
Figure 27: Error residuals predicted from the algorithm, for a whole year operation 43
Figure 28: Summer time period load profile pattern and the corresponding peak shaving area 44
Figure 29: Resulting curves from the algorithm, for day 35 44
Figure 30: Artificially created excess energy and the corresponding demand, for day 35 45
Figure 31: Diesel engine operation before and after the algorithm's implementation, for day 35 46

Figure 32: Algorithm output curves, for winter day 63 47
Figure 33: Algorithm output curves, for day 255 48
Figure 34: Day 63 net surplus energy area 49
Figure 35: Algorithm output curves, for a summer day (195) 50
Figure 36: Islandic power system configuration and proposed methodology 52
Figure 37: Renewable ninja PV power production, data generation process 54
Figure 38: Overview of the approach used to model PV power output [51] 55
Figure 39: Solar irradiation and PV power production data, for the year 2016 57
Figure 40: Typical week PV power output 58
Figure 41: Battery's equivalent resistance circuit diagram 59
Figure 42: Multi cell equivalent circuit diagram, of the battery module 60
Figure 43: Battery's dependence over temperature difference, ΔE(T) 60
Figure 44: BESS control system configuration 65
Figure 45: System's response after the control system implementation 67
Figure 46: Apros analogue modules 69
Figure 47: Apros binary modules 71
Figure 48: Apros electrical network modules 71
Figure 49: APROS complete simulation model 73
Figure 50: Dynamic simulation results for a typical winter week 76
Figure 51: Dynamic simulation results for a single day operation 77
Figure 52: Residual and SoC plots, for the whole year operation 78
Figure 53: Distribution of OLD and NEW diesel operation 80
Figure 54: Islands diesel engine drawing 82
Figure 55: Operational strategy algorithm for the diesel engines of the island 83
Figure 56: Specific Fuel Curve fitted on manufacturers data 84
Figure 57: Linear correlation between the fuel consumption and the loading factor 85
Figure 58: Unit commitment for the diesel operation, under the proposed methodology 85
Figure 59: Instantaneous fuel consumption for the OLD and NEW cases 86
Figure 60: Single diesel generator operation – new technical minimum 86
Figure 61: Battery behaviour for 8 days' time period 87
Figure 62: Single day operation BESS results 88
Figure 63: Battery actual vs scheduled power flows for day 63 89

1 Introduction

1.1 Background Information

Nowadays, fundamental concepts related with energy production and consumption are continuously evolving and being reformed towards the forthcoming energy revolution based on smart energy networks predominance. Due to constant environmental regulations and limitations, energy utilities are enforced to implement changes and alter their policy in order to achieve a more sustainable and renewable based operation [1]. This task may be more feasible for large scale, highly interconnected grids, but this is not the case for smaller islanded grids, where renewable production can be a significant proportion compared to the total system production and excess energy cannot be exported. Through this perspective, islands' power networks, that resemble the future structure of distributed microgrids in islanded operation, are highly dependent on precise forecasts and storage solutions, since grid stability and production/consumption balancing are met exclusively by the local power generation. This is primarily dependent on diesel generators. Abrupt changes in load conditions and sudden impulses of renewable energy injections into the grid, are usually counterbalanced by commissioning more diesel generators for peak hour demand, forcing them to experience cold start-ups or to operate in variable power setpoints which result in fuel-consuming ramp-ups. Both of these operational conditions are strongly related to high operating costs and reduced diesel engine lifetime, which in turn have a negative effect on grid operators illustrated by the high cost of the produced electricity. In addition, as Chua et al. stated in [2], commercial and industrial customers are subject to monthly maximum demand charges which can be as high as 30% of the total electricity bills, thus peak shaving can be an efficient way to reduce those charges and relieve diesel generators from cost-intensive and energy-demanding ramps-up, accelerating from base to the peak load.

Concerning the aforementioned inherent difficulties in operating islanded grids and managing the power flows between production and consumption, battery energy storage systems (BESS) have proved to be a very promising option for smoothening those instabilities and enabling higher renewable power penetration simultaneously. Such a system can be inter-connected to the energy grid, providing ancillary services with frequency control or load smoothening by peak shaving during the hours of the day with high demand (i.e. midday hours) with stored energy from day periods with relatively lower demand (i.e. night hours). However, the most suitable operation strategy of the BESS, which is determined by a centralized Energy Management System (EMS), is related with the shape of the load profile of the system and the type of renewable power generation. Thus, for an islandic power system, where the load profile presents a high peak in late night hours and high photovoltaic (PV) generation in daylight hours, peak shaving with BESS energy stored from PV generation seems a rational approach. Specifically, this is the case for most South European islands where the load profile is shaped mainly from activities related to tourism at night hours rather than energy devouring industries that operate during the daylight hours.

1.2 An overview of Smart Grids

Smart Grids (SG) are regarded as the next generation of power generation, transmission and distribution grids considering their capability of bidirectional power flow. This ability has been attributed to the renewable power sources and energy storage systems integration. As the number of decentralized renewable producers is constantly increasing, the need for higher capacities of the transmission system, that can afford the power congestion can be clearly noticed. Thus, the conventional power grids have to adapt to the constantly evolving environment by integrating smart energy management solutions and bidirectional operation. Also, energy storage systems and demand response techniques should have a great impact on the grid stability under uncertain power production and consumption. The future trends associated with SG are summarized according to [3] to the following:

- Creating a grid that is more efficient secure, reliable and controllable to enhance the data exchange capabilities
- Instant control capabilities and self-healing resources
- Easy integration of individual micro-generation units
- Fast distribution of smart technologies such as remote control, autonomous operating, sustainable and interactive communication
- Integration of smart appliances and consumer devices that can be controlled via demand response operation

At the following figure (Figure 1), the basic topology of a SG with all the communication and data exchange pathways is presented. Common issues that are related with smart grids secure control and operation are related with grid stability (frequency-voltage regulation), balancing the power generation with the demand, the impulse renewable power penetration which needs to be directly compensated and the ability for self-sufficiency. These issues are commonly faced by load forecasting, predictive and optimization algorithms, while during the recent years, more and more energy storage systems are integrated into large smart grids.

Regarding the smart grids concept, a smart control and management system is necessary in order to achieve the most efficient and optimized BESS operation. Thanks to recent development in time-series forecasting and the possibility to access a big amount of data related with the power system operation, an EMS could implement a predictive strategy based on consumption/production forecasts and an objective function minimization. Therefore, load forecasting is a necessary stepping stone in order to achieve better energy dispatch planning, which is of great significance for the stable operation of conventional generators.

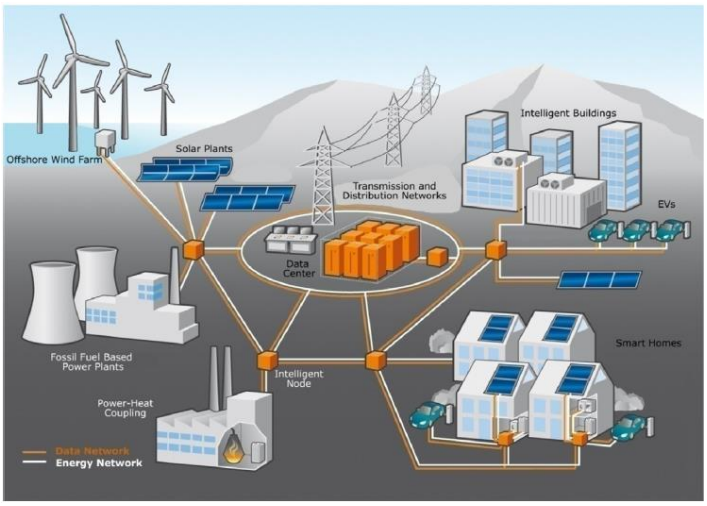

Figure 1: Smart grid basic topology [3]

1.3 Aim of this study

Regarding the present study, a novel predictive algorithm for peak shaving and diesel engine operation smoothing is proposed. This algorithm is combined with a load forecasting method and then integrated into a microgrid simulation model, that includes a detailed non-linear battery representation. In this way, the isolated power system of a South-European island is examined and the developed predictive open loop EMS is integrated into a dynamic simulation model. Compared to the studies mentioned in the previous section, the novel aspect of this study is the combined attributes of a machine learning method for load forecasting and a developed tailored made optimization algorithm with a custom modelled EMS and the dynamic simulation of a detailed Lithium (Li) battery model in Apros software. Therefore, a complete simulation framework for isolated power systems is proposed, combining load forecasting, predictive EMS algorithms and dynamic simulation models. Aim of this study is the development of a smart predictive control architecture for a BESS, based on load forecasting, for the optimum integration of PV power into an islanded power grid, through peak demand shaving and smoothening of the load curve.

2 Literature Review

2.1 Load Forecasting Techniques

Many studies concerning short term load forecasting for power grids implementing numerous methodologies and algorithms from the field of time-series forecasting have been published so far. Among them, various versions of ANNs have proved to be a common approach [4,5,6] and is also adopted in this study. In order to evaluate the performance of neural networks and their capability to forecast accurately, some statistical indicators are used such as Mean Squared Error (MSE), Mean Absolute Error (MAE) and Mean Absolute Percentage Error (MAPE) with the last being the most common for comparison actions [6]. In [7], Satish et al. proposed a combined synergy consisting of two ANNs, one for basic day ahead load forecasting and one for peak and valley forecasting, highlighting the strong correlation of temperature with load. Brodowski et al. [8] implemented a day ahead hybrid load forecasting using a divide and conquer hierarchical approach. The whole dataset was partitioned into smaller ones and each subproblem was resolved with a different ANN model. Their model is depicted in the figure below.

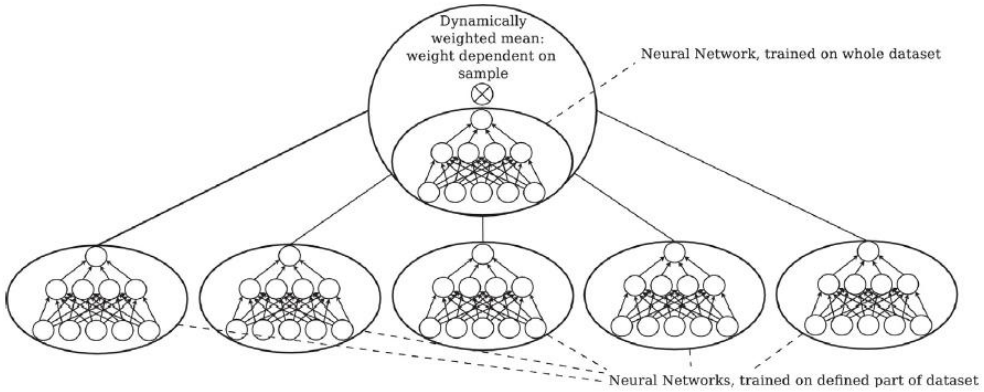

Figure 2: Structure of a hierarchical approximator variant with different ANN sub models combined together for a single hour power load forecast [8]

The Fuzzy C-means method was used for clustering the load data points and Principal Component Analysis (PCA) analysis for selecting the most suitable input features for each network. The combined result was considered as the final prediction. In this way they claimed to achieve lower MAPE than classic ANNs or Bagged NNs. In [9,10] authors achieved day ahead load forecasting using Kalman filtering combined with fuzzy logic. Specifically, in [9] a fuzzy rule-based logic was used to estimate Kalman filter parameters for structuring a fuzzy linear load model capable of 1h ahead predictions. This method could also be successively used for up to 60 days ahead predictions. Markoulakis et al. [10] used a Kalman filter to calculate the coefficients of a recurrent load model and discrete ANFIS networks for each hour in order to achieve 1h ahead forecasts. The ANFIS model is depicted below.

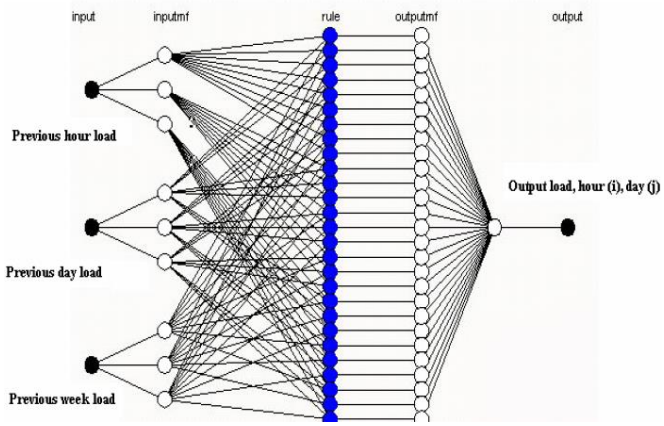

Figure 3:ANFIS network model for load forecasting, combining ANN structure with fuzzy rules [10]

In [11] the hourly load curve of Spanish power system was modelled as a linear function of low and high frequency components considering a Long-Term Demand Model (LTDM) based on macroeconomic parameters for low frequency and calendar, temperatures, daylight effects for high frequency components respectively. The model was used to forecast long-term annual peak and trough demand values and showed an overall improvement in MAPE compared with a NARX model which was used for validation. Ghasemi et al. [12] proposed a simultaneous load and price forecast using a multilevel algorithm with feature selection for inputs and optimization of the NLSSVM-ARIMA model parameters using Artificial Bee Colony. A Flexible Wavelet Packet Transform (FWPT) was used for price/load signal processing which resulted in better regression accuracy for the forecasting of those highly correlated variables. Thus, it was possible to find the proper actions that should be done on the Demand Side Management (DSM) in order to shape the load profile appropriately towards the minimization of the electricity cost. A Single-layer feedforward network was developed in [13] for hour and day ahead PV production forecasting whereas in [14] a weather forecasting platform was developed, including several forecasting algorithms among them neural networks, for solar irradiance forecasting.

2.2 Energy Management System (EMS) Algorithms

2.2.1 Residential EMS

Predictive Energy Management Systems (EMS) is based on high quality forecasting of electricity demand and renewable energy production, which is used for solving optimization problems related with operational setpoints and cost minimization. In the residential sector such systems have been integrated into small scale BESS, as in [15], where forecast-based algorithms with dynamic PV power feed-in limitations (in order to avoid curtailment) were formulated as linear optimization problems and used for optimal power use in a house. In this way, many operating strategies of battery charging and discharging could be accomplished, leading to increased self-sufficiency and less curtailed PV energy. In [16] a reactive power management algorithm was implemented to account for load forecasting uncertainties by introducing a range for the state of charge (SoC) planned trajectory which was obtained in terms of electricity cost minimization with increased battery lifetime and grid relief compensation. Another study was focused [17] on load forecasting for increasing battery's lifetime in PV-Battery interconnected residential network, whereas in [18] a Kalman load model was

developed for load forecasting based on past load values, temperatures and number of occupants in the house. In [19] MPC was implemented for a PV and battery residential system with load forecasting based on ANNs and in [20] a FLC (Fuzzy Logic Controller) was used for active power control which resulted in load profile smoothening, while the proposed fuzzy EMS compensated for forecast errors.

2.2.2 Power grid level EMS

The implementation of such predictive energy management systems for large isolated power systems and grid scaled BESS can be more challenging due to inherent difficulties related with system stability. In studies such as [21], load forecasting was used for a system with high PV penetration. Implementation of a parallel-series Complex Value NN and a splined-based load forecasting showed better results compared to a trivial persistence predictor. Thus, it was possible for a grid-scaled BESS operation to be optimized. The BESS connection to the system is depicted in the figure below.

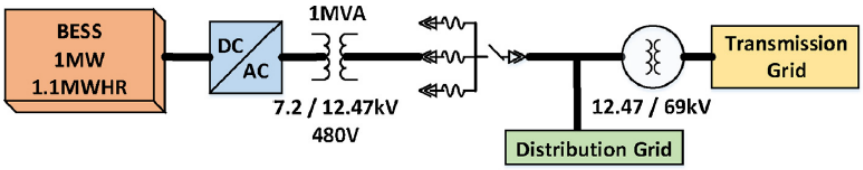

Fig. 3. BESS connection to distribution grid system.

Figure 4: BESS connection to the distribution grid system topology [22]

In other studies, [22, 23, 24] a simple linear regression model for load forecasting has been implemented in order to achieve optimal operation of a grid-scaled BESS for the power network of Hawaii island, considering also the large number of installed PV capacity on rooftops at the distribution grid. Two methods were introduced and compared for BESS power flow control, one based on dynamic programming and optimized SoC trajectory generation and one with real time control based on smoothing level and time period. This is also depicted in the following figure.

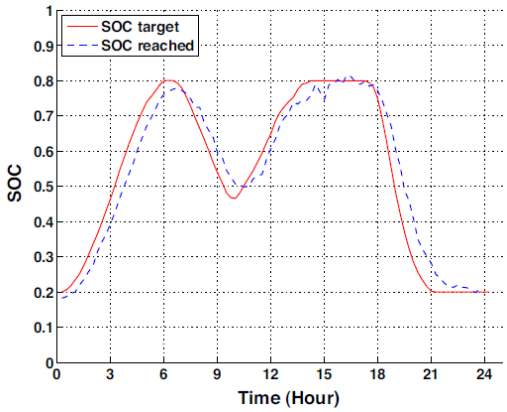

Figure 5:Target and achieved state of charge trajectories for the BESS operation [22]

By this approach, the flattening of the load curve by minimizing its deviation from a smoothing level was accomplished and curtailment issues from additional renewable generation were encountered. Both of the proposed methods were tested for 108 days and although load peak shaving and dampening of load fluctuations were achieved, the

BESS model was not detailed enough to include all the dynamic characteristics of charging/discharging processes. On the contrary, implementing an advanced load forecasting method resulted into better results compared to the first approach [24]. Halfmann et al. [25], implemented a predictive real-time BESS control based on load forecasting with ANNs to provide both peak shaving and primary frequency control for the Germany power system simultaneously. In this way, the network fee for the customers was reduced by achieving a greater value for Full Load Equivalent through peak shaving. Sossan et al. [26] combined a utility scale BESS with the dispatchable feeder concept for a university campus consisting of dispatchable buildings loads with considerable PV generation. The dispatch planning was formulated as a trajectory tracking problem which was solved using MPC for real-time feedback control of the BESS dispatch power, while at the same time compensating for day ahead load forecast errors, (as in the present study). Load forecasting was implemented using a vector-autoregression technique based on similar days and by incorporating a NWM (Numerical Weather Model. However, the authors highlighted the possibility for a better performing forecasting tool to be plugged in their control structure. The relation of forecast-based strategies with dispatch planning was also remarked by Mazzola et al. [27], investigating the impact of forecast accuracy on the operational cost of an isolated microgrid, the operation setpoints of which were obtained through a predictive optimization model. Load forecasts of different quality were produced which were then used by a rolling-horizon strategy for the next day and by solving a MILP optimization problem they obtained generation schedules. BESS module was modelled by HOMMER's software KiBaM set of equations while the operating cost of diesel generators was assumed to be proportional to the power output. Even though this may be considered as a common approach, it does not take into account the diesel engine efficiency variations in partial load during variable/transient operating conditions. Predictive energy management systems for a microgrid consisting of grid-tied BESS with PV generation were also examined in [28, 29] where load and PV generation forecasts were provided as input and used in combination with an optimization problem for minimizing renewable curtailment power or grid consumption and consequently the electricity cost. However, the ability for power exchange with the main power grid interconnection presents an operating advantage over isolated microgrids. Lujano-Rojas et al. [30], introduced a data driven ARMA model for wind power generation and load management in order to minimize the daily fuel consumption of a diesel generator via a BESS and controllable loads, for a small hybrid power system in Spain. A cascaded central long-term EMS down to a short-term balancing EMS were simulated by Colas et al. [31]. Load consumption was estimated according to the relevant daily time-period patterns and day ahead scheduling was obtained, while at the same time supercapacitors were used by a local EMS for primary frequency control. An application for peak shaving was reported by Kalkhambkar et al. [32] who used an improved energy loss minimization to a 34-bus system with the application of GWO algorithm while in [33] the size of the BESS was the subject of an optimization procedure for reducing electricity cost in a university via peak shaving.

3 Artificial Neural Network forecasting module

3.1 General Overview

Artificial neural Networks (ANNs) are intelligent systems that are successfully used to solve complicated problems in many different applications such as curve fitting, forecasting, pattern recognition, identification, classification, speech, vision and control systems [34]. ANN structure is based on our understanding of biological nervous system [35]. Neurons are the basic structural units of human's nervous system, which receive inputs in form of electrical signals from the different types of human body sensors (vision, hearing, touching, taste, smelling), combine them in some way and perform a generally nonlinear operation on them to produce the final result [36] This result is also in form of an electrical signal, which is then passed to the human body actuators in order to perform an action. The way that the neurons will process the inputs is based on their structure and the repetition frequency of a particular task. In this way the concept of learning is adopted from the nervous system and given specific input data, this system will try to adjust its structure in order to produce the required result. However, the extra value of this learning system is its ability to generalize the rules that builds based on specific input data and apply them to solve similar problems that have never been tackled before.

ANN models fundamentally comprise of multiple connected neurons and nodes. Each neuron is structured from three basic components that interact with each other and together they form the basic processing unit of a neural network. Those are the summing junction, the activation function and the threshold value. These basic processing units are interconnected and communicate through the different connection channels which consist of the neuron incoming input signals, the corresponding weights and bias of each input, and the output signals leaving the neuron. From this description it is clear that each neuron can be arranged as a three-layer module which consists of an input layer, a hidden layer and an output layer [37]. The structure and the operation of a neural network described above, is better and more thoroughly explained in the following.

3.1.1 Basic ANN structure

For a basic ANN structure, an input is conveyed through a connection channel which is multiplied by a specific weight value and then a bias is applied to the result in order to construct the activation function argument. The weight value acts as a scaling factor for each input while the biases impose a constant value to the weighted sum of the inputs, affecting the value of the argument of the activation function. Thus, it is possible to claim that the weight of each input affects its significance to each node for the output calculation and the biases allow for the shifting operation of the activation function to the left or right. Preventing the error surface from constantly passing through the zero point, may be critical for successful learning. In this way, every possible function can be approximated with an appropriate combination of non-linear similar functions, regardless of its shape, patterns or linearity Based on the previous description, the basic equations used by neural networks can be derived. Therefore, for n input signals x_k, the activation function argument u_j is calculated for the j neuron, by using n input nodes as given in Equation 1

$$u_j = \sum_{k=1}^{n} W_{jk} x_k - b_j \qquad \textit{Equation 1}$$

In order to generate the output y_j, the input argument u_j is transformed through a transfer function *f(u)* that can be linear or nonlinear. Each neuron output can be calculated as the weighted sum of the neuron's inputs, which are also outputs from a previous network layer, and after being filtered from the activation function. This can be mathematically expressed by the Equation 2 and in vector form for all the neurons of a layer by Equation 3.

$$y_j = f\left(\sum_{k=1}^{n} W_{jk} x_k - b_j\right) \qquad \textit{Equation 2}$$

$$\vec{y} = f(\vec{u}) = f\left(\boldsymbol{W}\vec{x} + \vec{b}\right) \qquad \textit{Equation 3}$$

where n is the number of the input signals, W_{jk} is the weight which corresponds to the strength of the connection channel (synapse) connecting input k to neuron j, and b_j is the applied bias. It is a common approach to describe the neural network equations in matrix/vector form as it allows us to use a more compact equation structure for many inputs - many outputs systems, as the layers of the network are. The activation function transforms the input to a predetermined output range of values, by which it is possible to map the effect of an input signal combination to the output of a processing unit (neuron). Thus, it is possible to estimate how "active" or how close to the threshold limits each neuron is under a certain input array. The simplest form of activation function for this purpose is the step function which takes the value of zero under a specified threshold input value and the value of one from that point and after. In this way, the neuron is inactive for input values less equal than the threshold and fully active for greater input values. However, this logic has a drawback which lies on the abrupt change of a neuron's state around the threshold value, allowing for two possible states and not any intermediate state. This problem can be faced with the use of a linear activation function which maps the input to the output with a specified analogy, allowing for a continuous range for the output value and not a binary one. Although this function solves the problem of discontinuity, it is not suited for curve fitting problems, as it is not able to approximate in detail the curvature of highly nonlinear shaped, such as sinewaves. These problems were countered with the introduction of non-linear, continuous and differentiable functions such as the logistic activation function or the hyperbolic tangent activation function which takes values in the range of [-1,1]. Other less commonly used activation functions include the ramp, the Gaussian and the arctan functions. In the following figure (Figure 6), the activation functions described above are illustrated based on [38].

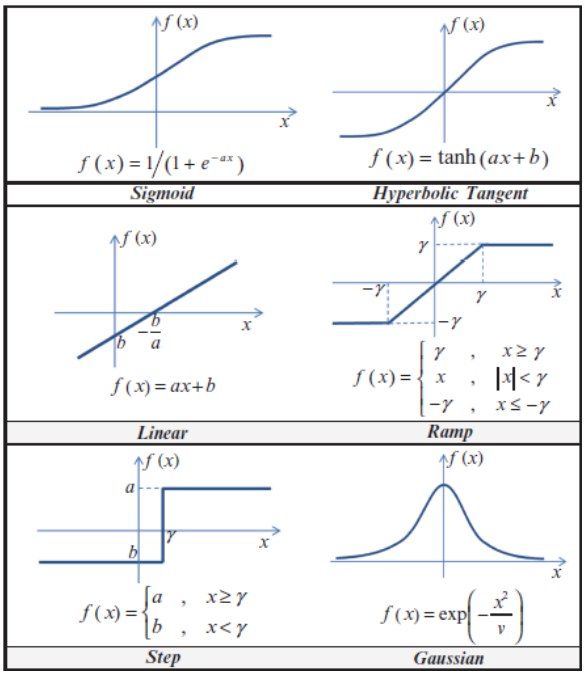

Figure 6: Commonly used activation functions [38]

Nowadays, a transfer function which has gained a lot of popularity especially for classification problems, is the rectified linear unit (ReLU). This has proved to give very satisfying results for deep learning applications and has recently been adopted for use in convolutionary neural networks (CNN). Recent advances in neural networks have been focused on the development/modification of activation functions that are integrated in neural network models and aim for better results. Such an advancement is the leaky ReLU function which is an updated version of the original ReLU. Despite the variety of the existing activation functions there are not unbreakable rules that must be respected in order to obtain the best possible results, as each function is directly related to the type of the problem under investigation. Nevertheless, based on rules of thumb and gained experience from other researchers the ReLU and sigmoid transfer functions seem to bring the best results in most cases. Regarding the present thesis, the choice of the activation function used in the developed neural network model was based on the literature [4, 5, 7, 8] and suited for forecasting and curve fitting problems. Thus, the logistic sigmoid transfer function presented in the following equation (Equation 4) was chosen for the hidden layer of the developed network and a linear function was adopted for the output layer. For further information about the structure and activation functions of neural networks, the reader should refer to [1, 38].

$$f(x) = \frac{1}{1 + e^{-x}} \qquad \textit{Equation 4}$$

Each layer is composed of many neurons that receive input from a previous layer and based on Equations [1-4] an output vector $\vec{y}$ is computed and passed to the subsequent layer until it reaches the output layer. Then the output of the last layer, which is also the output of the network, is compared with the target output vector $\vec{t}$. In this way, the error vector $\vec{e}$ is created, containing the values of the differences of the network's output with the target values $\vec{e} = \vec{t} - \vec{y}$. In the following figure (Figure 7), the structure of the developed model is presented.

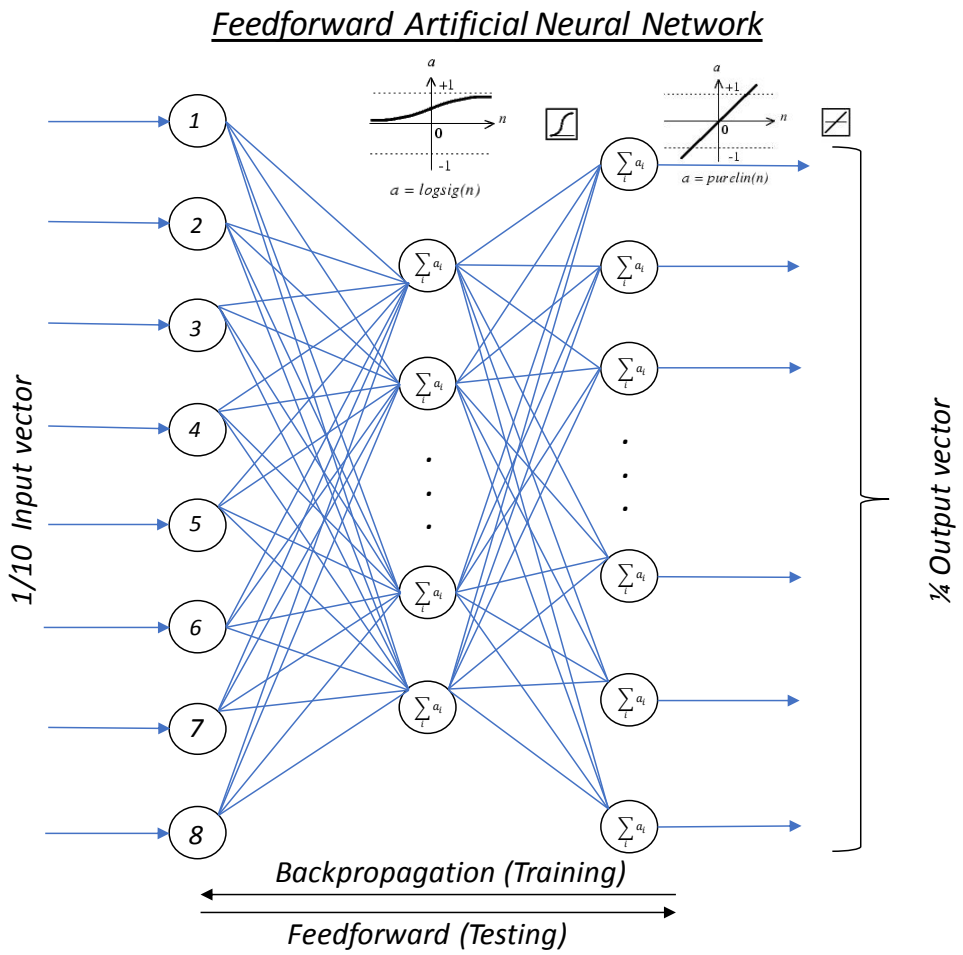

Figure 7: Basic feedforward ANN configuration with neuron's interconnections and activation functions

3.1.2 Training Process and Learning methods

The learning strategy is an algorithm that can be used to change and thereby train the network, so the network produces a desired output for a given input [39, 40]. Training is an important step of developing a neural network. It can be explained as the process of modifying the connection weights, in some orderly fashion, using a suitable learning method. The network uses a learning mode in which an input is presented to the network along with the desired output and the weights are adjusted so that the network attempts to produce the desired output. The weights, after training, contain meaningful information whereas before training they are random and have no meaning [40, 41]. Basically, there are three simple learning techniques which are unsupervised, supervised and reinforcement learning [42]. Because of the deficiency of back propagation training algorithms, faster algorithms such as LM and SCG learning algorithms are extensively preferred.

Supervised Learning

In this learning technique, inputs and targets are introduced to the network and the output is obtained. Then the error is calculated by comparing the output and target values. This process which is called an "epoch", is applied to the whole training dataset and is repeated until the error reduces to an acceptable value [34]. Then, once all the vectors of the training set have been used by the training algorithm, it can be claimed

that "one epoch has passed". In order to minimize the total error, the weights and biases between the input, output and hidden layers are updated at each epoch. In this way, the error is then propagated backward from the output layer to the input layer, a process which is named "backpropagation". (see Figure 7)

Unsupervised Learning

This method describes the training process of a network that does not require the matching of the networks output with a target vector. During this training session, the NN receives as its input many different excitations or input patterns and it arbitrarily organizes the patterns in different categories based on their similarity. When a stimulus is later applied, the NN provides an output response indicating the class/category to which the stimulus belongs. In case that any of the existing classes is not appropriately suited to the input, then a new class is generated. In this way, the NN decides on its own the distinguishing features that will be used for the classification of the objects presented to the network or even the prediction of a time series from raw data. Concerning the reasons explained above, this type of training is mostly used for classification or clustering problems.

Reinforced Learning

This type of training has currently gained much popularity, especially when combined with deep neural networks, the layers of which are dedicated to specific feature recognition. Unlike the previous technique, in this methodology there is a metric for the performance evaluation of the network under development which indicates whether the actual NN output is the same with the target output. In this way the response obtained from the network is biased to match a certain output and in order to achieve this, the generated error signal is on the form of a binary pass or fail option. Regarding the error of the NN output, the parameters are readjusted to achieve the desired output in a more brute-force aspect, not even considering an acceptable range, bearing the danger of non-ending training process. Thus, special care should be given when this method is applied.

3.2 Levenberg-Marquardt training algorithm

The Levenberg–Marquardt algorithm blends the steepest descent method and the Gauss–Newton algorithm that are described below. Fortunately, it inherits the speed advantage of the Gauss–Newton algorithm and the stability of the steepest descent method. It's more robust than the Gauss–Newton algorithm, because in many cases it can converge well even if the error surface is much more complex than the quadratic situation. Although the Levenberg–Marquardt algorithm tends to be a bit slower than Gauss–Newton algorithm (in convergent situation), it converges much faster than the steepest descent method. The basic idea of the Levenberg–Marquardt algorithm is that it performs a combined training process: around the area with complex curvature, the Levenberg–Marquardt algorithm switches to the steepest descent algorithm, until the local curvature is proper to make a quadratic approximation; then it approximately becomes the Gauss–Newton algorithm, which can speed up the convergence significantly [43]. In this part, the derivation of the *LM* algorithm will be presented in

four parts: (1) steepest descent algorithm, (2) Newton's method, (3) Gauss-Newton's algorithm, and (4) LM algorithm.

In the following we declare that $\vec{x}$ is the input vector applied to the network, $\vec{y}[M]$ is the output vector with *M* elements (24 in the present study), $\vec{w}[N]$ is the weight vector which contains (encapsulates) all the network weights and biases from each layer (*N* elements in total), *k* index refers to the iteration of the training algorithm which corresponds to the epoch of the training (as mentioned in 3.1.2) and $E(\vec{w}, \vec{x})$ is the total error function which is described as a mean squared function

$$E = \frac{1}{P}\sum_{p=1}^{P} \vec{e}_p^T \cdot \vec{e}_p = \frac{1}{P}\sum_{p=1}^{P} (\vec{t}_p - \vec{y}_p)^T \cdot (\vec{t}_p - \vec{y}_p) = \frac{1}{P}\sum_{p=1}^{P}\sum_{m=1}^{M} e_{p,m}^2 \qquad \textit{Equation 5}$$

where P is the number of training data batches used and p is the corresponding index for each training pattern applied. For better understanding, we mention that for the case studied in this thesis, a single data batch is composed of the same number of elements as the number of input variables (80). The error vector $\vec{e}_p$ for each batch is a vector containing *m* elements, which are calculated as the differences between the target and network output values, which are also *m* dimension vectors. From the above, it can be derived that the number of the data points *D* used for training is equal to number of the training batches P times the number of the input variables and therefore $D = P \times 80$.

Steepest Descent Algorithm

The steepest descent algorithm is a first-order algorithm. It uses the first-order derivative of total error function to find the minima in error space. Normally, gradient g is defined as the first-order derivative of total error function

$$\vec{g} = \frac{\partial E}{\partial \vec{w}} = [\frac{\partial E}{\partial w_1} \quad \frac{\partial E}{\partial w_2} \dots \frac{\partial E}{\partial w_N}]^T \qquad \textit{Equation 6}$$

With the definition of gradient g in the previous equation (Equation 6), the update rule of the steepest descent algorithm could be written as

$$\vec{w}_{k+1} = \vec{w}_k - a\vec{g}_k \qquad \textit{Equation 7}$$

where α is the learning constant (step size). The training process of the steepest descent algorithm is asymptotic convergence. Around the solution, all the elements of gradient vector would be very small and there would be a very tiny weight change.

Newton's Method

Newton's method assumes that all the gradient components $g_1, g_2, \dots, g_N$ are functions of weights and all weight are linearly independent:

$$\begin{cases} g_1 = F_1(w_1, w_2, \dots, w_N) \\ g_2 = F_2(w_1, w_2, \dots, w_N) \\ \dots \\ g_N = F_N(w_1, w_2, \dots, w_N) \end{cases} \qquad \textit{Equation 8}$$

where $F_1, F_2, \dots F_N$, are nonlinear relationships between weight and related gradient components. Then, by unfolding each g_i (*i=1,2,…,N)* in the previous system of equations and taking the first-order Taylor approximation we have:

$$\begin{cases} g_1 \approx g_{1,0} + \dfrac{\partial g_1}{\partial w_1}\Delta w_1 + \dfrac{\partial g_1}{\partial w_2}\Delta w_2 + \cdots + \dfrac{\partial g_1}{\partial w_N}\Delta w_N \\ g_2 \approx g_{2,0} + \dfrac{\partial g_2}{\partial w_1}\Delta w_1 + \dfrac{\partial g_2}{\partial w_2}\Delta w_2 + \cdots + \dfrac{\partial g_2}{\partial w_N}\Delta w_N \\ \cdots \\ g_N \approx g_{1,0} + \dfrac{\partial g_N}{\partial w_1}\Delta w_1 + \dfrac{\partial g_N}{\partial w_2}\Delta w_2 + \cdots + \dfrac{\partial g_N}{\partial w_N}\Delta w_N \end{cases} \quad \textit{Equation 9}$$

By combining the definition of gradient vector $\vec{g}$ in Equation 6, it could be determined that

$$\frac{\partial g_i}{\partial w_j} = \frac{\partial(\frac{\partial E}{\partial w_j})}{\partial w_j} = \frac{\partial^2 E}{\partial w_i w_j} \quad \textit{Equation 10}$$

And by inserting the Equation 10 to Equation 9 we get

$$\begin{cases} g_1 \approx g_{1,0} + \dfrac{\partial^2 E}{\partial w_1^2}\Delta w_1 + \dfrac{\partial^2 E}{\partial w_1 \partial w_2}\Delta w_2 + \cdots + \dfrac{\partial^2 E}{\partial w_1 \partial w_N}\Delta w_N \\ g_2 \approx g_{2,0} + \dfrac{\partial^2 E}{\partial w_2 \partial w_1}\Delta w_1 + \dfrac{\partial^2 E}{\partial w_2^2}\Delta w_1 + \cdots + \dfrac{\partial^2 E}{\partial w_2 \partial w_N}\Delta w_N \\ \cdots \\ g_N \approx g_{N,0} + \dfrac{\partial^2 E}{\partial w_N \partial w_1}\Delta w_1 + \dfrac{\partial^2 E}{\partial w_N \partial w_2}\Delta w_2 + \cdots + \dfrac{\partial^2 E}{\partial w_N^2}\Delta w_N \end{cases} \quad \textit{Equation 11}$$

Comparing with respect to steepest descent method, the second order derivatives of the total error function need to be calculated for each component of gradient vector. In order to get the minima of the total error function $E(\vec{w}, \vec{x})$, each element of the gradient vector should be zero. Therefore, by setting the left sides of the Equation 11 all zero and combining with Equation 6 we get

$$\begin{cases} -\dfrac{\partial E}{\partial w_1} = -g_{1,0} \approx \dfrac{\partial^2 E}{\partial w_1^2}\Delta w_1 + \dfrac{\partial^2 E}{\partial w_1 \partial w_2}\Delta w_2 + \cdots + \dfrac{\partial^2 E}{\partial w_1 \partial w_N}\Delta w_N \\ -\dfrac{\partial E}{\partial w_2} = -g_{2,0} \approx \dfrac{\partial^2 E}{\partial w_2 \partial w_1}\Delta w_1 + \dfrac{\partial^2 E}{\partial w_2^2}\Delta w_1 + \cdots + \dfrac{\partial^2 E}{\partial w_2 \partial w_N}\Delta w_N \\ \cdots \\ -\dfrac{\partial E}{\partial w_N} = -g_{N,0} \approx \dfrac{\partial^2 E}{\partial w_N \partial w_1}\Delta w_1 + \dfrac{\partial^2 E}{\partial w_N \partial w_2}\Delta w_2 + \cdots + \dfrac{\partial^2 E}{\partial w_N^2}\Delta w_N \end{cases} \quad \textit{Equation 12}$$

Regarding the above system of equations, there are *N* equations for *N* variables so that all Δw_i can be calculated. Then, considering the solution of the above system, the weight space can be updated iteratively. The above set of equations can also be written in matrix form as

$$\begin{bmatrix} -g_1 \\ -g_2 \\ \cdots \\ -g_N \end{bmatrix} = \begin{bmatrix} -\dfrac{\partial E}{\partial w_1} \\ -\dfrac{\partial E}{\partial w_2} \\ \cdots \\ -\dfrac{\partial E}{\partial w_N} \end{bmatrix} = \begin{bmatrix} \dfrac{\partial^2 E}{\partial w_1^2} & \dfrac{\partial^2 E}{\partial w_1 \partial w_2} & \cdots & \dfrac{\partial^2 E}{\partial w_1 \partial w_N} \\ \dfrac{\partial^2 E}{\partial w_2 \partial w_1} & \dfrac{\partial^2 E}{\partial w_2^2} & \cdots & \dfrac{\partial^2 E}{\partial w_2 \partial w_N} \\ \cdots & \cdots & \cdots & \cdots \\ \dfrac{\partial^2 E}{\partial w_N \partial w_1} & \dfrac{\partial^2 E}{\partial w_N \partial w_2} & \cdots & \dfrac{\partial^2 E}{\partial w_N^2} \end{bmatrix} \times \begin{bmatrix} \Delta w_1 \\ \Delta w_2 \\ \cdots \\ \Delta w_N \end{bmatrix} \quad \textit{Equation 13}$$

Where the formulated square matrix is the Hessian matrix:

$$\boldsymbol{H} = \begin{bmatrix} \dfrac{\partial^2 E}{\partial w_1^2} & \cdots & \dfrac{\partial^2 E}{\partial w_1 \partial w_N} \\ \vdots & \ddots & \vdots \\ \dfrac{\partial^2 E}{\partial w_N \partial w_1} & \cdots & \dfrac{\partial^2 E}{\partial w_N^2} \end{bmatrix} \quad \textit{Equation 14}$$

By combining *Equation 6* with *Equation 12* and *Equation 13* we get:

$$-\vec{g} = \boldsymbol{H}\Delta\vec{w} \; and \; so \; \Delta\vec{w} = -\boldsymbol{H}^{-1}\vec{g} \quad \textit{Equation 15}$$

Therefore, the update rule for Newton's method is

$$\boxed{\vec{w}_{k+1} = \vec{w}_k - \boldsymbol{H}^{-1}\vec{g}_k} \quad \textit{Equation 16}$$

Since the Hessian matrix $\boldsymbol{H}$ contains the second-order derivatives of the total error function, it gives a proper and more detailed evaluation on the change of the gradient vector compared to simple steepest descent method. By comparing Equation 6 and Equation 16 it is possible to observe that the inverted Hessian matrix is similar to the learning constant. However, in Newton's method this learning constant is constantly adapted based on the total error function.

Gauss-Newton Algorithm

One of the basic drawbacks of the Newton's method is that the Hessian matrix should be calculated at each iteration of the solving procedure for the weight vector updating. This operation is accompanied with a higher complexity and generally more computational time is necessary. In order to simplify this calculating process, the Jacobian matrix $\boldsymbol{J}$ is introduced as

$$\boldsymbol{J} = \begin{bmatrix} \frac{\partial e_{1,1}}{\partial w_1} & \cdots & \frac{\partial e_{1,1}}{\partial w_N} \\ \frac{\partial e_{1,M}}{\partial w_1} & & \frac{\partial e_{1,M}}{\partial w_N} \\ \vdots & \ddots & \vdots \\ \frac{\partial e_{p,1}}{\partial w_1} & & \frac{\partial e_{p,1}}{\partial w_N} \\ \frac{\partial e_{P,M}}{\partial w_1} & \cdots & \frac{\partial e_{P,M}}{\partial w_N} \end{bmatrix} \qquad \textit{Equation 17}$$

By replacing the error definition to Equation 5, then Equation 6 can be rewritten as

$$g_i = \frac{\partial E}{\partial w_i} = \frac{\partial(\frac{1}{P}\sum_{p=1}^{P}\sum_{m=1}^{M} e_{p,m}^2)}{\partial w_i} = \sum_{p=1}^{P}\sum_{m=1}^{M}(\frac{\partial e_{p,m}}{\partial w_i} e_{p,m}) \qquad \textit{Equation 18}$$

Combining Equation 17 and Equation 18, the relationship between Jacobian matrix J and gradient vector g would be

$$\vec{g} = \boldsymbol{J}\vec{e} \qquad \textit{Equation 19}$$

where the error vector $\vec{e}$ has the following form

$$\vec{e} = \begin{bmatrix} e_{1,1} \\ e_{1,2} \\ \cdots \\ e_{1,M} \\ \cdots \\ e_{p,1} \\ e_{p,2} \\ \cdots \\ e_{p,M} \end{bmatrix}$$

As a basic assumption of Newton's method, is that the Hessian matrix can be approximated with the help of Jacobian matrix as

$$\boldsymbol{H} \approx \boldsymbol{J}^T\boldsymbol{J} \qquad \textit{Equation 20}$$

From the above and by combining Equation 16, Equation 19 and Equation 20 the update rule of the Gauss-Newton method is derived as

$$\boxed{\vec{w}_{k+1} = \vec{w}_k - (\boldsymbol{J}_k^T\boldsymbol{J}_k)^{-1}\boldsymbol{J}_k\vec{e}_k} \qquad \textit{Equation 21}$$

Obviously, the advantage of the Gauss-newton algorithm over the Newton's method (Equation 16) is that the former does not require the calculation of second-order derivatives of the total error function, by introducing the Jacobian matrix $\boldsymbol{J}$ instead. However, the Gauss-Newton algorithm still faces the same convergence problem like the Newton algorithm for complex error space optimization. Mathematically, the problem can be interpreted as the matrix $\boldsymbol{J}^T\boldsymbol{J}$ may not be reversible.

Levenberg-Marquardt Algorithm

In order to make sure that the approximated Hessian matrix $\boldsymbol{J^T J}$ is invertible, the Levenberg–Marquardt algorithm introduces another approximation for the Hessian matrix:

$$\boldsymbol{H \approx J^T J + \mu I} \qquad \textit{Equation 22}$$

Where, μ is called combination coefficient and is always possible and $\boldsymbol{I}$ is the identity matrix.

From Equation 22 it is possible to observe that the elements on the main diagonal of the approximated Hessian matrix will be positive numbers. Therefore, with this approximation, it can be ensured that the matrix H is always reversible. By combining the last equations (Equation 21 and Equation 22), the update rule of the Levenberg-Marquardt Algorithm can be presented as

$$\boxed{\vec{w}_{k+1} = \vec{w}_k - (\boldsymbol{J}_k^T \boldsymbol{J}_k + \mu \boldsymbol{I})^{-1} \boldsymbol{J}_k \vec{e}_k} \qquad \textit{Equation 23}$$

As the combination of the steepest descent algorithm and the Gauss-Newton algorithm, the Levenberg-Marquardt algorithm switches between the two algorithms during the training process. When the combination coefficient μ is very small (nearly zero), Equation 23 is approaching to Equation 21 and Gauss-Newton algorithms is practically implemented. When the combination coefficient μ is very large, Equation 23 approximates the Equation 7 and the steepest descent method is practically applied.

3.3 Developed ANN model structure and training

3.3.1 The island under investigation

A forecasting model is a necessary subsystem that needs to be implemented in a predictive energy management algorithm capable of compensating future events. In this study, such a model was developed for future consumption values forecasting by implementing a simple single-hidden layer feedforward neural network. At this point, it is crucial to clarify that the original target island for which the proposed methodology of this thesis should be applied, was the Greek island of Astypalaia. This island was chosen based on the combination of its basic pattern appearing in the load curve (Figure 19), which is described by the highly peaked load values at night hours when there is not PV energy production, and the relatively high amount of installed PV panels. However, this island could not be adopted for this study, due to the fact that there were not available data for the load curve of past years, from the system operator. This drawback was significant regarding the development of the neural network module, which demands a high amount of past data in order to be trained appropriately.

This main drawback was resolved by the following trick. Since there were available data for the isolated power system of the Portugal island of Madeira, for 3 years' time period, it was decided to downscale those data to the magnitude of the power system of Astypalaia. This was achieved by deciding a scaling and applying it to the load curve of Madeira's system. ($Raw\ Data_{Madeira}[GWh] \xrightarrow{\div 360} New\ Data_{synthetic\ island}[MW]$)

Therefore, an "reference" island was created (Figure 9) with the location of Madeira and the demand curve at the order of magnitude of Astypalaia.

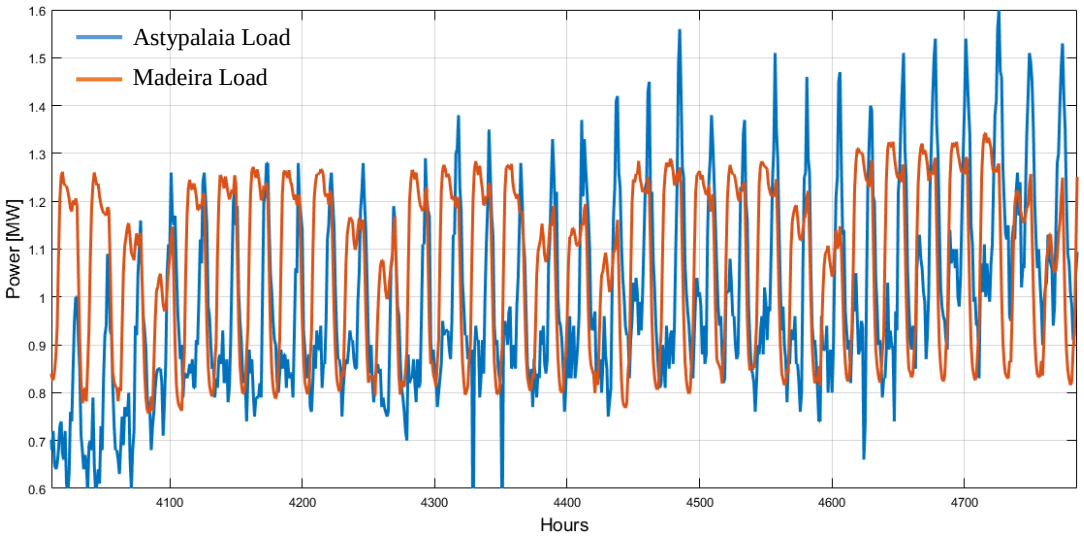

Figure 8: Summer load profile pattern of Astypalaia's system compared to Madeira's system

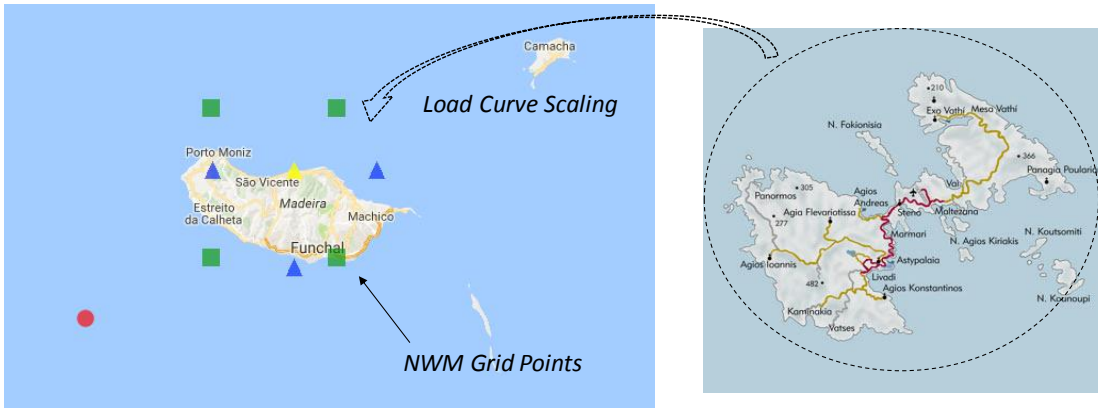

Figure 9: The "synthetic" island generation and the corresponding grid points of the Numerical Weather Model (NWM) for the temperature data

3.3.2 Data preprocessing

The first step for developing a neural network model concerns the data preprocessing. This refers to a set of actions that need to be applied to the dataset in order to divide the dataset to appropriate subsets and prepare the data format, in order to be inserted to the training algorithm described in 3.2. Provided that the purpose of the developed neural network module was to forecast the next day's load curve by estimating the demand values at a 24-hour basis for a whole year operation, the training dataset should be appropriately prepared. For this reason, at least a whole year of operation should be included in the training dataset in order to capture all the appearing patterns and periodicities. Based on this fact, the dataset of the load values which was provided by the grid operator of the island, was divided to the training set which contained load data from the years 2014 and 2015, and the test set which contained data for the year 2016. Regarding the termination criterion of the training process, the training dataset was

further partitioned to include the validation dataset, which accounted for about 4% of the whole training set.

A strong correlation between the trend of the load curve and the temperature data of the island was observed, making the latter as an appropriate input for the developed neural network model. The hourly temperature data was produced by the long validated CFSR [44] numerical weather model (NWM) from representative grid points displayed in Figure 9 near the most-highly inhabited areas of the island for the years examined, so that the correlation of weather phenomena with electricity consumption to be intensified.

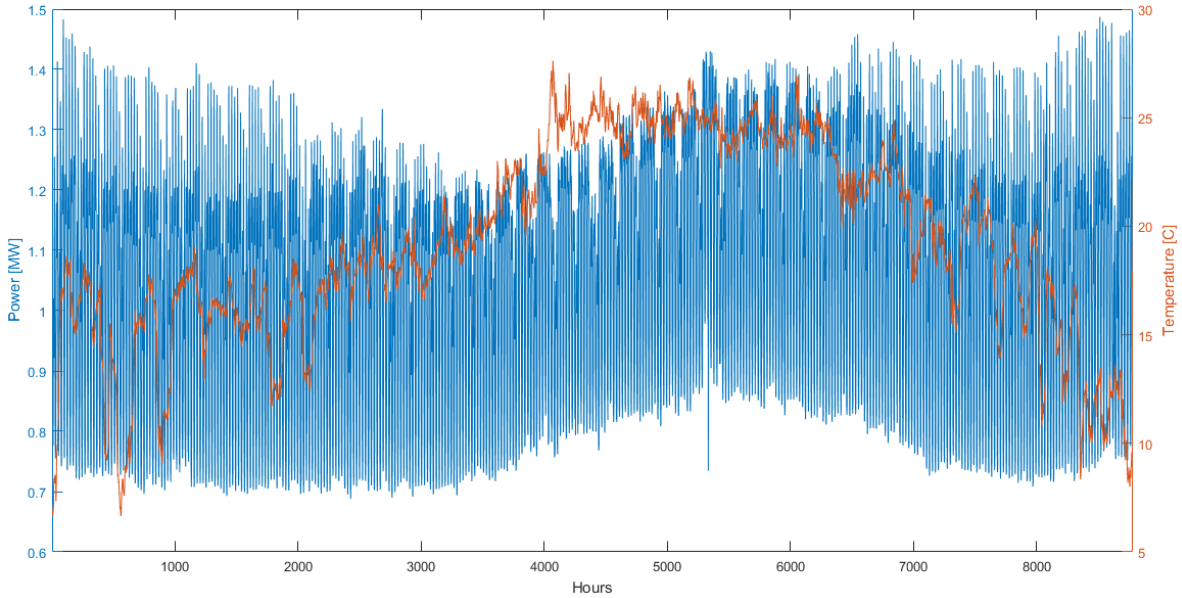

Figure 10: Yearly time period load curve correlation with temperature, for the test case system

The network's structure was chosen based on the well-known Kolmogorov theorem [45]. According to this, a single layer of hidden neurons with the appropriate number of perceptrons is considered to be enough for any function fitting problem, which is the case in our study. The inputs of the feedforward neural network were determined based on common input variables for similar networks referred in load forecasting studies and after a trial-and-error iterative procedure. Therefore, the inputs that were found to give the best results in terms of the MAPE defined as:

$$MAPE = \frac{1}{N}\sum_{i=1}^{N}\left|\frac{Forecsted\ Load_i - True\ Load_i}{True\ Load_i}\right| \qquad \textit{Equation 24}$$

are summarized to the following:

- *i)* 48 values of the hourly consumption data of the two previous days,
- *ii)* 24 values of previous day temperature data,
- *iii)* 7 binary values corresponding to the day of the week and
- *iv)* 1 binary variable which was used as an index for weekend days and working days.
- *v)* The network output consisted of a 24-variable vector containing the next day's forecasted load values.

In *Equation 24 N* is the number of data point used for the test dataset. The structure of the developed network is schematically depicted in Figure 11.

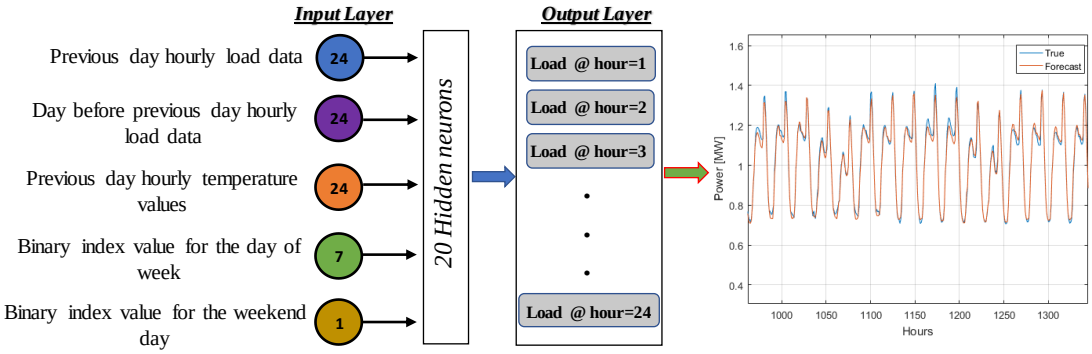

Figure 11: Developed network structure and data flow

The input variables before the training procedure were scaled in the interval [0, 1] based on Equation 25 so that every input has the same weighting despite the different physical scales that are related with the type of input variable. For the same reasons, the binary values were chosen to be 0 or 1.

$$\hat{x} = a + \frac{(b-a)}{(x_{max} - x_{min})}(x - x_{min}), \quad where\ [a,b] = [0,1] \qquad \textit{Equation 25}$$

3.3.3 Network Training

For the purpose of developing the neural network applied in this study, a supervised learning method was implemented. With this methodology of training, the input stimulus that it is applied to the network's neurons results in an output response which is compared with a prior desired output, namely the target signal. If the actual response differs from the target response, the neural network generates an error signal which is then used to calculate the appropriate correction that should be made to the network's synaptic weights. This is repeated until the actual output matches the target output, considering a validation subset of the dataset, whose output should be in an acceptable error range compared to the target response. This process is depicted in the following picture, where the developed network model is trained.

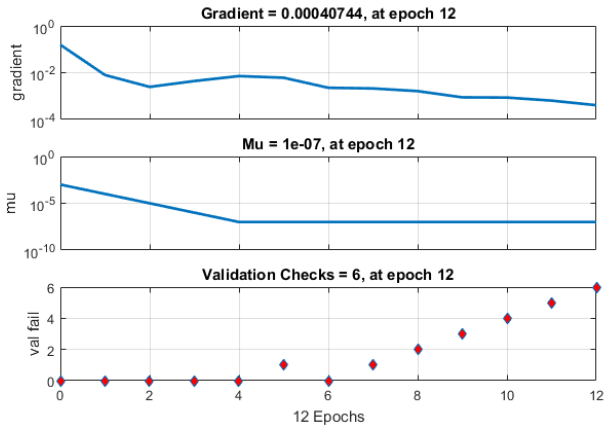

Figure 12: Training termination criteria and gradient vs epochs

The figure above (Figure 12), represents the training process of the network. As the backpropagation procedure is deployed, the gradient of the error is constantly

diminished, while at the same time the mu factor (parameter μ in Equation 23) is also minimized to a specific value, accelerating the training process, as described in 3.2. Regarding the termination criterion of the training, 6 check values of the networks output from the validation dataset were used and only after 6 successful test the training was terminated. In the following picture (Figure 13) the performance of the trained network is depicted. At this point, it is important to be stated that the developed network was initially trained in the way described above making it possible to acquire more accurate initial values for the weight and biases. Then the network was re-trained following the same process, given the acquired initial state. The plots presented in Figure 12 and Figure 13, correspond to the re-training process of the network, which is also the reason for the relatively low number of epochs. The performance of the network was based on the mean square error between the network's output and the actual value. As it is possible to observe, the blue line representing the training set is always below the red line representing the test dataset. This fact is in accordance with the MAPE measured for the aforementioned datasets where the training dataset stands for a lower MAPE value than the test set. This is because the training dataset was already used while the network was developed, thus its inputs are already known to the networks compared to the test dataset whose values have never been introduced to the network before.

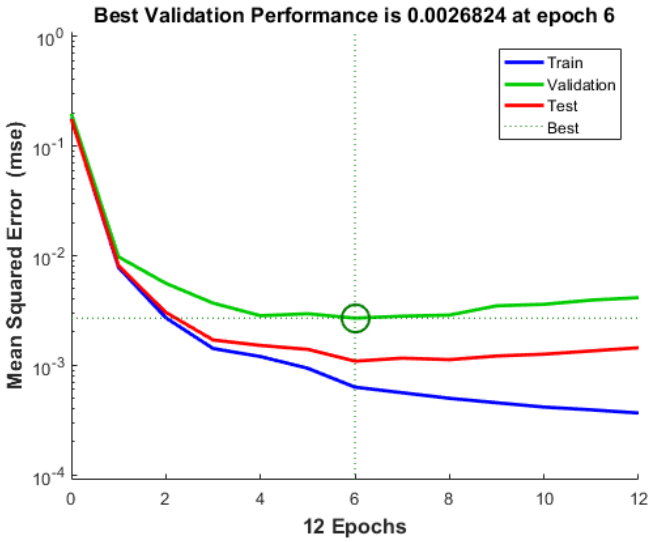

Figure 13: Mean squared error vs epochs for the re-training of the network

For the training procedure, as it was stated above, data from years 2014 and 2015 were used in a backpropagation algorithm based on the Levenberg-Marquardt error minimization algorithm. The mean squared error (MSE) was used as a termination criterion for the training procedure. The evaluation of the network output with the target values was determined with the correlation coefficient R as it is shown in Figure 15. The MSE parameter was first calculated for the validation data set, chosen to be around 4% of the training set, and then the overall network's performance was evaluated for the test set which was not ever used in the training process.

Network structure comparison

After determining the network's structure, a parametric investigation was conducted, regarding the number of neurons of the hidden layer that resulted in the best possible

MAPE. For this reason, the number of neurons at the hidden layer was varied and after the network's weights and biases were randomly initialized, it was trained and simulated to monitor the MAPE for each case. The results are depicted in Figure 14.

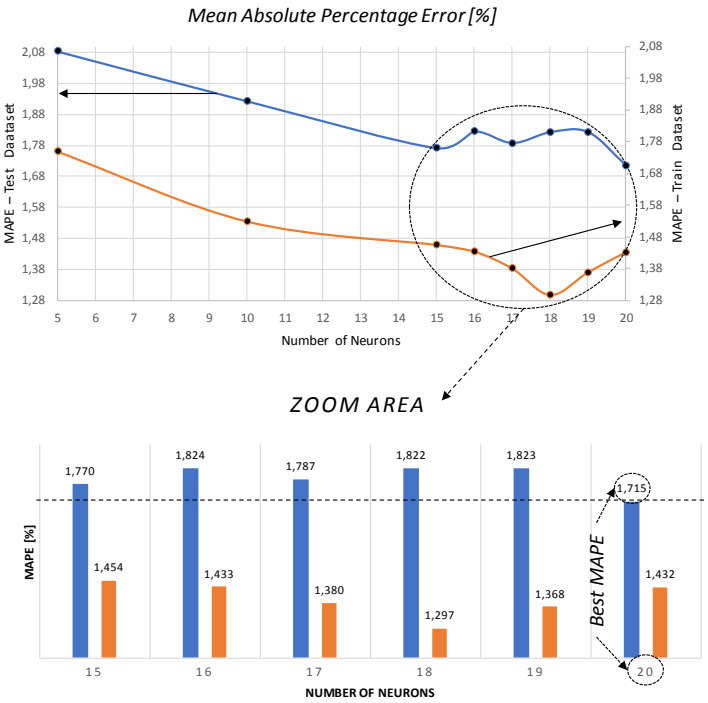

Figure 14: Parametric investigation of the neurons number in the hidden layer

As it can be observed, the number of neurons that resulted in the best MAPE was 20. From the above analysis, it was found that the MAPE was strongly affected from the neuron number, as it was improved for increasing the neuron number. Under 15 hidden neurons, the network was not satisfactory in terms of forecasting capability whereas in the range of [15-20], the network resulted in better MAPE values. However, as long as the training process requires an initialization step for the weight values, which is based on a random generator, it is characterized from stochasticity. For this reason, the parametric investigation was limited to the results of Figure 14. Moreover, the purpose of this study was not to achieve the best possible forecasting model but to present the synergetic effects of forecasting, optimization and dynamic simulation of the system.

After the network configuration procedure was completed and the best results were achieved, the correlation coefficient defined as

$$R^2 = 1 - \frac{\sum_{i=1}^{N}(y_i - t_i)^2}{\sum_{i=1}^{N}(t_i)^2} \qquad \textit{Equation 26}$$

was found to be R=0.99189, which considered as an acceptable value. In particular, from the following scatter plot it is possible to observe that the majority of the data points of the whole dataset (training, validation, test) are concentrated in the neighborhood of the perfect forecast line. The perfect forecast line is the straight line with an inclination of 45 degrees and represent the equality of the network's output with the actual value.

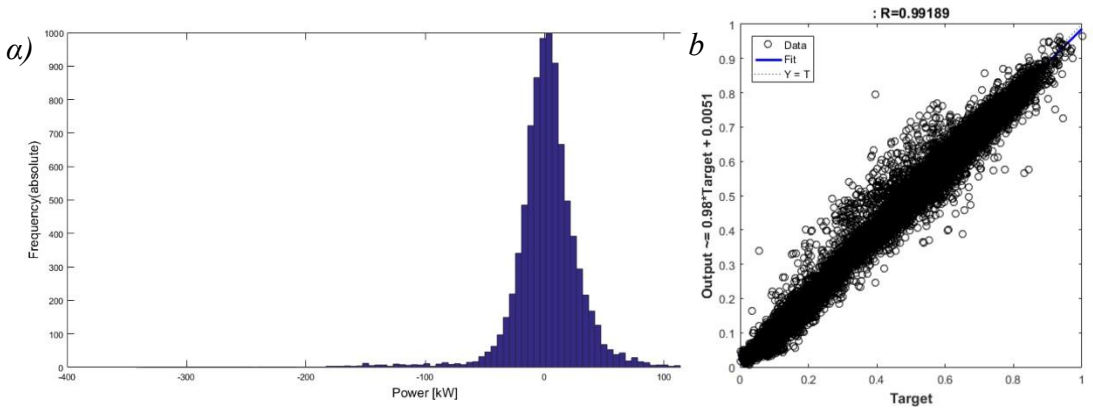

Figure 15: Test dataset achieved results metrics a) error histogram distribution, b) correlation coefficient

Further analysis on the network's performance can be evaluated from the residual plots and the histogram of the error values. As it is clear from the figure below, the variation of the error signal of the train dataset is less than the variation of the test dataset, though there is no specific correlation. This is an indication of good generalization aspect of the network, while there is no bias to certain values neither a particular trend. This is also depicted on the histogram of the errors of the test dataset, which present the expected normal distribution.

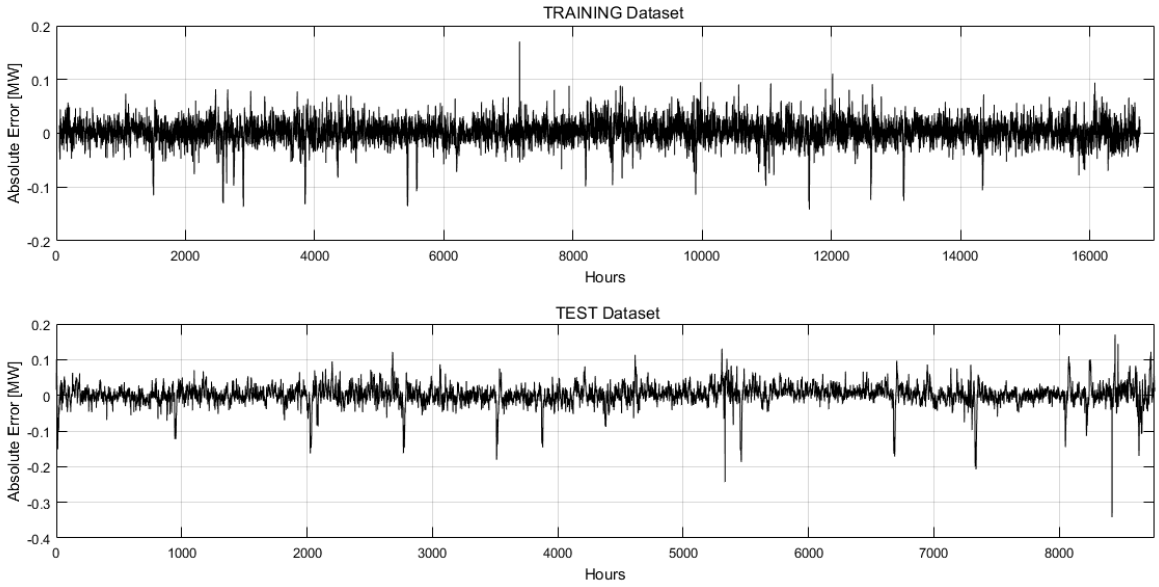

Figure 16: Error residual signals for the test and the train datasets

Thereinafter, the outputs were scaled back to their physical scales, the overall network's performance was evaluated for the test set and a MAPE=1.715% was achieved. The results of the load forecast are presented in detail in the following section.

3.3.4 Network achieved results

With the network's configuration determined and after the training process, the ANN model was deployed and tested for the test dataset (year 2016). In the following figure (Figure 17), the complete dataset, including the training and testing sets, is compared with the model's predicted outputs. Specifically, with the blue color, the training set is depicted and with the red color the test set is marked.

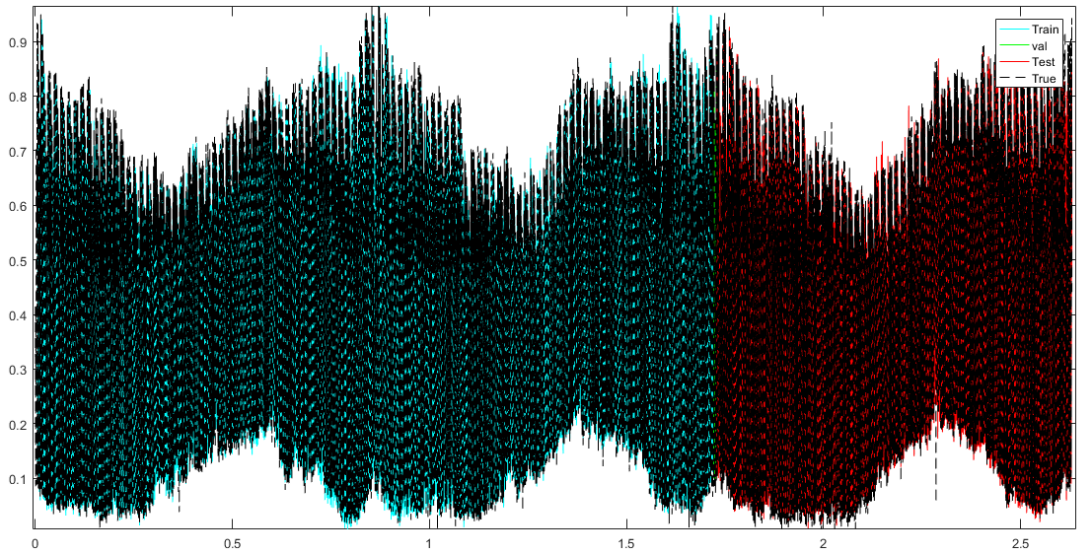

Figure 17: Training, test and validation data vs model output

As it is obvious from the above figure, there are multiscale patterns ranging from yearly down to daily timescales. The yearly based pattern is the most easily distinguished pattern, as the load values are generally higher during winter time periods and lower during summer time periods. This fact is justified from the weather effect on the consumption, as it was also illustrated in Figure 10. In this way, lower ambient temperature is generally correlated with higher consumption, excluding the situation of extremely high temperatures, which are noticed at the late summer periods, where the load curve takes high values. This fact is attributed to the use of heat pumps and air conditioning which are activated during summer. In the following figure, a zoom is applied to the test dataset, so that the result of the ANN forecasting is better visualized.

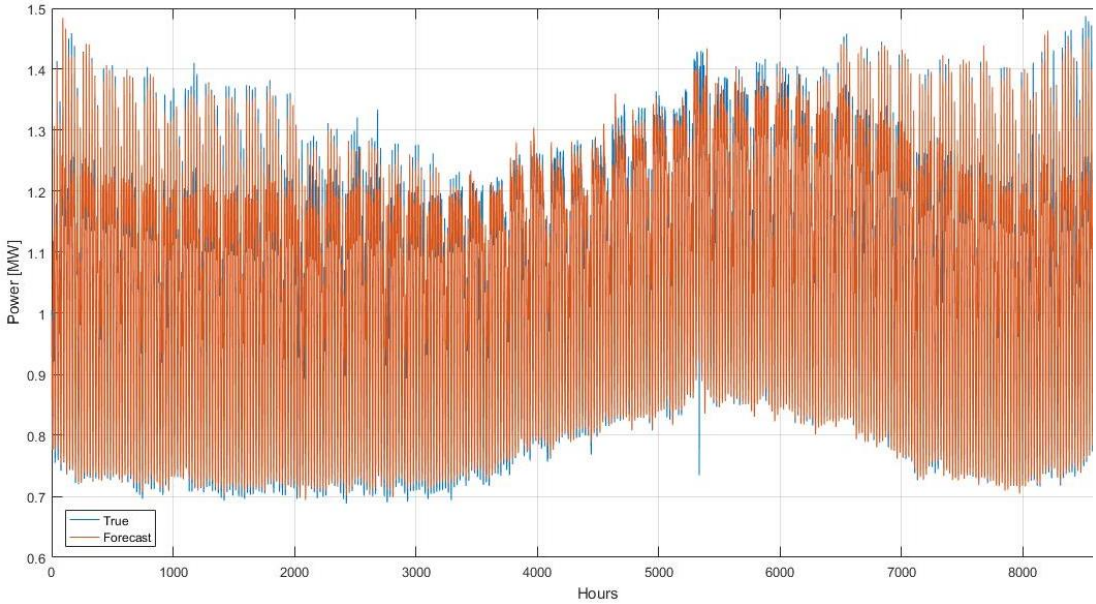

Figure 18: Actual vs forecasted load data for the test set (year 2016)

From the figure above, it is clearly depicted that there are intra-year patterns, which are related with the weeks of the year. Thus, the signal is repeated with a specific structure for each week of the year which is directly observable. It can also be stated that the

developed model has a very good overall efficiency and pattern capturing capability, as the orange curve (Forecasted values) is almost similar to the blue curve (True values). This is better illustrated in the following figure, where the intra-week patterns are depicted.

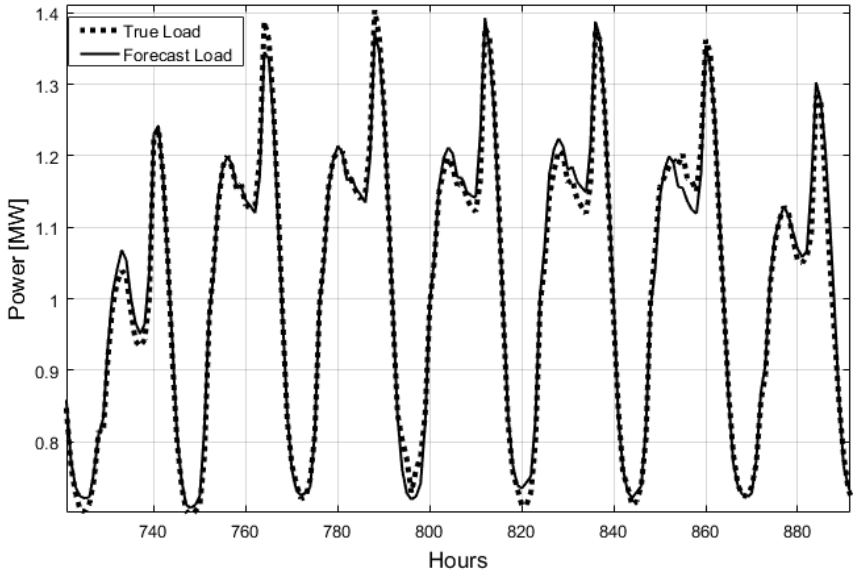

Figure 19: Actual vs forecasted load data for a typical winter week of the test set

From the above figure, the greater depth of detail of the developed network is depicted, where the separate actual data points at each hour are clearly illustrated. A whole week is presented starting from Sunday and as it can be noticed, the weekend days have a lower maximum value compared to the rest of the weekdays. This trend of the load curve is a common future to similar power systems and is explained by the significance of the industry/commercial sector in the total demand of the system. Thus, a region (island) with developed industry will be more affected by this pattern compared to a touristic region which the load curve is dominated by the residential sector.

After the prediction module with the ANN was prepared, the next step was its integration with the developed optimization algorithm described in the following section.

4 Optimization algorithm for peak shaving and load smoothing

In this chapter, an algorithm was developed to be integrated into the energy management system of the islandic power network, that could upgrade its operation by providing renewable energy in a more secure and stable way and by peak shaving the maximum demand values. The developed algorithm was suited for the specific island case investigated in this study but could be also implemented with few modifications to other similar power systems, where the load curve presents similar patterns. In the following section, the algorithm is described in detail.

4.1 Algorithm Description

4.1.1 Problem Description

After the load forecasting module was configured and tested, the demand values of the next day at an hourly basis could be predicted. This ability was taken into account for the development of a predictive Energy Management System (EMS) algorithm that could be used for the "smartening" of the power system, considering a more stable and robust operation. The facts that the load curve's most frequent shape and pattern was characterized by highly peaked values at late night hours and that the type of installed renewable sources was PV, were considered for the decision of the operational modes of the developed algorithm. In an effort to visualize the total load curve with its basic patterns during the test year (year 2016), Figure 20 is presented.

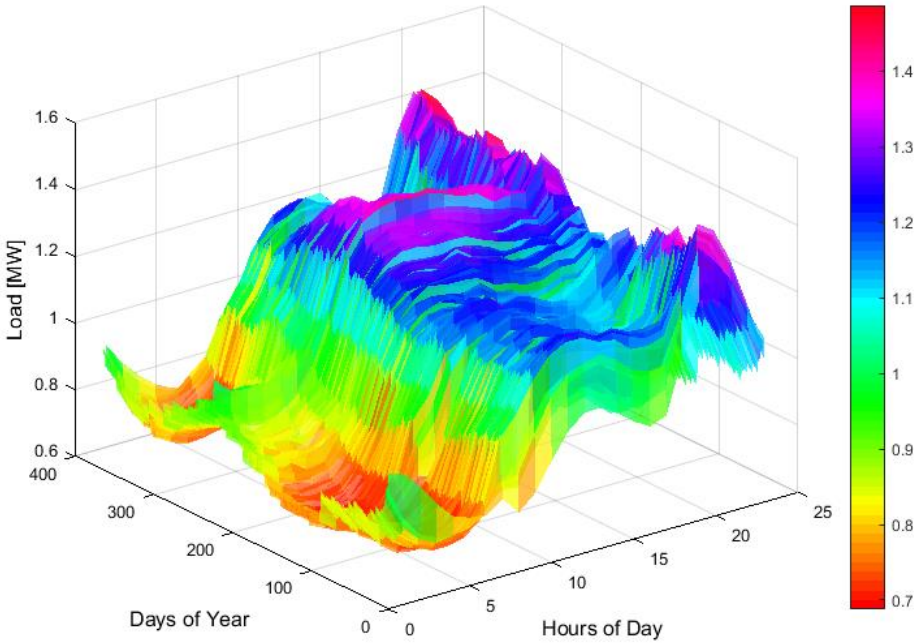

Figure 20: Ensemble of the load curves of the island for a complete year (2016)

From this figure, it can be proved that there are two demand spikes for the most of the year. The first demand spike is detected during the morning hours where everyone wakes up and starts consuming energy and the other is detected during the evening hours where most people return from work and once again they begin to consume energy in their homes. Considering the shape of the load profile, it can be concluded that especially for the winter period, the peaked values of load are detected during the

night hours where the renewable installed PV power is not available. From Figure 20, it can be shown that the island's power system has maximum peak demand values about 1.3-1.5 MW, which are currently covered by conventional diesel generators that operate at low partial loads. The installed capacity of PV power is approximately 300 kW, accounting for around 20% of the peak values. Regarding the above, it is rational to consider the following targets be countered by the algorithm:

1. Peak shaving of the maximum demand values of each day of the year
2. Smoothing the operation of the diesel engines during the off-peak hours
3. Avoiding the "duck" shape evolution to the load curve, concerning the constantly increasing PV power penetration to the grid
4. Ensuring 100% renewable energy penetration

Concerning the point 3, the "duck" shape is presented in the following figure (Figure 21) and is a trend that is constantly evolving and affecting the net load power curve. The net load power curve is defined as the total load curve subtracting the PV power production curve. The resulting curve (which is named net load curve) is the one that will have to be covered by the rest thermal-conventional power production units. As more and more solar PV are integrated into the grid, it starts dramatically suppressing net load during midday, when the sun is out. The net load curve sags in the middle of the day (like a belly) and then swoops back up when the sun goes down (like a neck).

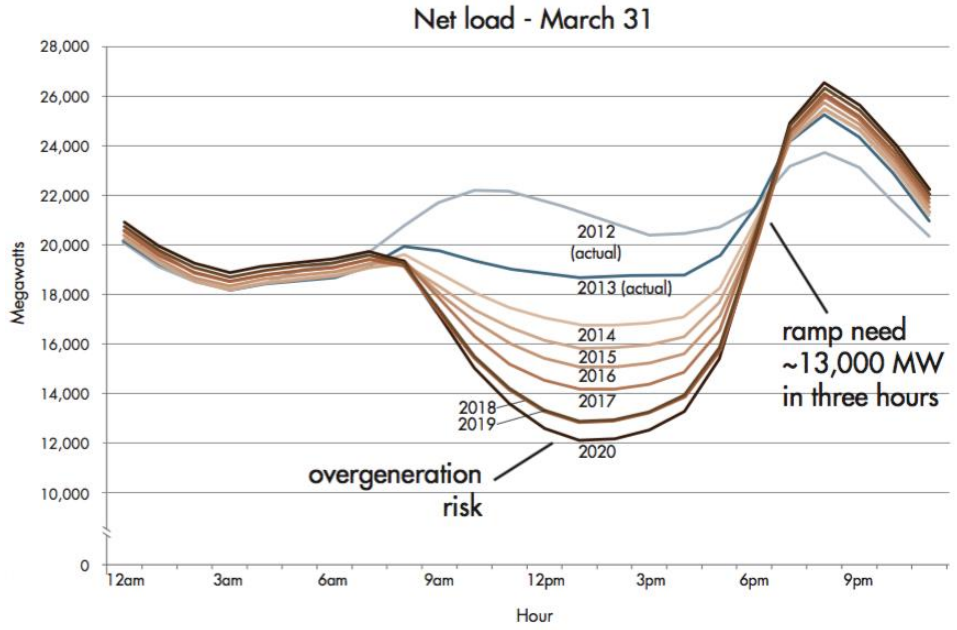

Figure 21: The "duck" net load curve, illustrating steep ramp needs and overgeneration risk [46]

The figure above was taken from the system service operator of California [46] and the "duck" shape evolving through the years from the increasing PV power generation is depicted. It is also clear that this effect is accompanied by an overgeneration risk which is due to the technical minimum operating point of the thermal units. The "duck" shape is also directly related to the need for higher ramp rates because of the sudden load change. These effects will have a negative impact on the stable and smart operation of a future isolated grid with high renewable penetration. The main idea for encountering the above effects and achieving a smoother, robust system operation was to take

advantage of the load forecasting ability and to combine it with an energy storage system (ESS) in order to save a specific amount of energy that could be injected to the power grid later. For the purpose of this study and based on the fact that battery energy storage systems (BESS) have recently made a resonant entrance to the power market and are constantly evolving [47], such a system was considered for the storage ability needed in our case study.

4.1.2 Synthetic Power Curve

Regarding the above concerns, a BESS capable of saving renewable energy when it is not required and releasing it at night peak demands is a meaningful strategy. However, a BESS should operate with an optimum plan in order to be appropriately integrated into the system and minimize the pay-back period of the investment. In addition, considering that this would be a grid-scale BESS and that the installed renewable capacity in the island, for the time being, is not high enough to cover the load curve at any point, the PV energy storage should be optimized. At this point, for the purpose of explaining the algorithm flow, it was considered that the PV production curve for the whole year at an hourly basis, was already obtained and could be used from the algorithm. More details about the PV power curve production and the way that it was generated can be found in the next chapter where the system modelling is described.

The first step of the algorithmic procedure, was to determine the inputs. Those were decided to be the 24 variables vector, which contained the demand values of the next day, as they were predicted from the ANN model and the 24 variables vector containing the hourly values of the total PV energy production of the corresponding day. Then the peak reduction level was decided and set to be at 0.1 MW less than the maximum demand value of each day. This value was determined based on the load curve data observation and was evaluated from the values of the peak region relatively to the mid-day load values. However, this parameter could be subjected to optimization in an upgraded version of the algorithm and in this way, it could be matched for each day specifically instead of taking an average constant value. After the peak reduction level or peak shaving level was determined, based on the load forecasting of the next day, the area to be removed after the peak reduction was calculated. This is better visualized in the following figure (Figure 22). In this figure, the load curve of the next day is depicted with the solid line and the peak reduction level that is decided to be implemented, is represented with the dashed line. This line, should cross the load curve at two separate points and in this way a closed area is shaped. This region, which is basically the area under the load curve subtracting the area under the dashed line and is depicted as the grey region in Figure 22, corresponds to the total energy that will be eliminated after the algorithm operation and the generation of the new diesel engines setpoints. It is also clear from the units of the two axes of Figure 22 that the aforementioned area, represents the energy values based on the following definition:

$$E_{1\to 2}[MWh] = \int_{t_1}^{t_2} P(t)dt \qquad \textit{Equation 27}$$

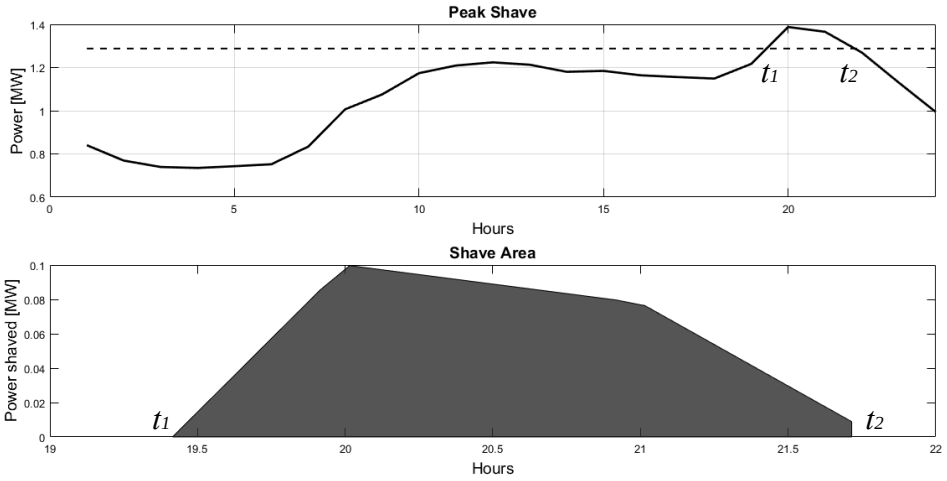

Figure 22: Peak reduction level and the corresponding area between t_1 and t_2

With the above input parameters defined, the next step was the creation of the combined curve. For this, the "offset" value concept was necessary. The offset value was defined as a constant load value and at the first step of the algorithm it was initially set equal to the base load value, defined as the minimum of the daily load curve. This, offset value was used for the initial combined curve generation, which was later updated during the iterations of the algorithm. The combined curve was defined as i) the summation of the load curve and the PV power curve for the load values that were smaller than the offset value and ii) as the summation of the PV power curve with the offset value, for the load values that were greater than the offset value. This is also mathematically described as below:

$$P_{combined}[MW] = \begin{cases} P_{PV} + P_{load}, & for\ P_{load} < P_{offset} \\ P_{PV} + P_{offset}, & for\ P_{load} \geq P_{offset} \end{cases} \qquad \textit{Equation 28}$$

4.1.3 The "elevator" concept

After the initialization of the algorithm parameters and providing the input values described in the previous section, the next step was the implementation of the "elevator" concept. This was basically the core process of the algorithm according to which the desired effects could be obtained. At this point, we highlight that the main output of the algorithm was a 24-variable vector containing the diesel engines operating setpoint values for each hour of the next day. This was actually the dispatch planning for the power generation concerning the unit commitment of the next day.

Initially, as it was stated earlier, the offset value was considered at the base load which was the minimum of the daily load. The PV production curve was then superimposed to this offset level and in this way, the offset value was used as a carrier for the total PV power generation curve. The offset level was constantly increasing by a constant step value which was set equal to *dP=1 kW*. This process was repeated until sufficient surplus area was created. The surplus area was defined as the amount of energy that was overproduced compared to the demand of the corresponding time period. The procedure of updating the offset value is depicted in Figure 23. In this way, the offset level acted as an "elevator" for the PV production curve and at the same time as an upper limit for the diesel operation during the off-peak hours.

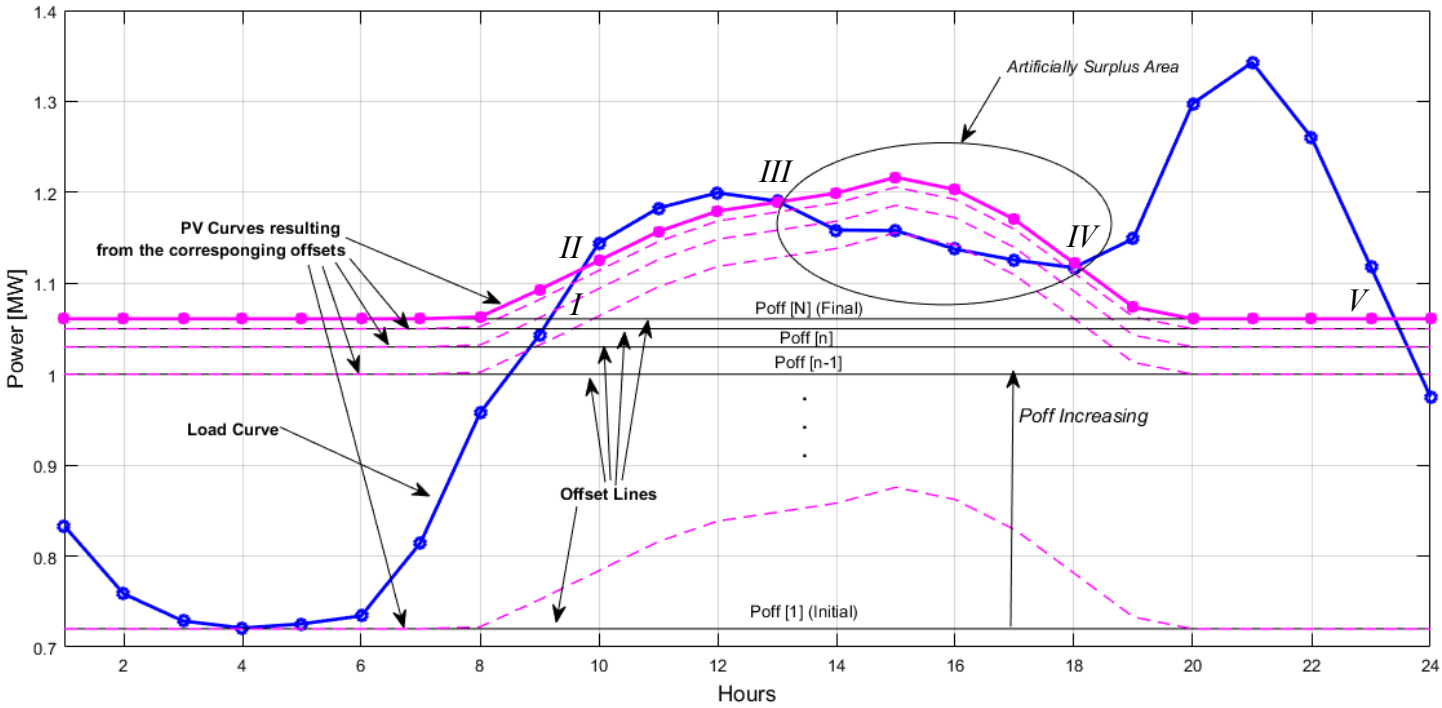

Figure 23: The elevator concept with the corresponding cross points

From the figure above, the process of updating the offset value is described. Initially, the first offset value *Poff [1]* is set equal to the minimum of the daily load curve. Then, the PV power production curve, the magenta curve, was added to this line and after each update it is transferred upwards, until the first cross point (cross point I) between the offset line and the load curve, was noticed to be at the sunlight time period. This condition was necessary to be satisfied because if the curves were intersected before, then it would be impossible to "generate" an artificial surplus, because the offset would still be very low, as it may be observed in Figure 23. Regarding the cross points as they are depicted in Figure 23, it is possible to observe two separate regions. The one region is defined from the cross points II and III and the other from the cross points III and IV. The first region defines an area in which the combined curve resulting from the updates of the offset would be under the load curve, meaning that the demand values would be higher than the total energy produced for the specified time period and therefore the BESS should provide an additional amount of energy. For the second region (points III and IV), the inverse would be happening meaning that the instantaneous produced energy would be greater than the total demand and consequently the BESS should be able to store additional energy. The situation described above is depicted in Figure 23 for the cases *Poff [n]* where n corresponds to the number of iteration. At this point it should be clarified that concerning the region created from the points I to III, in case that the BESS cannot provide the necessary power, then the diesel generator should violate the upper limit rule defined by the offset value and maintain the balance of the system. The process described above should be repeated until the value *Poff [N]* was reached. This would mean that the net energy (energy to be stored to the BESS minus the energy to be provided by it) should be at least equal to the total energy that would be needed later for the peak shaving to be applied. The above process is also explained from the following figure (Figure 24).

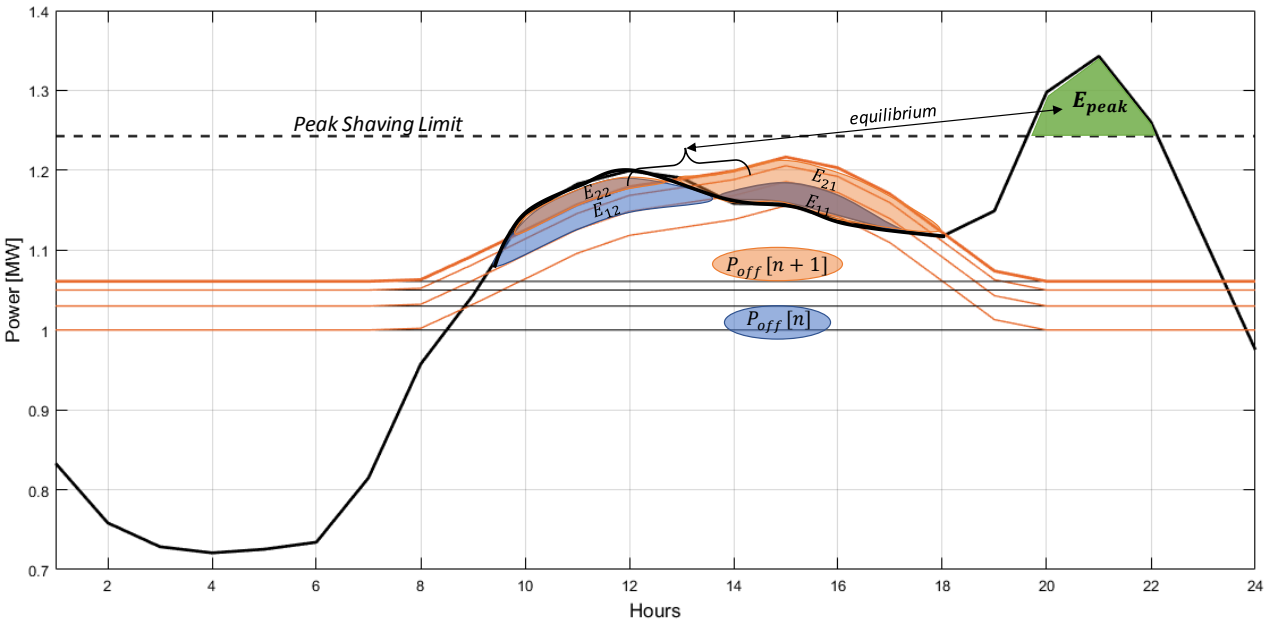

Figure 24: The equivalent areas generated by the "elevator" technique and the equilibrium pursuit

Regarding the figure above, (Figure 24) it can be derived that each update of the offset level, resulted in a new artificially created surplus area, which was calculated as the net difference E_{11}-E_{12} for the blue case or E_{21}-E_{22} for the orange case, as depicted above. At this point, it is important to be stated that the variables E_x represent energy values [MWh] which are also area values under the Power vs Time curve. From this point of view, for the blue case, the net difference would be negative E_{11}-E_{12} <0, meaning that not sufficient surplus energy would have been created and the offset level should be updated. In this way, after updating the offset level, the method resulted in the orange case, in which the net difference would be positive E_{21}-E_{22} >0. After each update, the aim of the developed algorithm was to converge to the target value, E_{21}-E_{22}→E_{peak}. The termination criterion of the algorithm could be represented by E_{21}-E_{22} ≈ E_{peak} within an acceptable convergence bandwidth described with the variable ε. Thus, this iterative procedure was terminated when the net surplus was at least equal with the peak shave area (green area). The aforementioned statement could be described mathematically as:

$$\int_{t_I}^{t_{IV}} (P_{combined} - P_{load})\, dt \geq \int_{t_1}^{t_2} P_{load}\, dt \qquad \textit{Equation 29}$$

where ε was considered around 10^{-3}, t_I and t_{IV} the cross points depicted in Figure 23, and t_1 and t_2 the cross points defined by the peak shaving level, depicted in Figure 22. In order to calculate the above areas as more accurately as possible, a linear interpolation was considered between the hourly values of demand and production, which in general is quite close to the true case. Specifically, as it can be noticed in the following figure (Figure 25), the intervals in which the above areas where calculated were discretized in a fine way (*N* intervals from the following equation) so that the area calculation, which was based on the trapezoid rule, could be accurate enough for our purpose. The integrals of the corresponding areas were numerically calculated based on the following way:

$$\int_{t_1}^{t_2} P(t)dt \approx \sum_{k=2}^{N} \frac{P(t_{k-1}) + P(t_k)}{2} \Delta t_k$$ *Equation 30*

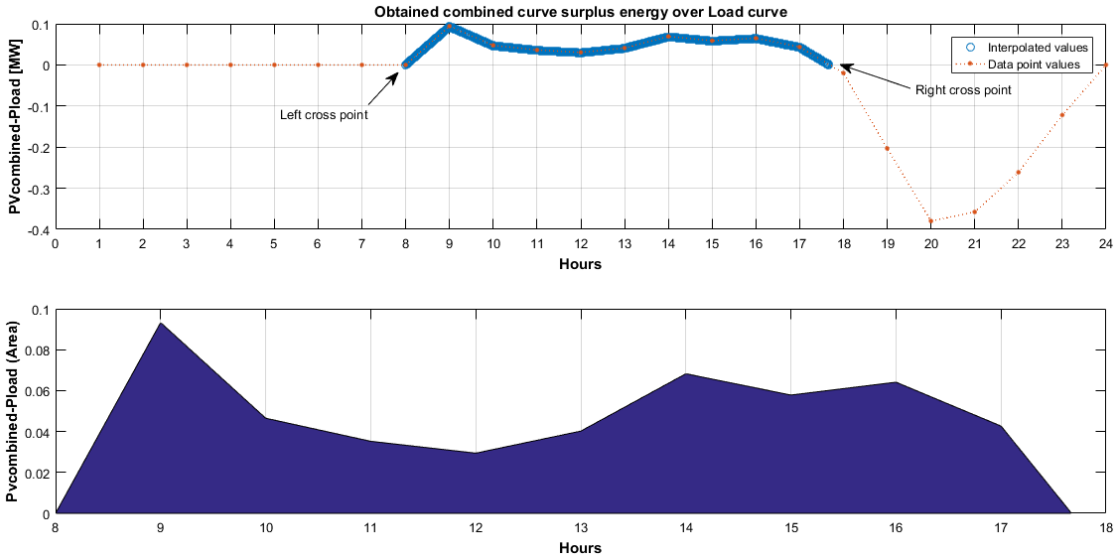

Figure 25: Numerical discretization and integration of the interval that corresponds to the surplus energy generation

The overall algorithm described in the above sections is depicted through the following flowchart.

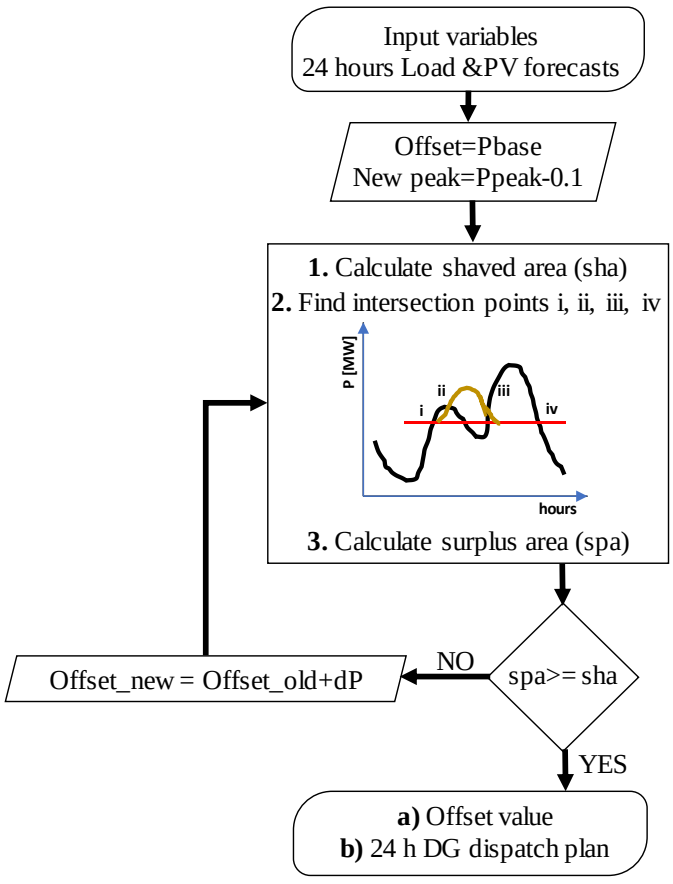

Figure 26: Developed algorithm flowchart

4.2 Acquired diesel engines setpoints

The developed algorithm described in the previous section, was applied to each day of the year under investigation (i.e. year 2016) and was based on the load forecasting for the same year. The main target was to be implemented via an Energy Management System which would operate the power system of the island in a prescribed/predefined optimal and robust way. This was achieved by planning the diesel generators operation and integrating it with the BESS operation in a predictive way, considering the ultimate targets of the supervisory system, summarized in 4.1.1. The developed algorithm, was also capable of storing only renewable energy produced from the PV panels, as long as the storage could be initiated only when there was enough surplus energy. In this way, a 100% renewable penetration could be guaranteed, devoid of technical minimum limitations or sudden load changes. From the following figure, it is possible to observe the residual ε during the algorithm calculations for the days of the year. It is quickly proved that the algorithm converges to the specified target value almost for every day of the year, excluding 7 days (35, 94, 97, 241, 248, 290, 301). In these days, considering the safety of the system, the algorithm specified a higher surplus energy from the one that would be really needed.

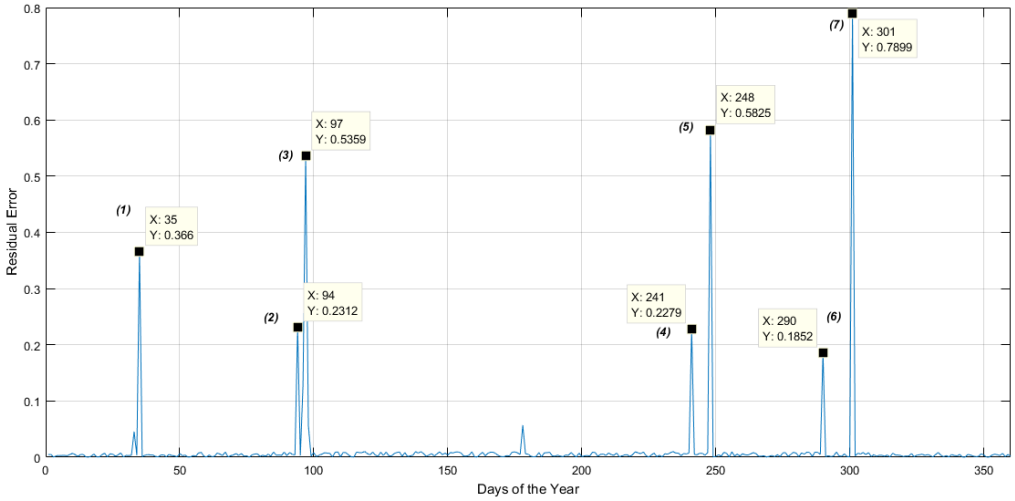

Figure 27: Error residuals predicted from the algorithm, for a whole year operation

Thus, it is possible to set a new 24-hour based operation plan for the diesel generators consisting of the offset value that is achieved from the algorithm and the new shaved peak, which were also the outputs of the procedure. In the following sections the results of the algorithm are presented for indicative days from different seasons of the year, with the corresponding comments.

4.2.1 Algorithm outputs for different time periods

The whole year could be divided into two basic time periods, the winter time period and the summer period. This division is based on the pattern appearing to the load curve of a typical day during each season. The winter time period pattern is depicted in Figure 22 whereas the summer time period pattern is depicted in the figure below (Figure 28). It can be noticed that during the winter time period, the load curve presents the pattern that was suitable for the implementation of the developed algorithm whereas the pattern of the summer time period was not ideally suited. This was due to the fact that the curve was not peaked during the late evening hours, as was the case with the winter pattern,

but instead it was constantly at high levels of load values. This fact was attributed to the intensive use of cooling and air conditioning of the industrial equipment during the hot days of summer with relatively higher temperatures compared to the winter time period. In this way, the concept of PV energy storage in a previous time period, that could be used later during the peak hours, was not applicable. This was due to the fact that the peak values of the load were present during the morning and midday hours, were the PV generation could be directly injected to the grid.

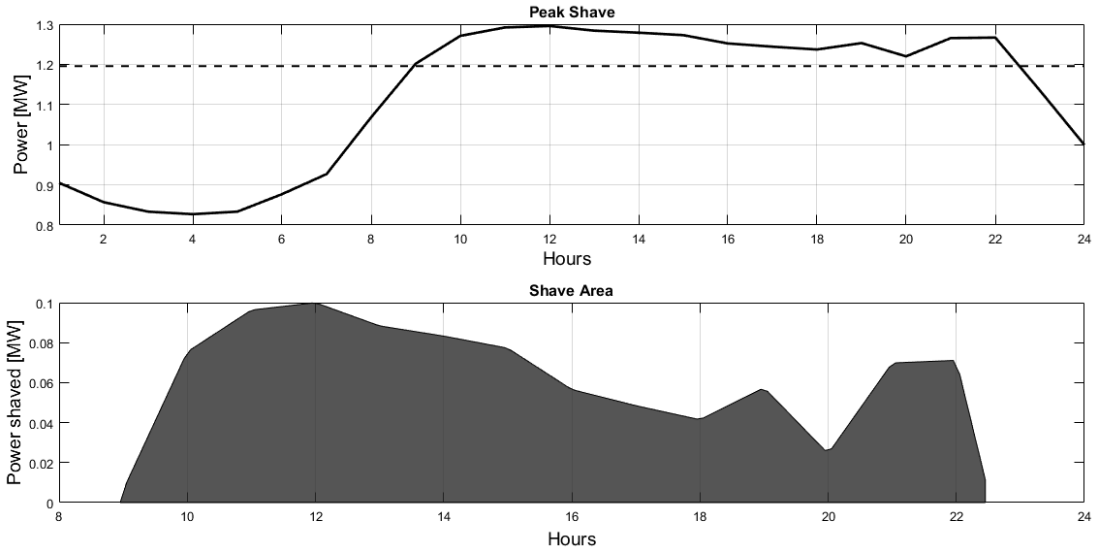

Figure 28: Summer time period load profile pattern and the corresponding peak shaving area

Winter time period

For the period of the year that was related with months 1-3 and 9-12, the winter time period pattern was mostly noticed. For these cases, the algorithm predicted the results as they are depicted below. Specifically, in the figure below (Figure 29), results are presented for day 35 (February).

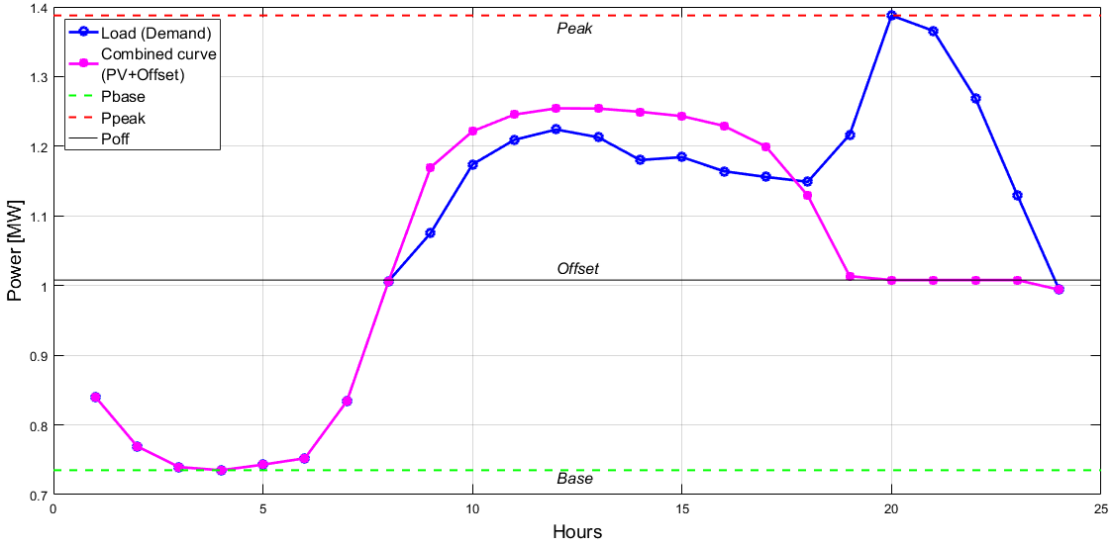

Figure 29: Resulting curves from the algorithm, for day 35

In the figure above, the combined curve that the developed algorithm prescribed, is directly recognizable as the magenta curve. It is also possible to observe the high and low limits of the offset value, marked with the green and the red lines respectively. These are the lowest and highest demand values of the day, which define the range of possible values that the offset variable could gain. For that specific day of the year, a relatively smooth PV production curve accompanied by a smooth load curve can be noticed, which is mainly characterized by its peaked values late at the evening (hour 20:00). However, the PV production is maximized earlier in the same day, during the morning - afternoon time period (11:00-13:00). At this time period, a curved section of the plot is followed from a hollow one which is overlapped from the combined curve. In this way, an excess surplus energy amount is possible to be artificially created. Part of this energy is used instantaneously in order to cover partially the current demand values and the rest of it is intended for storage in the battery, in order to be available later on the peak hours. This fact is better explained in the following figures.

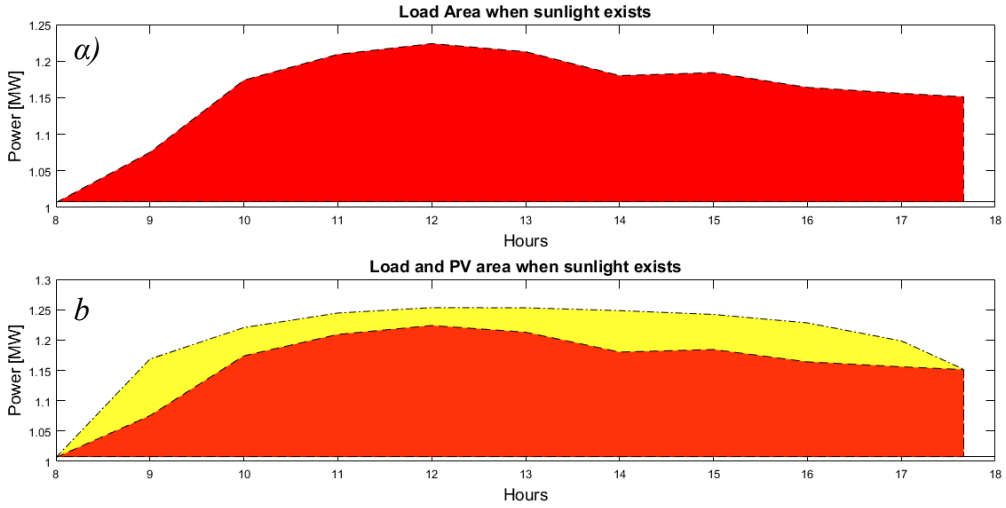

Figure 30: Artificially created excess energy and the corresponding demand, for day 35

From the above figure, it is possible to observe the area between the load curve and the offset value, as defined from the developed algorithm for a typical winter day. The corresponding load profile is presented in Figure 29. The red area represents the amount of energy that will be needed to be covered from the current PV energy production, assuming a perfect forecast for the load curve of the next day. This assumption is based on the fact that given the load curve of the next day and the PV power generation, the developed algorithm estimates the offset value, which is interpreted from the diesel engine operation perspective, as the maximum allowed value, regarding the time period [08:00-18:00]. Thus, the red area of Figure 30 a, which is generated for every day with a similar winter demand profile, is generally partially covered from the current PV power production or even from stored energy in the battery system. In case neither of these power sources is capable of matching the demand of this area, a violation of the upper barrier posed for the diesel engine from the offset value is necessary, so that the system balance is preserved. In Figure 30 b, two regions are depicted. The orange region which corresponds to the red area above and the yellow region which corresponds to the excess energy area to be stored for later peak shaving capability. The orange area is actually the overlapping of the combined curve with the load curve and the offset line barrier whereas the yellow area is the net surplus energy and corresponds to the section

of the magenta line in Figure 29 which is over the load curve. As it is possible to notice, both of these areas are suddenly interrupted at the right end at about 17:40. This fact is attributed to the transition of the combined curve to values lower than the current demand values and since the excess energy to be stored has to be renewable (i.e. PV power) the storing capability is interrupted, in order to avoid storing grid energy in the battery. The possibility to store power from the grid has been investigated in other studies [48,49,50] and is considered to achieve better results when combined with a time of use (TOU) tariff and an electrical power price daily profile. Nevertheless, in this study, this effect is not allowed and stored energy of the BESS is forced to be renewable, in order to inject clean renewable energy to the power grid of the island and consequently improving the renewable penetration. From the following figure, the diesel engine planning is possible to observe.

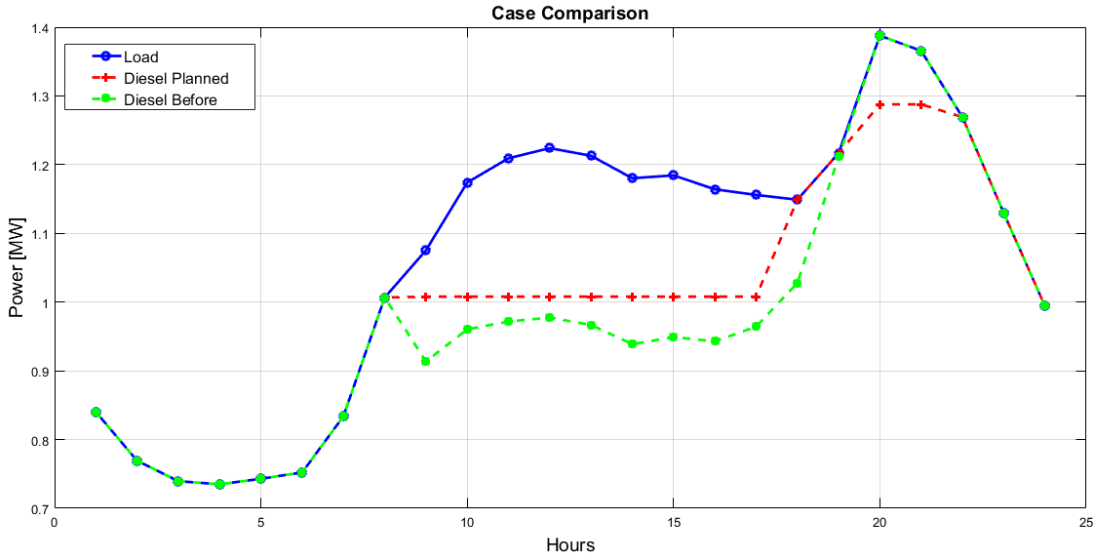

Figure 31: Diesel engine operation before and after the algorithm's implementation, for day 35

In the above figure, (Figure 31), the diesel engine planned operation is plotted with red cross line. The blue line at the same plot, represents the load curve (as also depicted in Figure 29) and the green line represent the net load curve of the same day. At this point, it is considered as a good option to remind that the net load is defined as the total load of a single day subtracting the renewable power generation that corresponds to this day. Thus, the green dashed line is related with the operation of the diesel engine of the island in case that the whole PV generated power could be injected into the grid, the time that it is produced. As this may be possible for a flexible small-scale power grid, this is not the case for a large power grid which is interconnected with many conventional thermal power plants. This is due to the achieved technical minimum operation that is prescribed for these units and the related start-up and shut-down dynamic operation modes. The last, are related with rapid and abrupt changes in the loading state of the thermal units which are subject to technical limitations. This in turn, may result in curtailment issues and valuable renewable energy is not injected into the grid, for stability reasons. This drawback is countered by the developed algorithm, as long as a stable diesel operation with predefined ramp-ups is achieved. At the same time, the renewable power production is ensured and smoothly integrated with the diesel and BESS operation. However, the developed algorithm may present an

additional advantage over larger power grids with high inertia, achieving a robust operation by scaling up the aforementioned benefits. For our case of the islandic power system, the operational setpoints of the diesel engines are depicted with the red dashed line in Figure 31 and as it is evident, it is smoother compared to the green line. In this way, sudden changes in loading of the diesel engines resulting from the uncertain PV power production are avoided while at the same time the ramping rate is diminished regarding the peak shave of the night hours. In the figures below, the results that are achieved from the algorithm are presented for other winter type load profiles.

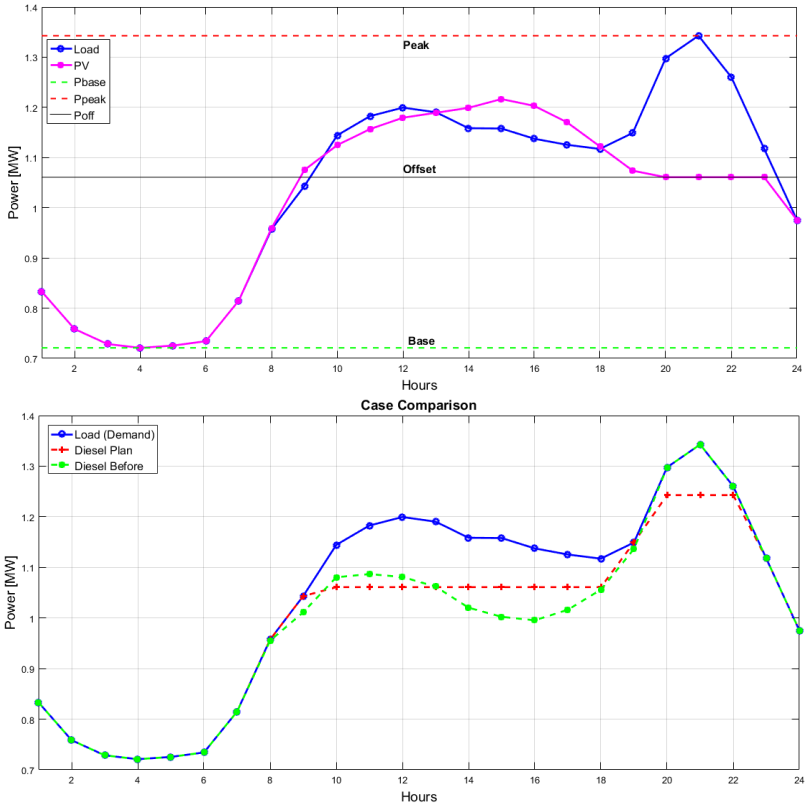

Figure 32: Algorithm output curves, for winter day 63

In Figure 32 and Figure 33, the combined curves and the diesel operation planning for two different winter days, as it is outputted from the algorithm, is presented. Specifically, in Figure 32 results are presented for a winter day before summer while in Figure 33 results are presented for a winter day after the summer time period. For the load profiles of those days, it can be easily observed that the "duck" phenomenon is intensified and this has a significant effect to the diesel net load operation, which is depicted from the green lines. For both cases, and especially for day 255, a highly curved valley is located right before the night hours peak demand. This effect is directly related with the high ramp rate needed to be covered by the diesel engines in a relatively short time period. This ramp up of the diesel engines is associated with higher fuel consumption during acceleration while at the same time it is considered an important factor for extra stressing of the engine. Thus, this dynamic behavior may result in a higher maintenance cost and more frequent component failure.

Regarding Figure 32 and Figure 33, another fact to be noticed is related with the combined curve during the morning hours [08:00-12:00]. As it can be observed, during these time periods the load curve is over the combined curve, meaning that the total

produced power at that time period will be insufficient and additional power will be needed. This fact is associated with the combined effect of the morning peak demand that can be observed in the load profile with the relatively lower PV power production in the morning hours, compared to midday hours.

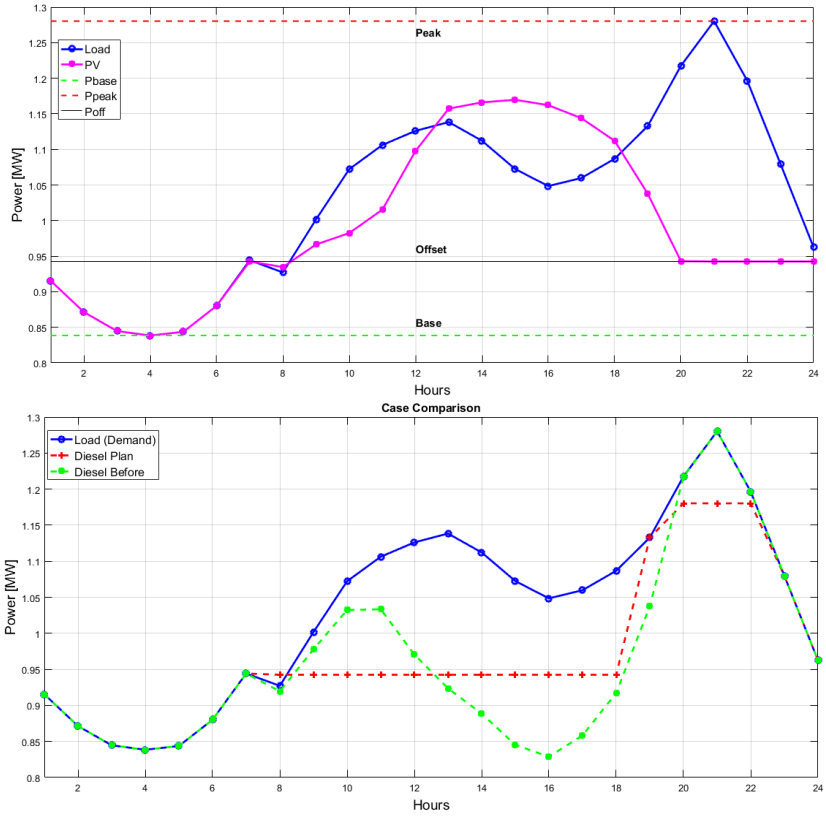

Figure 33: Algorithm output curves, for day 255

However, despite the issue of the early hours, which will be faced with additional power, the algorithm still considers the net surplus PV energy to be equal with the peak energy demand for later use and this fact is well depicted in the following figure for day 63

α)

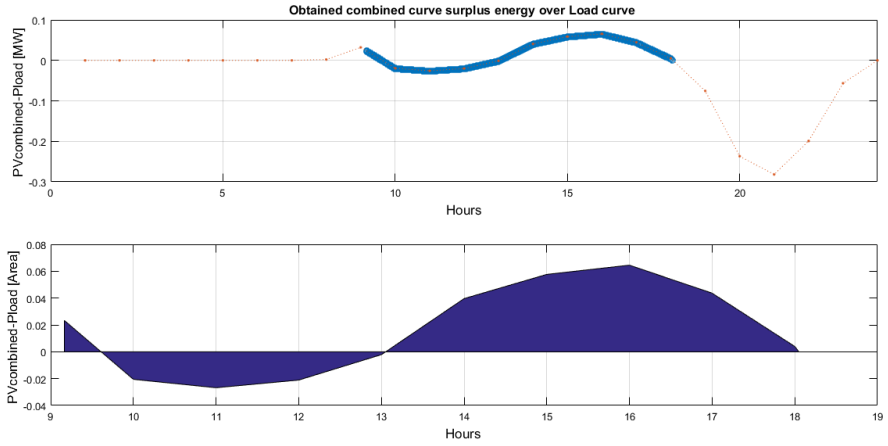

b

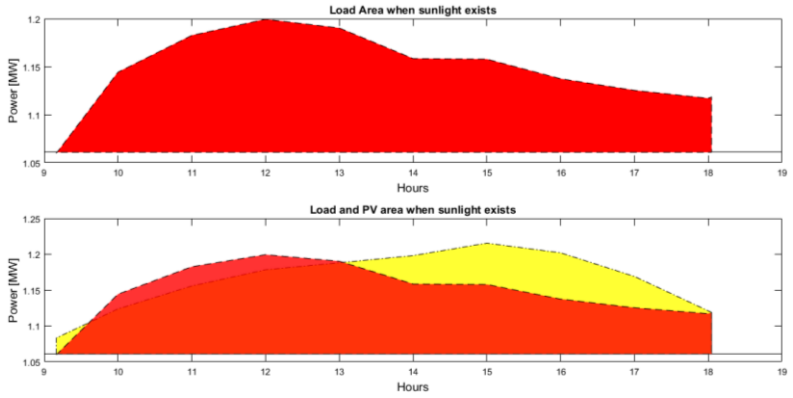

Figure 34: Day 63 net surplus energy area

As it is possible to observe in Figure 34, the load area between the load curve and the offset value, for the time period of the PV power generation, is not constantly under the corresponding area of the PV energy produced. Because of this, in Figure 34 a, the blue area which is located among the hours 09:40-13:00 is negative meaning that for this time period the total demand will be greater than the current PV power production. This is also depicted in Figure 34 b where the orange area overlaps the yellow area for the same time period. However, the situation is reversed during the time period 13:00-18:00 where the system is capable of overproduction and consequently artificial surplus energy is created. This is also illustrated from the same figure (Figure 34 b) where the yellow area is over the orange area representing the demand energy at that specific period.

Summer time period

In the section above, the operation of the developed algorithm is described for the load curve pattern which are more frequently observed during the winter time period where the peak demand is displaced at the evening hours where there is not PV power production. Though this is the case for the winter time period for the specific islandic power system under investigation, the same pattern is also observed during the summer time period for many islandic power systems. For small-scale systems in which the load is commonly shaped by the residential factor and the touristic activities, the peak demand is constantly placed at the night hours, when the majority of those activities requires energy consumption. Nevertheless, in order to observe the behavior of the algorithm during the summer time period for the power system investigated in this study, the algorithm was executed for a whole year period, including each day of the year. The results that can be found in the following figures are consistent with what was expected from the beginning, as long as the current version of the algorithm is suited for the load profiles depicted in Figure 22. The load profile which was mostly observed during the summer time period is presented in Figure 28. As it is obvious, the shape of the load curve during this day is not similar with the winter profile as a single peak area is not distinguished, especially during the night hours. This can be further explained from the dashed line which separates the peak shaving area to be calculated so that the algorithm takes the necessary actions to output the appropriate offset level as described above. Following the same logic, the algorithm resulted in the following results, depicted in the figures below.

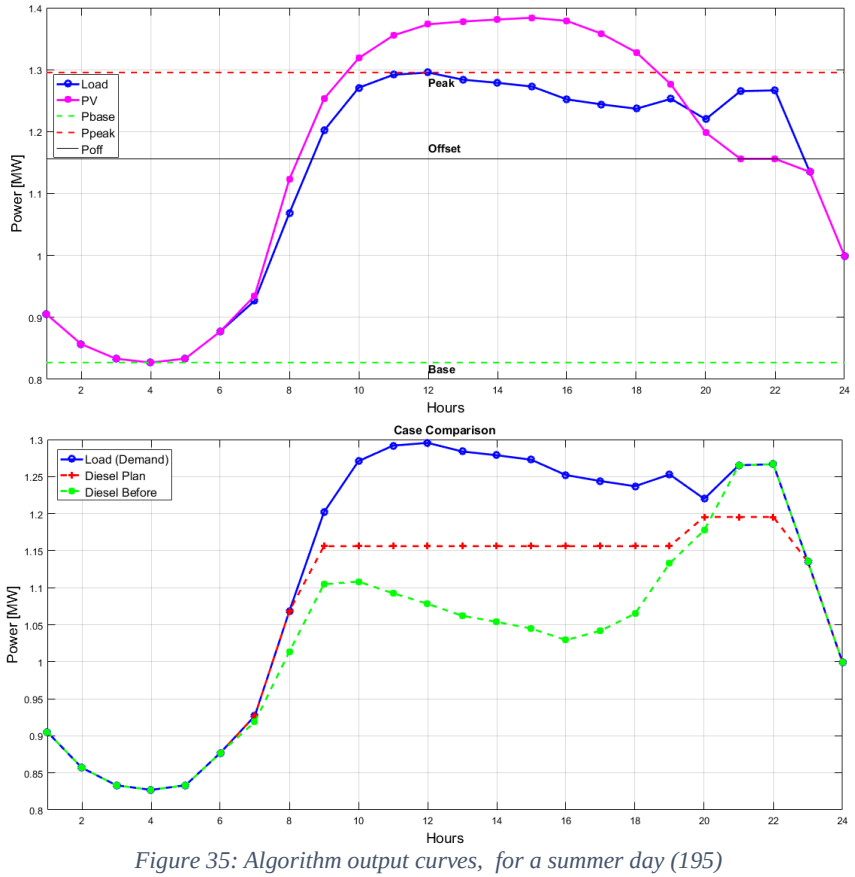

Figure 35: Algorithm output curves, for a summer day (195)

Results are presented for the middle day of the summer which is 15 July and correspond to day 195 of the year. From the figures above, it is possible to observe that the combined curve is formulated as it was described from the algorithm and based on Equation 28. Because of this, the offset value is decided to be placed in a position by which enough surplus energy will be created to cover the peak demand region. However, the peak demand includes a whole area between the hours 09:00-22:30 as it can be observed in Figure 28 and it is not deferred compared to the maximum PV power generation which is located among the hours 12:00-14:00 (Figure 35). For this reason, although the algorithm predicts the necessary offset value to store the appropriate amount of energy in the BESS for later use, the stored energy cannot be used later on the day as long as the peak is happening at the same time period with the storage time period. This fact can be also further explained from the concept of storing PV energy to be used when it is actually required, while for the summer days, the time period in which this energy is required coincides (collides) with the PV power production time period. Thus, there is no need for storing the energy and instead this energy could be used instantaneously. The only possible scenario for storing energy in a similar case could arise from the technical minimum of the diesel generators and to avoid curtailment. In this scenario, the BESS should anticipate the extra amount of energy and should inject it back to the grid during the late-night hours. Nevertheless, as it is possible to observe in Figure 35, the diesel operation can be still smoothed and the peak shaving ability of the system is preserved.

5 Modelling of the island's power system

After the development of the prediction module with the artificial neural network model and the development of the energy management algorithm that supervised the power flows of the system, the next step was to model the system configuration and its basic components, so a dynamic model of the system is created. This model should integrate the above modules and should combine the dynamic simulations with the proposed predictive strategy, as developed in the previous section. In this way, a complete framework could be simulated and the combined effects of a dynamic model and an energy management system could be investigated.

5.1 General System Configuration

The complete system configuration and the proposed methodology are depicted in the following figure.

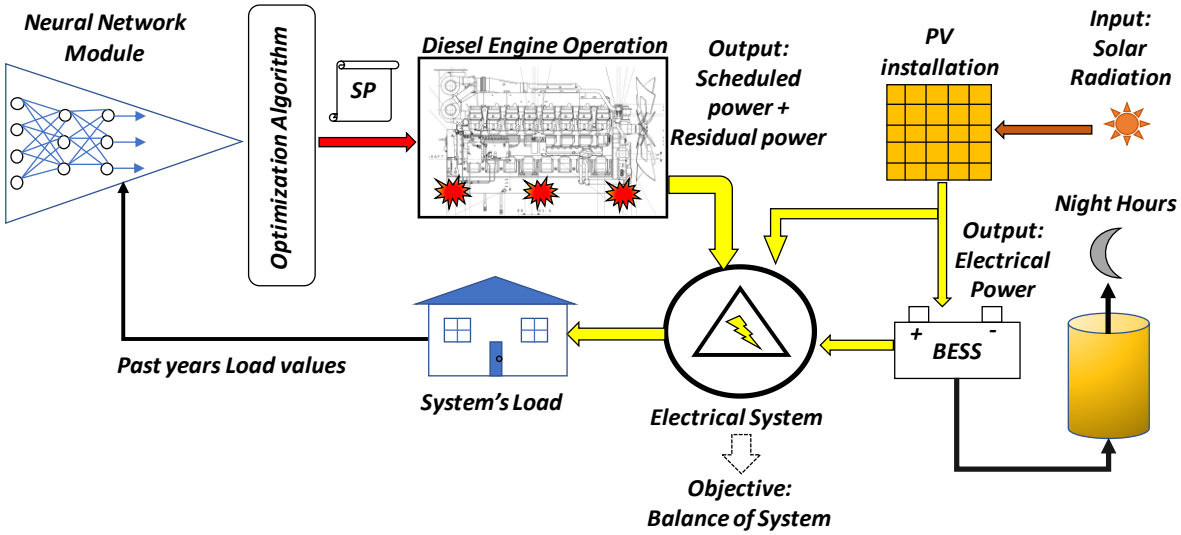

Figure 36: Islandic power system configuration and proposed methodology

From the figure above, it can be noticed that the objective of the operation of the different system components, that needs to be satisfied from the central EMS, concerns the system stability and balance. This objective constitutes the main priority of the system's operational algorithm, while in a secondary level aims for the implementation of the logic described in the previous chapter (4.1.1). The power system's balance is modelled as the congregation of the signal flows coming from the various energy system components, representing the individual power flows that have to be in an equilibrium so that the balance of the system is preserved. This can be mathematically formulated with the following expression:

$$\left| P_{residual}(t) = \sum_{i=1}^{N_p} P_{inflow,i}(t) - \sum_{i=1}^{N_c} P_{outflow,i}(t) \right| \leq \varepsilon \qquad \textit{Equation 31}$$

where in the above equation $N_p = 3$ stands for the different possible energy injections to the grid from each energy production system which are the diesel engines, the PV system and the BESS, while $N_c = 2$ stands for the different possible energy sinks which

are the system's load and the storage energy to the BESS. In the above equation, a relaxation variable is also defined as ε for the system balance, allowing for small and sudden perturbations in the balance of the system, which are associated with control actions and deviations in a very small-time scale compared to the hourly-based analysis which is implemented for the power system simulation. The balance of the system should be preserved at each time step of the simulation and in cases that this is not possible with the current configuration, the BESS should compensate for restoring the balance and if even this is not feasible, then the diesel engines should be operated appropriately, as it will be described in a later chapter. At this point we summarized the system's basic parameters in the following table.

Table 1: Technical specifications of the power system under investigation

Maximum load demand [MW]	1.5
Installed PV power [kWp]	300
Diesel engine maximum power [MW]	2
Battery maximum power injections [kW]	159
Battery capacity [Ah]	2000
Power electronic (inverter losses)	10%

In the above table, the basic characteristics of the power system under investigation depicted in Figure 36 are presented. At this point, it is important to be emphasized, that the BESS selection was based on typical values for grid scale battery applications and the primary concern was to simulate a BESS in the order of magnitude with the demands of the system. However, the BESS size was not optimized to match the system requirements in the most efficient or economically feasible way, as this is a topic for another study. Thus, the BESS module presented in our simulations was used to simulate the storage capability of the system and it was focused on the dynamic behavior modelling of similar systems, integrated into a complete operational framework. Further details about the BESS are given in a next section of this chapter. The diesel module was operated based on the setpoints acquired from the developed algorithm of the previous chapter (4.1) and at a smaller time scale, based on the real time controls of the system, to preserve the balance. The PV module was introduced to the system modelling as a timeseries of PV power generation for each day of the year under investigation (2016), considering the system losses from the power conversion and the power electronics associated with its operation. In the following section, a detail representation of the PV system modelling is presented.

5.2 Photovoltaic power production modelling

In this section, the simulation platform for generating PV energy production data is described. Regarding the purpose of this study, the PV simulation was a necessary input to the developed algorithm and had to be considered as an input in a previous step from the total system simulation. This fact can be explained by the combined curve described in 4.1.2, where the PV generation data is necessary to be superimposed to the offset level in order to evaluate the corresponding areas of interest. Thus, the solar energy data were generated before the algorithm implementation for the year under investigation (2016) and were considered as perfect forecast for the purpose of the system simulation.

This was decided for the better assessment of the quality of load forecasting, integrated into a supervisory energy management system, as it is proposed in this study.

The simulation platform used in this study to estimate the solar energy production data was based on the model developed by [51]. This simulation platform, the operation of which is described below, is comprised of an open-source code available at the website [*www.reneables.ninja.com*]. Screenshots of the website application used for the data generation of this study can be found in the following figures.

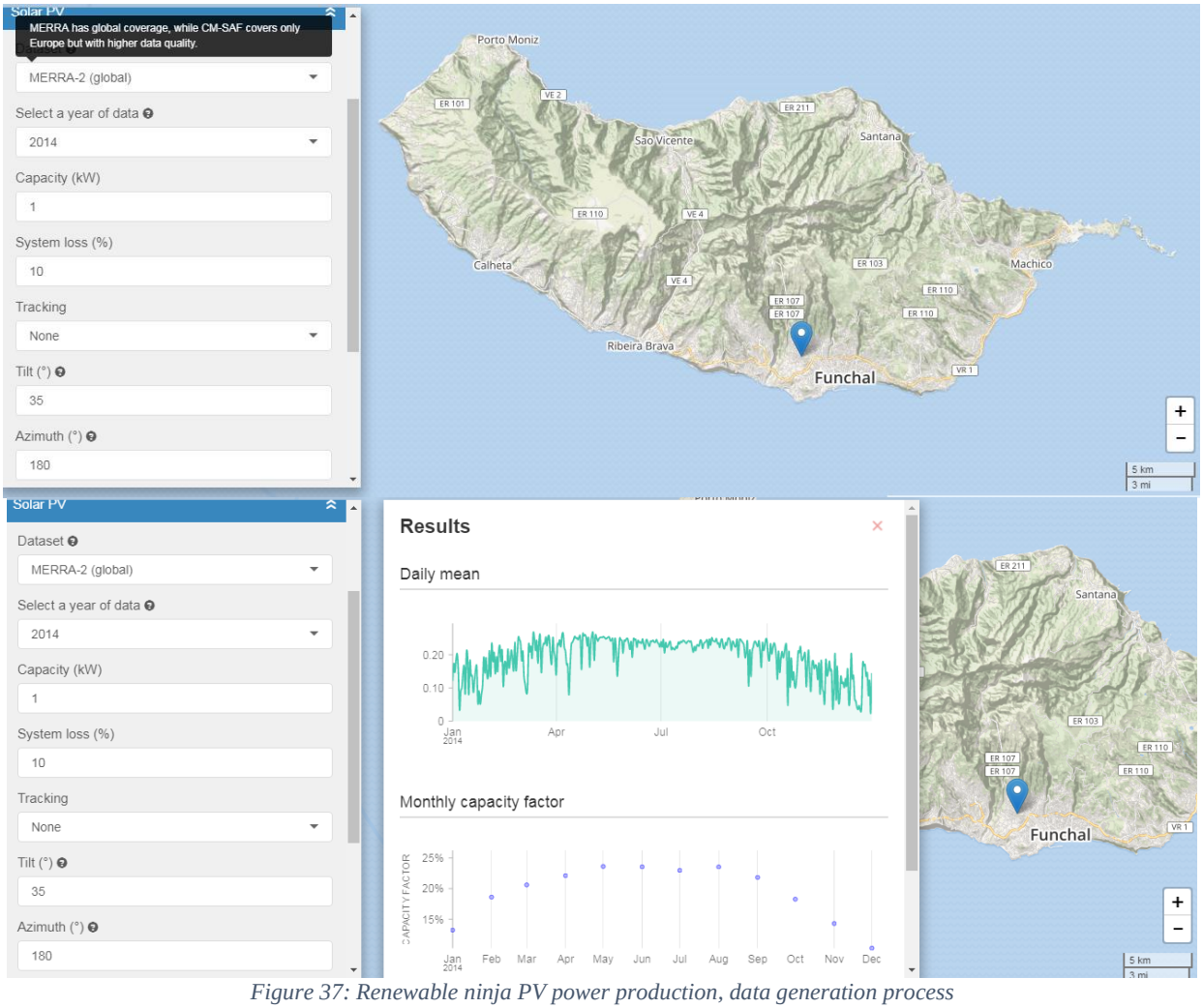

Figure 37: Renewable ninja PV power production, data generation process

From the figures above, it is possible to observe the graphical application developed from [51] for the data generation. The first step for this is the determination of the point of interest, for which data needs to be generated. As it can be observed from Figure 37, for our case, the point selected was chosen to be in a close distance from the island's capital city (Funchal). In that way, it was possible to represent the installed residential PV modules, which are mainly placed at inhabited areas, with an equivalent PV plant located at the same geographical area. At this point, it is important to be stated that the different points for which the data could be generated, were limited to the grid resolution of the simulation platform. The data generated from other intermediate points were basically extrapolated values between the calculation nodes across a specific geographical region. For this reason and taking into account the relatively short distances of the island's morphology, the point which was selected for data generation

in our study, was a representative data point for the whole island. As a next step for the data generation process, the user defined inputs were considered. From Figure 37, those inputs can be observed and are summarized for our specific case study in the following:

- Weather Dataset to be used: MERRA
- Selected year for data generation: 2016
- Installed Capacity: 300 kW
- System Loss: 10%
- Tracking capability: 2-axis tracking
- Tilt: 0°
- Azimuth: 180°

The above parameters were chosen based on the following criteria. The MERRA dataset was chosen instead of the other possible dataset SARAH, due to the better generalization effect of this dataset for worldwide located countries and not specifically for European countries. In other words, this dataset (as it is also proposed from the developers of the platform) is most favorably suited for international data generation whereas the other dataset which is more suitable for European countries. The year of the data was set as the year under investigation (2016) which was also the test year of the developed ANN model. In the figure below, the process of the PV data generation from the simulation platform is presented:

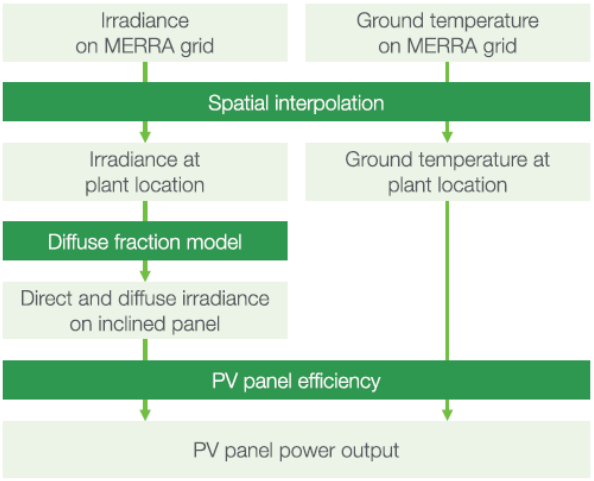

Figure 38: Overview of the approach used to model PV power output [51]

Based on the configuration depicted in the figure above, the following methodology was adopted for calculating the PV output.

The installed capacity was approximately equal to the total installed capacity of the island (Astypalaia) considering that the panels have a tilt angle of zero and an azimuth angle of 180. The tilt angle corresponds to a horizontal plane solar panel, meaning that the panels is placed on a horizontal rooftop for example. The azimuth angle was chosen appropriately (180°) in order to correspond to a southward facing direction. Then, with those inputs, the simulator is capable of producing a timeseries of PV energy production data, based on the basic modelling equations presented below. At this point, it is important to give the following definitions

- Direct Normal Irradiation (DNI): It is the amount of solar radiation received per unit area by a surface that is always held perpendicular (normal) to the rays that come in a straight line from the direction of the sun at its current position in the sky
- Diffuse Horizontal Irradiation (DHI): It is the amount of radiation received per unit area by a surface (not subject to any shade or shadow) that does not arrive on a direct path from the sun but has been scattered by molecules and particles in the atmosphere and comes equally from all directions.

During the PV output calculation, the simulator is provided with both direct and global irradiance, from the corresponding MERRA dataset and then the irradiance on the plane of the PV panel can be estimated. In case of a fixed azimuth angle and tilt angle, the plane incidence angle is given by

$$a = \cos^{-1}(\sin(h) \cdot \cos(t) + \cos(h) \cdot \sin(t) + \cos(a_p - a_s)) \quad \textit{Equation 32}$$

where h is the sun altitude, α_p is the panel azimuth, t is the panel tilt and α_s is the sun azimuth angle. Then, the direct and diffuse plane irradiance can be computed from the global irradiance as follows

$$I_{dir,p} = \frac{I_{dir,h} \cdot \cos(a)}{\cos(\frac{\pi}{2} - a_s)} \quad \textit{Equation 33}$$

$$I_{dif,p} = I_{dif,h} \frac{1 + \cos(t)}{2} + a(I_{dir,h} + I_{dif,h}) \cdot \frac{1 - \cos(t)}{2} \quad \textit{Equation 34}$$

where α is the surface albedo (set equal to 0.3). The model can also simulate tracking systems with single or two axes of rotation, as it was the case selected for our simulations. Finally, the power output from a given panel could be calculated from the in-plane irradiance determined in the previous step. This could be done with the following set of equations [52]

$$P_{PV}(I_p, T_{mod}) = P_{PV,STC} \cdot \frac{I_p}{I_{p,STC}} \cdot \eta_{rel}(I_p', T') \quad \textit{Equation 35}$$

$$\eta_{rel}(I_p', T') = 1 + k_1 \ln I_p' + k_2 (\ln I_p')^2 + T'(k_3 + k_4 \ln I_p' + k_5 (\ln I_p')^2) + k_6 T'^2 \quad \textit{Equation 36}$$

where $P_{PV,STC}$ is the power at standard test conditions (STC) of $I_{P,STC}$=1000 *W/m2*, and $T_{mod,stc}$=25°C, η_{rel} is the instantaneous efficiency while I_p' and T' are normalized parameters to STC values $I_p' = \frac{I_p}{I_{p,STC}}$ and $T' = T_{mod} - T_{mod,STC}$. The coefficients k_1-k_6 are estimated from a fitting model based on experimental data measured at many different sites. The instantaneous relative efficiency depends on the instantaneous irradiance and module temperature T_{mod}. Under slowly changing conditions, the module temperature can be estimated from the ambient temperature and the irradiation in the following way:

$$T_{mod} = T_{amb} + c_T I_p \qquad \textit{Equation 37}$$

The coefficient c_T describes how much the PV module is heated by the solar radiation

The system loss coefficient was considered at around 10%. Additional losses are caused by the PV system's components, primarily the inverter (which converts a panel's DC output into AC power for on-site use or exporting to the power grid), and these are estimated with an additional static loss. In addition to temperature data, the DTI data contain DC and AC output. They therefore allow estimating inverter efficiencies. The mean efficiency across all sites is 0.90, with a standard deviation of 0.04. This suggests a reasonable assumption for inverter losses is 10%, which is used for all simulation results presented here. This is a conservative assumption since the systems in the DTI dataset are about 15 years old, and newer inverters may perform better [51]. In the following figure, the simulator input irradiance (orange time series) and the output PV energy (yellow time series) are depicted

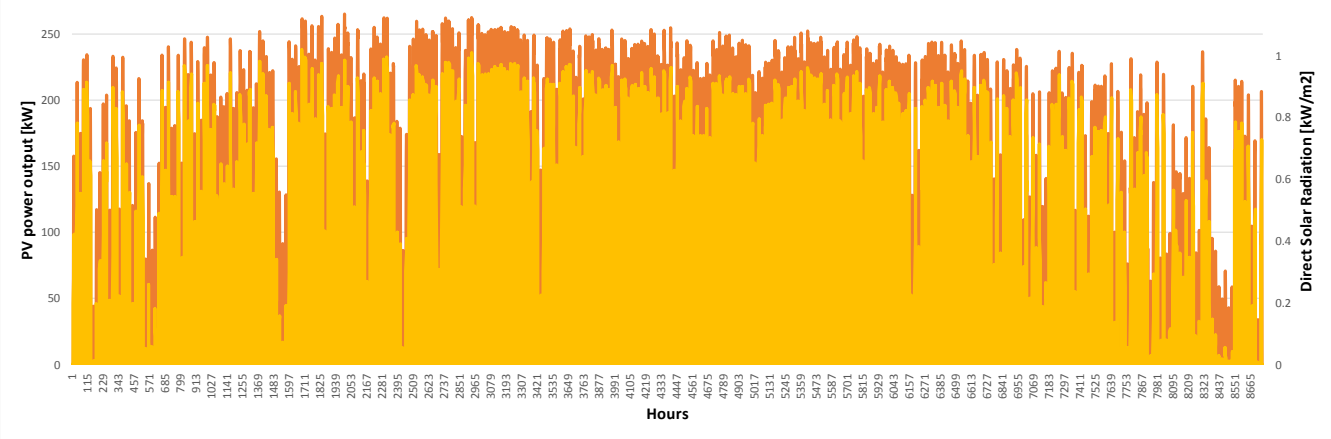

Figure 39: Solar irradiation and PV power production data, for the year 2016

As it is possible to observe in the figure above, the yellow data series has a direct correlation with the orange data series in an almost linear way, which is also validated from Equation 35. It is also clear that during the summer time period, the PV output energy is maximized compared to the winter time periods, which are characterized from lower mean values and some days of partial or complete cloud covering. This clouding factor effect can be noticed from the sudden drops of the irradiance level, which is most of the time accompanied by a drop in the PV energy output. For greater detail and to illustrate the variation of the PV output for a single day, the next figure is presented.

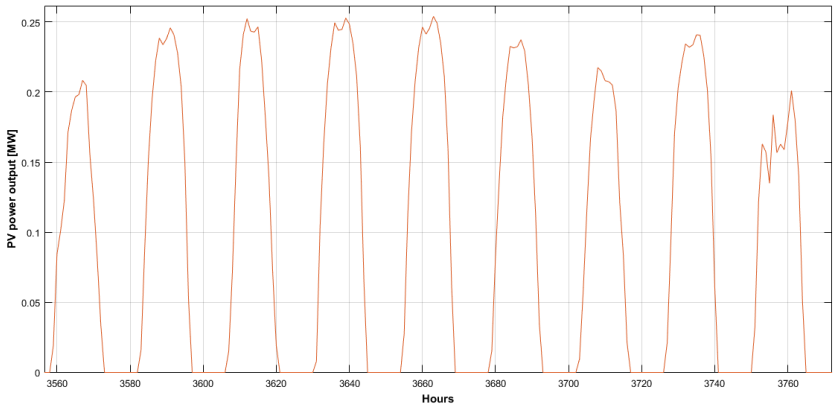

Figure 40: Typical week PV power output

As it can be noticed in the figure above, the solar energy is maximized during the midday hours of each day, while sudden and small-time scale effect such as a sudden cloud motion covering the panels may affect the smoothness of the PV energy production pattern. However, this fact comes in agreement with the more realistic point of view of this thesis, as these solar data are generated based on experimental data measurements, model calibration and data assimilation. The battery module component is discussed in detail in the following section.

5.3 Battery Energy Storage Modelling

In this section, the battery modelling of the battery energy system is described. The battery model was based on the modelling methodology of the Lithium battery module of Apros simulation software and are described in the next section. Apros simulation platform, is a dynamic process simulation software developed by VTT Fortum, which is based on built in modules, representing different areas subsystems, ranging from chemical and thermal systems to electrical ones. This allows for integrated multi-domain analysis and simulation while at the same time, control and automation systems can be integrated to the physical models. In this way, it is possible to simulate complete system models in a more realistic approach, estimate the dynamic performance of the system and evaluate different operating scenarios and centralized management algorithms. In the following section, the battery electrical model with the corresponding parameters, adopted in our study are presented.

5.3.1 Electrical model of the battery system

The lithium battery is a module type for the simulation of one-phase DC energy storage and DC energy injection. There are two operational modes associated with this module, charging and discharging. The battery module, is actually a DC voltage source modeled with a current source, a variable internal resistance network and an energy charging level indicator (counter). The battery is discharged or charged according to i) the voltage level of electrical node that connects battery with the rest of the system and ii) the remaining capacity (amount of stored energy) of the battery. If the capacity of the battery is greater than zero (>0) and the voltage of the connection node of the battery is below the open circuit voltage of the battery, the battery is discharged (it produces electricity). If the capacity of the battery is less than the maximum capacity and the voltage of the connection node of the battery is above the open circuit voltage of the battery, the battery is charged (it consumes electricity). The internal resistance of the

battery is calculated according to the input properties of the component and the current is adjusted to get the correct open circuit voltage. The basic modelling equations of the Lithium battery module are described below. The single cell circuit model depicted in Figure 41 is translated into the following differential equation for the node voltage as a function of time:

$$U(t) = V_{OC} - R_{series} + R_{cycle} \cdot I - \left(I - C_{transient}\frac{dU_{ts}}{dt}\right) \cdot R_{tr_{sh}} - \left(I - C_{transient,long}\frac{dU_{tl}}{dt}\right) \cdot R_{tr\_ln} + \Delta E(T) \quad \textit{Equation 38}$$

In the following figure the internal resistance network of the battery model is presented.

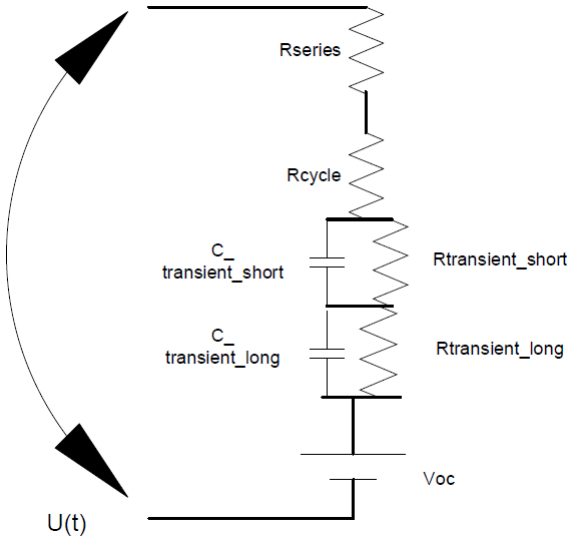

Figure 41: Battery's equivalent resistance circuit diagram

Regarding the possibility to combine many battery cells in series and in parallel connection in order to obtain battery cell arrays for higher capacitance and power levels, the corresponding current values are given by

$$I_p = \frac{m-1}{m} I \quad \textit{Equation 39}$$

$$I_{cell} = I - I_p \quad \textit{Equation 40}$$

The variables above are also depicted in the following multi-cell diagram of the battery

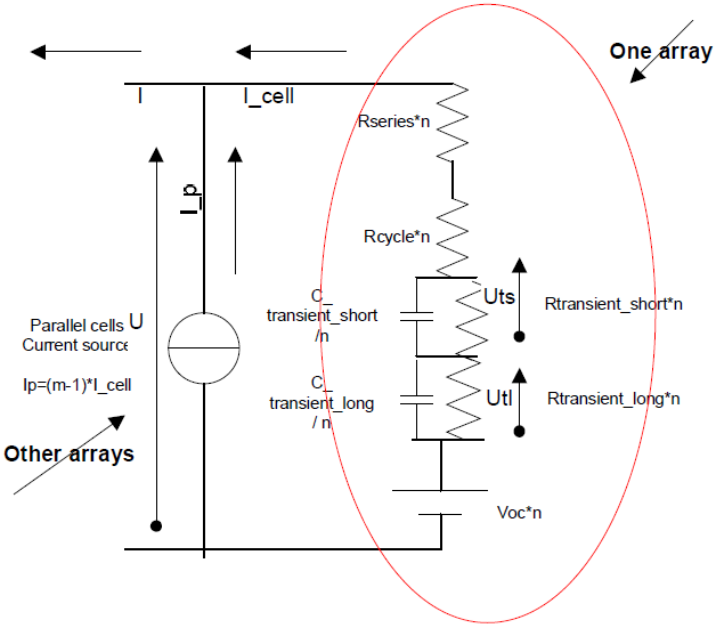

Figure 42: Multi cell equivalent circuit diagram, of the battery module

Regarding the variables from the previous equations, the following are clarified

U_{ts}: refers to the voltage over the transient short resistance

U_{tl}: refers to the voltage over the transient long resistance

n: refers to the number of cells in series (n=199 in this study)

m: refers to the number of cells in parallel (stack size is n x m) (m=169 in this study)

In order to simplify Equation 38 for numerical stability reasons in Apros simulation platform, the following equation is adopted instead

$$U(t) = V_{OC} \cdot n - \frac{n}{m}\left(R_{series} + R_{cycle} + R_{tr\_sh} + R_{tr\_ln}\right) \cdot I + n \cdot \Delta E(T) \qquad \textit{Equation 41}$$

In the above equation, R_{series} is responsible for the instantaneous voltage drop in battery terminal voltage. The other component of series resistor, R_{cycle}, is used to explain the increase in the battery resistance with cycling. The components R_{tr_sh} and R_{tr_ln} of the battery RC network are responsible for short and long-time transients in battery internal impedance respectively [53]. The term $\Delta E(T)$ is related with the battery temperature and its effect on voltage and is estimated from experimental data based on the following plot

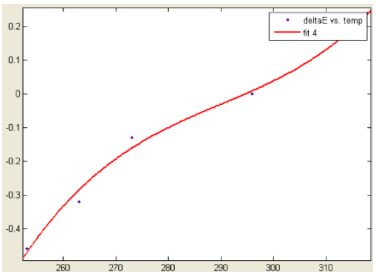

Figure 43: Battery's dependence over temperature difference, ΔE(T)

In the figure above, the blue dots represent the experimental data values and the red line presented below corresponds to the fitter model, which is then used in Equation 41.

$$\Delta E(T) = 3.938 \cdot e^{-6T^3} - 0.003426 \cdot T^2 + T - 97.96 \quad \textit{Equation 42}$$

Regarding the open circuit voltage and the resistance of the battery's network model, the state of charge of the battery (SoC) needs to be calculated. The battery SOC can be expressed as

$$SOC = SOC_{init} - \int (i_{bat}/C_{usable})dt \quad \textit{Equation 43}$$

The SOC can consequently be calculated by dividing the current capacity of the battery with the maximum capacity s follows

$$SOC = \frac{C}{C_{max}} \quad \textit{Equation 44}$$

Then, the open circuit voltage of a single cell can be calculated. The open circuit voltage and the internal resistances of the battery network model, depend on the state of charge, the battery temperature and user-given coefficients, as it is described from the following set of equations

$$V_{OC}(SOC) = voc_1 \cdot e^{voc_2 SOC} + voc_3 + voc_4 \cdot SOC + voc_5.SOC^2 + voc_6.SOC^3 + \Delta E(T) \quad \textit{Equation 45}$$

$$R_{series} = R_{s1} e^{R_{s2} SOC} + R_{s3} \quad \textit{Equation 46}$$

$$R_{series\_n} = n \cdot R_{series} \quad \textit{Equation 47}$$

$$R_{tr\_sh} = R_{ts1} e^{R_{ts2} SOC} + R_{ts3} \quad \textit{Equation 48}$$

$$R_{tr\_sh\_n} = n \cdot R_{tr\_sh} \quad \textit{Equation 49}$$

$$R_{tr\_ln} = R_{tl1} e^{R_{tl2} SOC} + R_{tl3} \quad \textit{Equation 50}$$

$$R_{tr\_ln\_n} = n \cdot R_{tr\_ln} \quad \textit{Equation 51}$$

where in the above equations *sh* stands for *short* and *ln* stands for *long*. The cyclic resistance depends on the number of full cycles (N_{eqv}) and is given from the following equations

$$R_{cycle} = k_3 \cdot \sqrt{N_{eqv}} \quad \textit{Equation 52}$$

$$R_{cycle\_n} = n \cdot R_{cycle} \quad \textit{Equation 53}$$

The capacity of the battery is updated after each time step according to the current flowing from or to the battery as

$$C(t) = C(t - \Delta t) - I \cdot \frac{\Delta t}{3600} \qquad \textit{Equation 54}$$

where Δt is the simulation step in seconds. At this point it is important to be stated that in order to simulate the dynamic behavior of the BESS in detail, taking into account the small-time scales of the transient electrical physical phenomena, the simulation step was decided to be much smaller compared to the hourly based time scale of the power variables of the grid under investigation. For this reason, a linear approximation was considered for the intra-hourly values for the concerned variables of the simulation. The chosen time step was Δt=0.2 s and the coefficient 3600 was used in Equation 54 for unit conversion as long as the unit of time is seconds and the unit of the capacity is ampere-hours (Ah).

The capacity of the battery was limited between the values 0 and the maximum capacity which is set as an initial parameter. This fact is in line with the current trends of the batteries industry, which is constantly upgrading the materials, the structure and the quality of the produced batteries. This results in an overall efficiency upgrade and allows for the development of deep charge/discharge batteries, maximizing its useful capacity and consequently the capabilities of a BESS. In order to better simulate the degradation of the battery's material and its ability for energy storage, a capacity fade model was integrated into the battery model of this study. Capacity fading refers to the irreversible loss in the usable capacity of a battery due to time, temperature and cycle number. Generally, a battery is considered to be usable until reaching the 80% of its initial capacity [54, 55]. So that, modeling the capacity fading is important for predicting the remaining life of the battery. The irreversible loss causing capacity fading is associated with degradation of the battery, and the loss occurs whether the battery is inactive (so-called "calendar life" losses) or exercised ("cycle life" losses) [56]. Both calendar and cycle life losses of a battery appear to be linear with time and dramatically increase with increasing temperature [55]. Therefore, the effect of temperature must be considered while modeling the capacity fading for a battery. The calendar and cycle life losses lead to a capacity correction factor to determine the remaining usable battery capacity. Thus, the capacity fading was modelled considering the correlation between the battery temperature and capacity. In this way, the maximum capacity of the battery was calculated as a fraction of the nominal capacity considering both calendar and charging losses, based on the following equations

$$C_{max} = C_{nom} \cdot CCF \qquad \textit{Equation 55}$$

$$CCF = 1 - (f_{sl} + f_{cl}) \qquad \textit{Equation 56}$$

where *CCF* is the capacity correction factor and represents the aging of the battery, f_{sl} is the lifetime storage loss fraction and f_{cl} is the lifetime cycle loss fraction. The loss fractions are integrated over the simulated time period and in this way the integral of the storage loss fraction is calculated as

$$f_{sl} = \int sl_1 \cdot e^{\frac{sl_2}{RT}} \cdot \frac{dt}{100 \cdot 2592000} \qquad \textit{Equation 57}$$

The parameter R is the gas constant (8314 J/kmolK) and the coefficient 3592000 is used for time unit conversion from months to seconds. The lifetime storage loss fraction is updated according to the formula

$$f_{sl}(t) = f_{sl}(t - \Delta t) + \ sl_1 \cdot e^{\frac{sl_2}{RT}} \cdot \frac{dt}{100 \cdot 2592000} \qquad \textit{Equation 58}$$

The losses per cycle can be then represented according to

$$\frac{\partial SOC_{cycle}}{\partial N_{eqv}} = k_1 N_{eqv} + k_2 \overset{\frac{\partial}{\partial t}}{\Rightarrow} \frac{\partial SOC_{cycle}}{\partial t} = (k_1 N_{eqv} + k_2) \frac{\partial N_{eqv}}{\partial t} \qquad \textit{Equation 59}$$

Where in the previous equation k_1 and k_2 are constants and the equivalent number of full cycles, integrated over the simulated time period can be calculated based on the following equation

$$N_{eqv} = \int \frac{\frac{1}{2}|I_{bat}|}{3600 \cdot C_{max}} dt \qquad \textit{Equation 60}$$

Then, the number of full cycles can be updated according to the next formula

$$N_{eqv}(t) = N_{eqv}(t - \Delta t) + \frac{\frac{1}{2}|I_{bat}|}{3600 \cdot C_{max}} \qquad \textit{Equation 61}$$

Next, the lifetime cycle loss fraction can be updated with the formula

$$f_{cl}(t) = f_{cl}(t - \Delta t) + \left[N_{eqv}(t) + k_2 \left(N_{eqv}(t) - N_{eqv}(t - \Delta t)\right)\right] \qquad \textit{Equation 62}$$

The coefficients k_1, k_2, k_3 in the above equations, depend on the temperature of the battery and further detail can be found in [52]. Summarizing the above, the battery modelling in Apros software is based on the equivalent electrical network and is described from equations [41-61]. In the next section, the control configuration of the BESS is presented.

5.3.2 Control configuration of the BESS

For the implementation of a complete simulation framework based on forecasting capability, as it is proposed in this study, a top to bottom approach should be followed for the development of the management algorithm responsible for controlling the power system operation. In the previous sections the supervisory algorithm was developed (4.1) that was responsible for the generation of the operational planning of the diesel engines, regarding the next day. This was achieved by the developed network, taking into account the predictions of the demand values of the next day. (3.3.4). The diesel engines operation planning was achieved by the developed algorithm. In that way, the next day's setpoint planning was estimated, in order to achieve the peak shaving and the load curve smoothing. This planned diesel setpoint information was directly related

with the operation of the battery, which should track a planned power delivery trajectory, which was also derived from the algorithm.

From the above it is evident that the operation of the BESS was predefined based on the prediction module and the algorithm. However, the planned trajectory could not be implemented in the real dynamic operation of the power system for the following reasons. At first, the power system's demand values were slightly different from the forecasted demand values which can be attributed to the neural network errors. Despite the overall good quality of the network prediction, which resulted in a satisfactory mean absolute percentage error (MAPE=1.715%) for the year of the simulation (2016), when focusing on specific load values, the error could be higher relatively to the overall system performance. Thus, during the dynamic simulation of the power system with a fine time resolution, the instantaneous errors of the forecasting module could result in significant deviations from the expected values and consequently the balance of the system could be risked. Another source of error regarding the dynamic simulation of the power system with the integration of the supervisory algorithm comes from the current state of the battery system. As long as the detailed BESS model described in the previous section (5.3.1) was not considered from the algorithm that generated the setpoint values, it was not possible to estimate the different possible states of the battery during the setpoint calculation. The variables that have the most direct and significant impact on the state of the battery are the current capacity C, the state of charge (SOC) and the maximum possible current injection. The last limitation comes from the maximum possible power delivery from the battery. Another important factor that could not be estimated before the dynamic simulation was the aging impact and the degradation of the battery's maximum capacity.

For the reasons described above, it is clear that in order to preserve the system balance and to track in the best possible way the predefined system operation, a real time control system should be employed. This would basically monitor the system for sudden changes and consider the appropriate actions to be made for restoring the balance. In the following figure, it is possible to observe the control system configuration adopted in this study.

In the figure below, a schematic representation of the real time charge / discharge controller of the BESS is presented. As it can be noticed, a cascade configuration was introduced, which was based on simpler proportional-integral single input single output controllers. This setup was adopted based on the simplicity of its structure and the commonly available PI controllers in industry. From Figure 44 it is possible to observe that there are two different controllers, one for the charging process control and another for the discharge process control. Both of them acquire their setpoints based on the output of a centralized controller which is responsible for regulating the system residual. The power system residual can be found in Equation 31 and is basically an indicator of the excess or shortage of energy in the power system. Thus, the setpoint of this controller was set to zero (0) so that the error is regulated and the balance of the system is preserved.

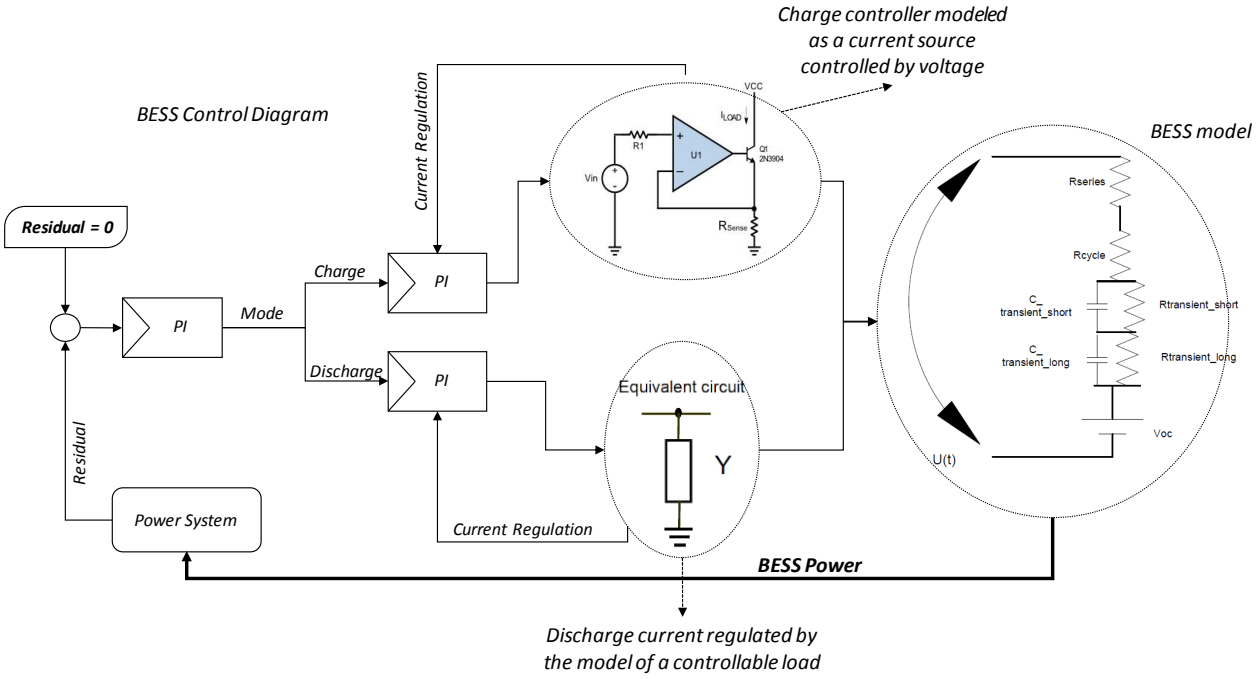

Figure 44: BESS control system configuration

Then, the central controller fed its output to the other controllers which were devoted to the current regulation of the battery. Specifically, the discharge process was modeled with a controllable load whose equivalent circuit is depicted in Figure 44. In this way, the discharge current injected from the battery to the grid was regulated by changing the value of the internal resistance of the controllable load and consequently, the appropriate amount of power was injected into the grid. Regarding the charging mode, the power that was stored inside the battery was controlled by regulating the charging current with the help of a voltage controlled current source. In this way, a DC controllable source model was used for the current regulation task during charging. The corresponding equivalent circuit of the adopted DC source model, is depicted in Figure 44. This is basically a circuit composed of an ideal voltage source, a resistor, an operational amplifier and a MOSFET power electronic module, operated as a linear regulator.

At this point we present the basic equation describing the action of a PI controller, as a transfer function (filter) and as it was numerically calculated in each time step of the simulation in Apros software.

$$PI(s) = \frac{k_p s + k_I}{s} \qquad \textit{Equation 63}$$

$$CO(t) = k_c \cdot e(t) + \frac{k_c}{T_i}\int e(t)dt \overset{Discrete}{\Longrightarrow}$$

$$CO(k) = K \cdot scale \cdot e(k) + CO(k-1) + \frac{K \cdot scale \cdot \Delta t}{T_i} \cdot \left(\frac{e(k) - e(k-1)}{2}\right) \qquad \textit{Equation 64}$$

From the above equations we have the following:

- CO(k): Controller Output signal at time step *k*
- e(k): controller error at current time step *k*, defined as SP-MV, where SP is the setpoint value and MV is the measured variable
- k_c: the controller gain
- K: discrete controller gain
- k_p: the proportional gain
- k_I: the integral gain
- T_i: the reset time [s]
- Δt : simulation time step [s]

The controller gain is related with the integral parameters as follows

$$k_I = \frac{k_c}{T_i}$$ *Equation 65*

The scaling factor that is used during the controller calculation in Apros, is defined as

$$scale = \frac{Max\ CO - Min\ CO}{Max\ MV - Min\ MV}$$ *Equation 66*

The parameters that were used for the simulation of this study were calibrated based on the trial and error method, conducting experiments and observing the response of the system. The parameters with which the best response was achieved are presented in the following table.

Table 2: Controller parameters

Controller	*Operation*	*Gain*	*Time const.*	*Max. meas.*	*Min meas.*	*Max output*	*Min output*
Residual	Direct	1	1	1000	-100	1000	0
Charge	Direct	1	10	100000	0	900	750
Discharge	Direct	1	1	1000000	0	1000000	0

For better understanding of the table above, the following are clarified. The direct operation of the controllers means that they produce a proportional output based on the input, with the same direction. Thus, for greater error values, greater output is produced. The time constant is counted in *seconds* time units. The output value of the charge controller corresponds to *Voltage* units, the output of the discharge controller corresponds to *Watts* and the output of the residual controller to *kiloWatts*. The residual controller was configured with a negative minimum measurement limit, to account for possible negative residual energy measurements, while the other controllers' measurements limits, based on their physical representation, lied in the positive range. The achieved response plots are presented in the following figures.

The achieved response plots are presented in the following figures.

Figure 45: System's response after the control system implementation

From the figures above, it is possible to observe that the controllers are capable of quick balance restoration with a relatively short response time and low overshoot. Specifically, the SOC and the residual power are simultaneously plotted and the transition from charging to discharging states of the BESS and vice versa is remarked. Also, a detailed view is presented, from which it is possible to observe the system behavior after a discharge command.

In the following chapter, the system modelled in Apros software and simulation results are presented.

6 Power system model dynamic simulations

In this chapter, the dynamic simulation of the model described above integrated with the predictive BESS controller is presented. The input parameters that were considered for the dynamic model development in Apros software, were based on the modelling equations of the previous chapter, the forecasted power demand output from the neural network module and the diesel engine predicted setpoint trajectory. Then, the corresponding dynamic equations were solved and the dynamic behavior of the system was observed. As it will be discussed in detail in the following section, the simulations indicated that the initial goals set at the beginning, namely peak shaving and smoothing of the system load curve, could be achieved.

6.1 Apros model description

The model of the power system that was described in a previous chapter was implemented in Apros simulation platform considering the following modelling guidelines. Thus, for a dynamic simulation, the selection of suitable control structures is essential in order to accurately describe the behavior of smart power grids during transients. The automation components, explained below [57], include measuring devices, analogue and binary modules, signal sources and controllers. For the better understanding of the developed Apros model, the modules used are identified and discussed in detail in the following section.

6.1.1 Apros modules description

Measuring devices

Measuring devices collect data on the physical properties and transmit them in analogue signals. The output signal of a measuring device can be used as an input signal for a control structure or for other purposes such as operation monitoring or data recording. The most significant variables that can be measured during the simulation of a power grid, include the current and voltage magnitudes, the state of charge of a battery and other related variables. Those devices maybe depicted in Figure 48.

Analogue modules

Analogue modules are used to modify analogue signals. In these modules, the output signal is always analogue, but in addition to the analogue input signal, a binary signal may be found for controlling tasks. The analogue modules can be divided in three groups, namely basic, static and dynamic modules. These are explained in detail in the following sections.

- *Static modules*

Analogue static modules include delay, memory, switch, deadband, hysteresis, limiter, Max and Min selector, polyline and square root. Some of the static modules such as deadband and limiter are a source of discontinuity, which in return may result in numerical instability of the simulation. However, those were suitably used in our simulations as it was necessary for the logic implementation of the energy management system. The basic analogue modules used in our simulation are presented below:

- *Basic analogue modules*

Analog basic modules are adder, multiplier, divider, mean value, setpoint and signal splitter. The adder module is applied to add or subtract the signals $y_{in,1} \pm y_{in,2} \pm \ldots \pm y_{in,i}$. The multiplier module can be used for a multiplication of analogue signals as $y_{in,1} * y_{in,2} * \ldots * y_{in,i}$. An amplifier is a special case of the multiplier module and used to amplify the input signal y_{in} by a factor of KP. The result is $y_{out}=k_p * y_{in}$. The term "setpoint" refers to the target value of a variable. The set-point module may have two operation modes (normal and tracking). In normal operation, the output signal is constant. For example, the control system of the power system, aims for maintaining a constant setpoint of zero residual energy, so that the balance is preserved, while the charge and discharge slave controllers are constantly tracking the setpoint that the upper controller imposes.

- *Analogue Switch module*

The switch module can be considered as a selector between two analogue signals. It has two analogue input signals, a binary input signal and an analogue output signal. The output signal follows the first input signal, if the binary input is TRUE and follows the second input signal, if the binary input is FALSE. This can be described mathematically with the help of the following equation:

$$y_{out} = \begin{cases} y_{in,1}, & for \;\; y_{bin} = 0 \\ y_{in,2}, & for \;\; y_{bin} = 1 \end{cases} \qquad \textit{Equation 66}$$

- *Analog limiter module*

A limiter limits the signal $y_{in,1}$ within a predefined range using a high limit value L_{high} and a low limit value L_{low}. If the value of the input signal is between the given limits, the value of the output signal follows the value of the input signal. These can be expressed as:

$$y_{out} = \begin{cases} y_{in,1} & for\; L_{low} \le y_{in,1} \le L_{low} \\ L_{low} & for\; y_{in,1} < L_{low} \\ L_{high} & for\; y_{in,1} > L_{high} \end{cases} \qquad \textit{Equation 67}$$

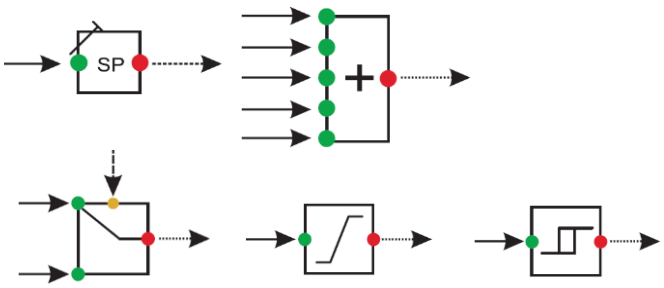

Figure 46: Apros analogue modules

Binary modules

Binary modules (Boolean logic elements) are required for selection purposes in many control circuits. In such modules, the input can be binary or / and analogue signals, while the output is always binary. Therefore, when an expression is evaluated by binary

modules, the output signal is ether zero or unity (zero means FALSE and unity means TRUE). The most relevant binary modules used in the dynamic simulation of a power grid are explained below.

- *Basic binary modules*

In the following figure, the basic binary modules (AND, OR and NOT) are depicted. The logical operator "AND" is applied in order to perform a logical operation AND for binary signals. The output signal is TRUE, when all input signals are in TRUE state. If one of the input signals is in FALSE state, the output signal is FALSE. This can be described from the following equation:

$$y_{out} = \begin{cases} 0, & for \;\; y_{in,1} = 0 \; or \; y_{in,2} = 0 \\ 1, & for \;\; y_{in,1} = 1 \; and \; y_{in,2} = 1 \end{cases} \quad \textit{Equation 68}$$

Using the logical operator "NOT", the state of the binary input signal can be inverted. It has only one input signal and one output signal and is operated based on the equation

$$y_{out} = \begin{cases} 0, & for \;\; y_{in} = 1 \\ 1, & for \;\; y_{in} = 0 \end{cases} \quad \textit{Equation 69}$$

- *Binary switch module*

The switch module is a selector between two binary signals. It has two input binary signals, an output binary signal and an input binary control signal. The state of the output signal follows the state of either of the two input signals depending on the control signal and can be mathematically expressed as

$$y_{out} = \begin{cases} y_{in,1}, & for \;\; y_{con} = 1 \\ y_{in,2}, & for \;\; y_{con} = 0 \end{cases} \quad \textit{Equation 70}$$

- *Limit value checker module*

The limit value checker compares the analogue input value to a given limit value LV, resulting in the following output signal:

- FALSE, if the value of the analogue input signal is greater than the given limit value
- TRUE, if the value of the analogue input signal is smaller than the given limit value.

This relation can be expressed mathematically using the following equation:

$$y_{out} = \begin{cases} 0, & for \;\; y_{in} \geq LV \\ 1, & for \;\; y_{in} < LV \end{cases} \quad \textit{Equation 71}$$

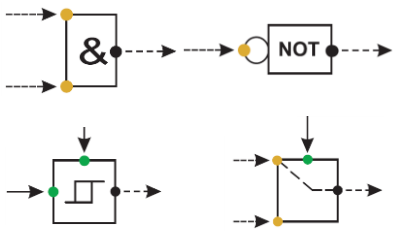

Figure 47: Apros binary modules

Electrical node, switch, load and source

The main function of the electrical node is to connect the electrical modules to each other. The switch is located between two electrical nodes of the electrical circuit. The order of nodes is insignificant, but they have to be same type, either DC or AC nodes. The switch is controlled by a logical input. If the input signal is in TRUE state, the switch is closed. In this case, the switch is a kind of a transparent module type, i.e. the electrical nodes on both sides of the switch have the same voltage. If the input signal is in FALSE state, the switch is open and there is no connection through this module to another node. In addition to the above modules, the DC source module was also used to model the connection of the BESS to the power system. This is actually a voltage controlled current source where the voltage setpoint can be set. In this way and considering the internal resistance of the source, the circuit current is calculated. This current is the same that is responsible for charging the battery system. Thus, for adjusting the amount of power that will be stored into the battery, the voltage of the DC source was controlled which in turn regulated the current injected into the battery. The reverse process was followed for the battery discharge where the connected load to the node of the battery, (as depicted in Figure 48) was controlled by changing the active load setpoint, which in turn affected the resistance of the load and finally the current drawn from the battery. In this way, the discharge power could be controlled with the Apros modules presented in Figure 48. The relation between the active load value and the resistance is given in the following equation

$$Y_L = \frac{1}{R_L} = \frac{P_L}{V_L^2} \qquad \textit{Equation 72}$$

where Y_L is the admittance (the reverse of resistance R_L), P_L the active load power and V_L the nominal voltage of the node which is connected with the Apros load module as it can be noticed in Figure 48. In the figure below, the basic Apros electrical modules described above are depicted.

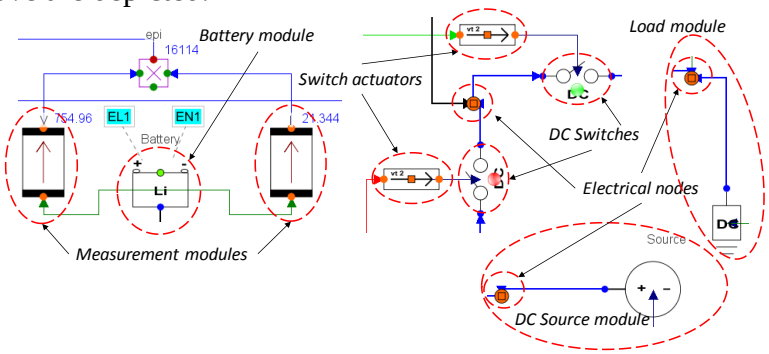

Figure 48: Apros electrical network modules

6.1.2 Signal based EMS algorithm in Apros

Combining the signal and electrical modules described above, it was possible to develop the system model in Apros software platform. It was also possible to model the energy management system that supervised the system operation, based on the previously developed strategy. In Figure 49, the complete Apros model is depicted. From this picture it is possible to observe the following basic subsystems: the system inputs, the power system balance, the battery model, the charge and discharge controllers and the EMS. The balance of the system, was modeled as a signal adder that was responsible for the summation of all the incoming signals which represented power flows. The result, which was named as residual for our simulation, was considered as an output signal and was then fed to the balance of system controller. The BESS was modelled based on the Lithium battery module with the corresponding set of equations described in 5.3.1. The battery charger with the DC source and the load was modeled as described in the previous section (6.1.1) and finally the EMS was modeled as described in detail below.

In the following table, the whole EMS operation is described as a truth table. The different possible states of the system are investigated and the corresponding logic controllers take the corresponding values. It must also be stated that for all Apros binary modules, the output emerging from the bottom port is the logical reverse of the output of the upper port. For the better understanding of the operational modes of the system the table below with the Figure 49 have to be simultaneously observed. It is also important to state for nomenclature reason that from the Figure 49 and the following table it is $\boldsymbol{P_{off} = P_{SP}}$ and it is basically the input that encapsulates the diesel power setpoint as derived from the algorithm of section 4.2.

Table 3: Truth table for the EMS operation, corresponding to Figure 49

Charging Mode (State = False) / Discharge Mode (State = True)				
System Check $(P_{PV} + P_{SP} - P_L > 0)$	***PV Check*** $(P_{PV} > 0.001)$	***State***	***MODE***	
TRUE	TRUE	FALSE	CHARGE	
FALSE	TRUE	TRUE	DISCHARGE	
TRUE	FALSE	TRUE	DISCHARGE	
FALSE	FALSE	TRUE	DISCHARGE	
Idling Mode (AND = False)				
System Surplus Check $(\lvert P_{PV} + P_{SP} - P_L \rvert > 0.1)$	$\boldsymbol{P_{SP} > P_L}$ $(P_{SP} - P_L > 0.001)$	$\boldsymbol{P_{SP} \cong P_L}$ $(\overline{P_{SP} > P_L})$	***AND***	***MODE***
TRUE	FALSE	TRUE	TRUE	-
TRUE	TRUE	FALSE	FALSE	IDLE
FALSE	TRUE	FALSE	FALSE	IDLE
FALSE	FALSE	TRUE	FALSE	IDLE

The above conditional controllers are explained below. The complete Apros model figure is presented in the next page.

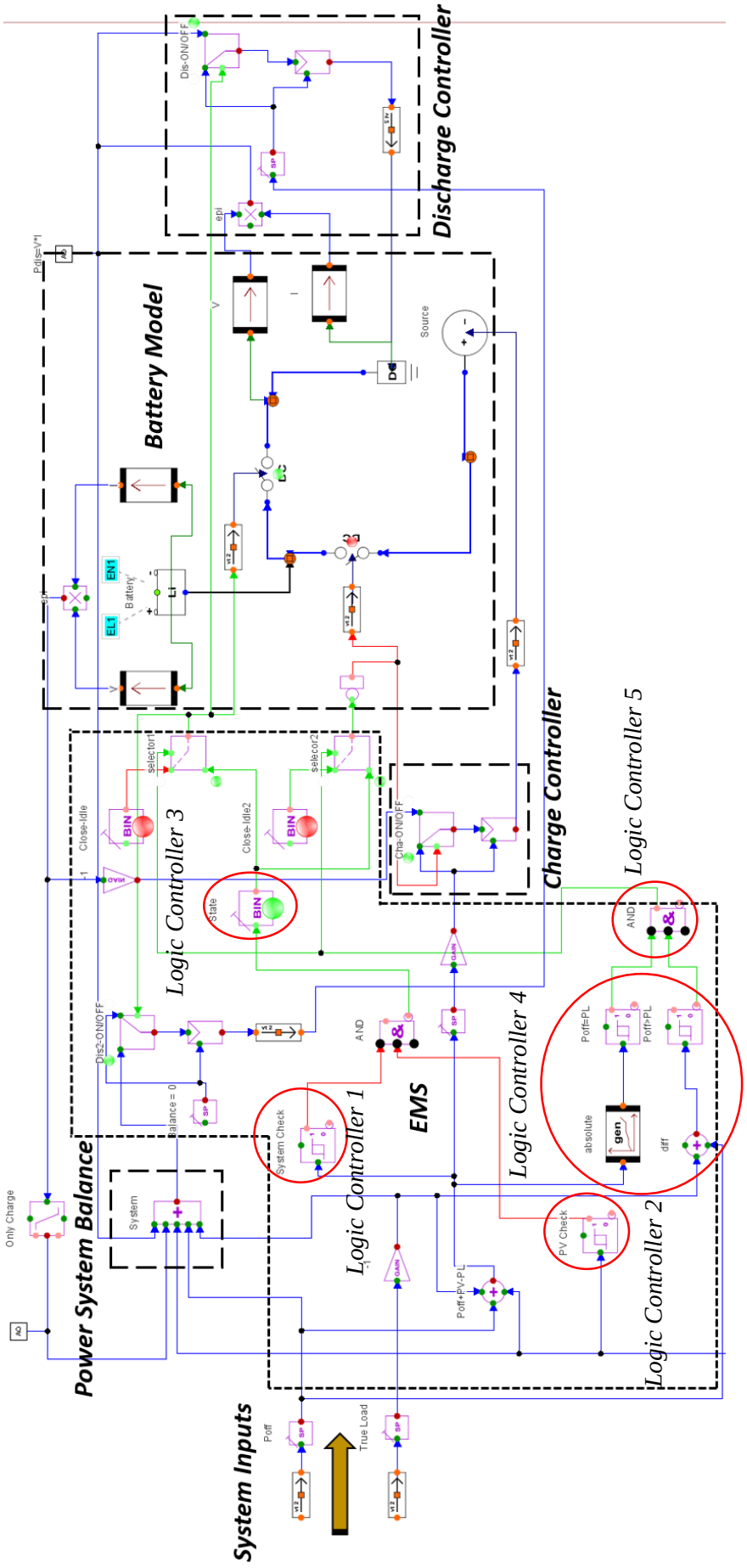

Figure 49: APROS complete simulation model

Table 4: Description of the logic controllers used in Apros EMS model

Logic Controller		Purpose/Description	Condition
1.	*System Check*	Check the balance of system and the residual	$P_{PV} + P_{SP} - P_L > 0$
2.	*PV Check*	Check whether there is available PV energy	$P_{PV} > 0.001$
3.	*State*	Responsible for changing the switch positions in the electrical network	$y_{out} = \begin{cases} 0, & for\ \ charge \\ 1, & for\ \ discharge \end{cases}$
4.	*System Surplus Check*	Responsible for detection of diesel setpoint matching the demand and not charging the battery with non-renewable energy	$\lvert P_{PV} + P_{SP} - P_L \rvert > 0.1$ and $P_{SP} - P_L \leq 0.001$
5.	*AND-selector1-selector2*	Responsible for the idling state management of the battery	$y_{out} = \begin{cases} 0, & for\ \ idle \\ 1, & for\ \ no\ idle \end{cases}$

The logic controllers that based on their operation the system changes states and which are also depicted in Figure 49 and referred to **Table 3** are the following: *System Check*, *PV Check*, *State*, *System Surplus Check* ($P_{off} \approx P_L$), *AND-selectror1-selector2*The condition in which the state is not described as true or false in **Table 3** but instead the value is dashed, is due to the fact that this state is mainly related with the charging state, which is the task of other logic controller.

In the case that **i)** $P_{PV} \geq 0$, **ii)** $\lvert P_{PV} + P_{SP} - P_L \rvert > 0.1$ and **iii)** $P_{SP} - P_L > 0.001$ $\xrightarrow{False} P_{SP} - P_L \leq 0.001$,the diesel power is very close to the demand and therefore additional PV energy is produced, which in turn means that charging mode should be selected. In all the other cases, either the system is balanced and therefore there is no need for energy storage or supply, or the excess energy attributed to diesel overproduction. For both of the cases described above, the battery should remain in idling mode.

Regarding the Figure 49 it is remarked that the signals are distinguished in binary and analog ones based on their color. The blue connections represent analog values signals while the red or green lines represent binary signal values. The coloring is based on the current signal value. Therefore, the red signals represent false values and the green signals true values. The electrical circuit connections are also colored in blue since analogue values are also transferred through them. The only exception is the battery connection which is colored as black line.

Concerning the controller 1, its main operation is related with the check of the balance between produced and consumed energy in the system. Specifically, the sum of the PV power and the setpoint power at each time step is the same variable as the combined curve which was produced from the algorithm of section 4.1.2. The controller 2 is devoted for tracking the hours of the day that PV power is produced, while the controller 3 is responsible for executing the command of charging or discharging by integrating the logic circuit with the electrical circuit. The controller 4 is tasked with the detection of diesel power overproduction compared to the current demand. This is important because in case that the diesel power is greater than the demand value, then the system

should not consider a charging mode because the battery should store only renewable energy. However, this is implemented by a threshold value, in order to clearly distinguish the situations when the diesel is capable of providing the predicted power and when this cannot be achieved and further or less power should be used. The use of the absolute value function is applied in order to detect energy excess with simultaneous overproduction of diesel engines, or just to represent the system balance, at the same time. Then, the appropriate command is passed to the battery system via the controllers who regulate the battery power. The threshold values at the mathematical conditions of Table 4 are in kilowatts *[kW]*. For unit consistency and greater accuracy, the power signal flows are given as kilowatts *[kW]* at the input section. Any necessary unit conversion (i.e. *W to kW*) is implemented with the help of analogue gains (described in 6.1.1). The controller 5 checks the mismatch of the diesel setpoints with the current demand with the help of a small threshold value. The input demand values are the true load values and not the forecasted demand values. The controller 5, is responsible for the idling state of the battery and is activated when the state should transit from charging or discharging mode to idling mode and vice versa.

Another issue to be discussed regarding the charge and discharge controllers of the Apros model depicted in Figure 49 is related with the setpoints. As it can be observed, the measured value (which is transferred through a value transmitter module) that enters the controller module is first passed through an analogue selector module, the operation of which is described in 6.1.1. In the selector, the two analogue inputs are i) the setpoint value of the controller and ii) the analogue value of the current measurement. This configuration was selected so that when a specific controller is not used during a specific time period in the simulation, the measurement value follows the setpoint value. In this way, the controller deviation is forced to be zero which means that no control action is calculated on its output. However, if this configuration was not used, then the moment that the controller would be turned on and off, the control deviation would be instantaneously very big, resulting in impulse control spikes in the output. This could affect the system behavior, especially for the transition times and especially when the controller is used once again in the simulation.

One last think to be considered is that the controllers used in Apros have built in anti-windup protection that prevents them from going into saturation mode. This phenomenon is related with the actuator limited range of values and the integrator which is continuously integrating the constantly increasing control error (deviation). This flaw is countered with the control integral term reset, when the controller output reaches its limit values. In this way, the integral term of the PI controller is set back to zero instead of building up more and more error, for the constantly increasing deviation.

In the following section, the results of the dynamic simulation of the model described above, are presented in detail.

6.2 Dynamic simulation results

6.2.1 System operation results for short time periods

After the system model configuration is completed, the power system yearly operation is simulated with the rules and the operational strategies mentioned before. Thus, it is possible to estimate the performance of the predictive EMS algorithm regarding the

impact of load forecasting to the real time operation of the BESS. As it was described in the previous section, the system power balance was used as a criterion for power generation-consumption balancing and it was monitored in order to be constantly zero (i.e. no over/under production was allowed). For that reason, the battery power delivered to the system was controlled according to this specification. However, at specific times over the year period, the power balance was not achieved due to isolated large forecast errors or operational limitations owed to the state of charge of the battery. This surplus or deficit of energy was considered to be compensated by the diesel engines supposing a flexible operation with small deviations around their base scheduled operating point, as forecasted. A good overall performance of the system was obtained with a significant success in smoothening the load curve around the engines predicted operating points. As it makes clear in Figure 50, the new achieved operation of the diesel engines consisted of basically two levels, one related with the offset obtained from the optimization algorithm and one owed to successful peak shaving implementation. In this picture, the indicative simulation results for a one-week duration are presented, making possible the comparison of two different operational strategies of the diesel engines. The first approach namely "OLD Diesel" corresponds to the net load curve which is related with the diesel engine operation if the system could absorb all possible PV energy production, meaning zero curtailment, despite the lack of load forecasting. The second approach namely "NEW Diesel" corresponds to the proposed methodology.

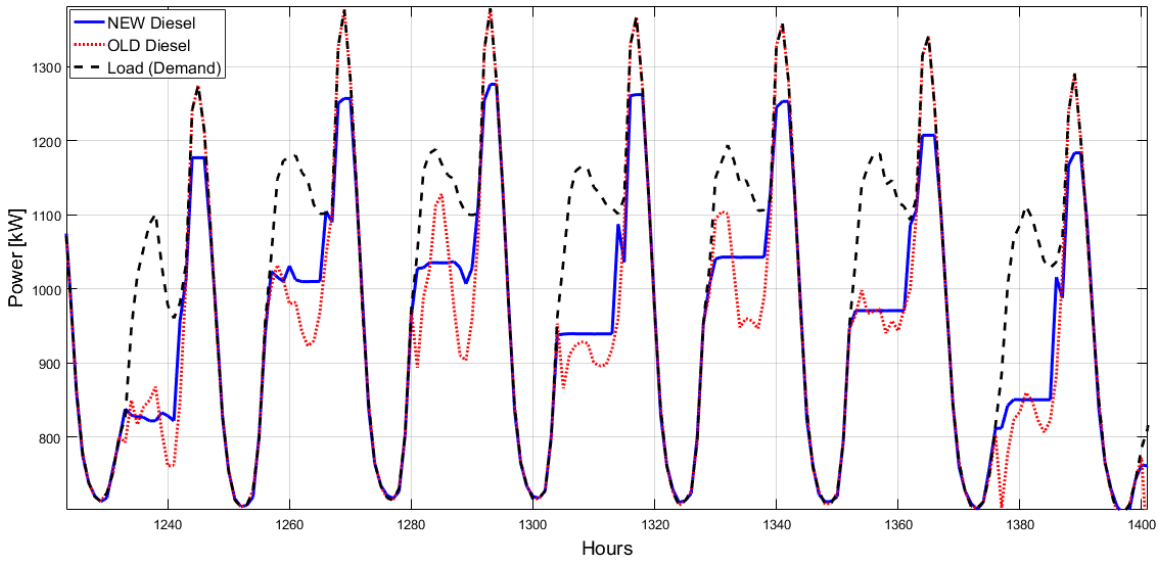

Figure 50: Dynamic simulation results for a typical winter week

According to the previous figure, it is clear that the NEW Diesel operation curve is much smoother than the OLD one while the produced PV energy is completely absorbed by the system by supplying the artificially achieved excess PV power at the time periods of peak shaving. This ensures that all renewable energy produced is supplied to the grid resulting in a predicted and planned zero curtailment.

In Figure 51 the achieved results during a single day operation of the week presented in Figure 50 are shown. As it is evident, with the proposed methodology the diesel engines operate in a more monotonic mode, owed to the calculated offset level and it is possible to avoid in a great extent the valleys and crests due to the PV generation at the

specified time-periods. These time varying, and unplanned operating conditions are eliminated with the proposed BESS operation and this has a significant improvement to the magnitude and the gradient of the engine's ramp-up for the following peak event (Figure 51). Under this scope, a more precise dispatch planning of the diesel engines can be obtained and the allocation of fewer additional engines to cover the ramp-up of the load curve can be achieved. In addition, the acceleration rate of the engines, depicted through the gradient of their operation at Figure 50 is decreased. The arrows in Figure 51 are used to illustrate the variation of the diesel operation for both the old and the new case, in increasing and decreasing power production to meet the changing demand. Provided that this is directly related with immense fuel consumption decreasing this gradient results in a less aggressive engine operation and a more cost-effective fuel consumption.

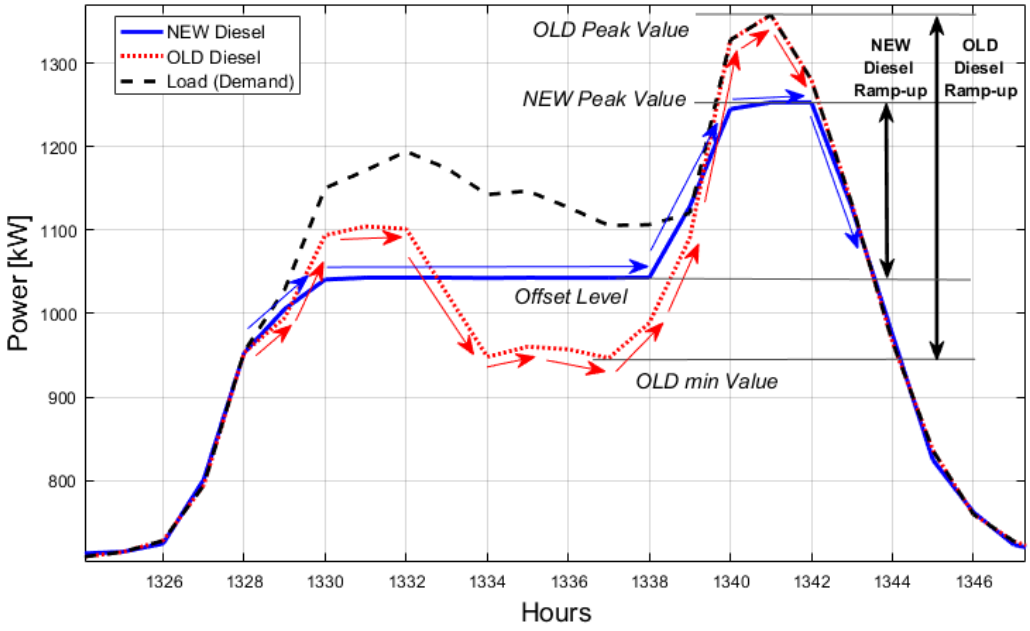

Figure 51: Dynamic simulation results for a single day operation

The effect of the ramp-up reduction is associated with the simultaneous reduction of the new peak maximum demand value that the diesel engine should encounter, via the relatively higher diesel engine operation during the off-peak time periods. This fact is attributed to the offset level which was decided by the algorithm and the constant setpoints imposed for the corresponding time period. In case of absence of the storage system, then in order to have zero curtailment and inject all possible PV produced power to the grid. Therefore, the net load that would correspond to the diesel power generation, would be unstable and constantly changing, based on the amount of PV power injected. This effect could be intensified or weakened depending on the day of the year, the season, the weather phenomena and the load profile of the specific day. However, by implementing this methodology, a predictive operation of the diesel engines combined with the BESS is possible to overcome the aforementioned instabilities and at the same time reduced the maximum power injected from them to the grid. This effect, considering the generally decentralized renewable production and the dispersion of PV panels could have a great impact on the maximum demand charges which is considered as a mutual benefit for the utility that provides the energy and the customer that is charged based on the peak demand and the energy mix of the current

time. Another effect of the methodology proposed, considering the result behavior of the system depicted in Figure 50 and Figure 51, which will be discussed in detail to the next chapter, is related with the dispatch operation of the diesel units. This could also have an economic impact on the electricity price and combined with the higher renewable penetration for each hour of the day, could further decrease the cost of electricity of the system.

6.2.2 System operation result for the whole year

Although the operational strategy proposed in this study is suited for special cases, as it was aforementioned in previous chapter section (4.2.1), the simulation conducted in Apros software referred to a whole year operation. In this way, the same operational strategy, which was decided based on the developed predictive algorithm was also applied for the summer time periods during which the load profile was not ideally suited for the specific algorithm implementation. Nevertheless, the system was simulated for all the year and the total results are presented below with the help of the yearly distributions.

In the following figure, the plots of the state of charge of the battery and the residual power described in previous section (5.1) and specifically with Equation 31, resulted from the whole year simulation of the system, are presented.

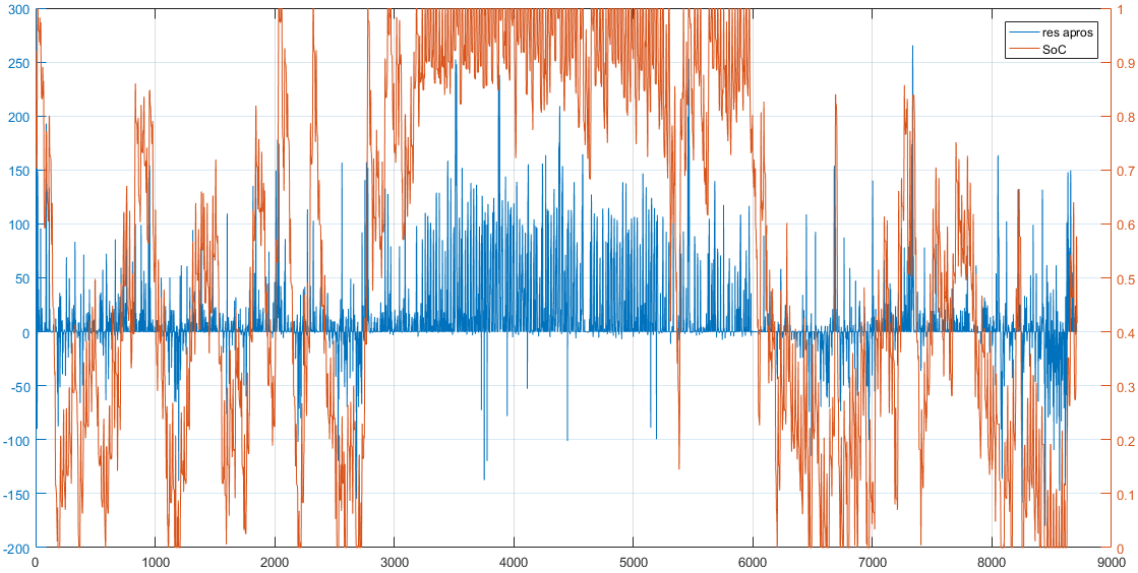

Figure 52: Residual and SoC plots, for the whole year operation

From the figure above, it is possible to observe SoC values represented with the green line and the residual values with the blue line. The SoC takes values in the range of [0,1] meaning that when it is 0, the battery is empty and when it is 1, the battery is fully charged. Along the whole year operation, there are some instances that the battery is fully discharged due to large forecast which are correspond to greater peak energy demand than predicted. Also, the efficiency degradation effect and the limited rates of charging and discharging power are also related with the aforementioned instances. Nevertheless, there are two main regions that are clearly distinguished in Figure 52, the one is the central region which is described by high values of the SoC and corresponds to the summer time period and the other are the two side regions that are described from lower SoC values and correspond to the winter time periods. These regions are derived

from the different daily load profiles characterizing those seasons and the logic of the developed supervisor algorithm. Therefore, during the summer time period, the battery is at the majority of the time fully charged and cannot be discharged later when the peak demand occurs, because this peak demand is happening at the same time period with the storing time period. This is also the reason that the residual energy is larger and in the direction of overproduction, meaning that the system has a relatively high amount of excess energy and the diesel engines should be operated in lower loading conditions. However, these issues could be resolved by allowing the system's battery to be discharged during the night hours but this should be studied in conjunction with the diesel operation limits. Regarding the system operation at the winter time periods, during which the developed algorithm works better, it can be observed that the state of charge of the battery is constantly swinging between higher and lower values. As long as the average maximum SoC at these time periods is around 75%, it can be stated that the battery's capacity size could be decreased, allowing for a smaller battery to be integrated. However, this could also be optimized in another studied, as described in detail in the last chapter.

In order to further evaluate the performance of the methodology developed in this thesis for the whole year operation, (though it is better applicable when the peak demand is misaligned with PV production which is the case for winter periods), a statistical indicator is employed. Specifically, the kurtosis feature is calculated for the reference case (Diesel + PV) and the case proposed (Diesel + BESS + Predictive EMS) by implementing the following formulas:

$$kurtosis = \frac{\sum_{k=1}^{K}(x(k) - x_m)^4}{(K-1){x_{std}}^4} \qquad \textit{Equation 73}$$

$$x_{std} = \sqrt{\frac{\sum_{k=1}^{K}(x(k) - x_m)^2}{K-1}} \qquad \textit{Equation 74}$$

$$x_m = \frac{1}{K}\sum_{k=1}^{K} x(k) \qquad \textit{Equation 75}$$

where x(k) is a signal valuefor $k=1,2,\ldots,K$, and K is the number of data points, x_{std} the standard deviation and x_m the mean value. This feature which is commonly used in vibration analysis for bearings health monitoring, expresses the quality of the data values distribution around the mean value of the dataset. The latter has a direct relation with the concertation of the data values around some central values and therefore it can be an indicator of the peak frequency of the signal. Thus, a signal with a high frequency of peaked values will typically have a greater kurtosis value compared to a smoother signal. Therefore, the quantification of the results of this approach is accomplished through the calculation of the kurtosis feature for the signals of interest in our study. Therefore, for the signals "NEW Diesel" and "OLD Diesel" depicted in Figure 50 and as obtained from the simulations, the kurtosis values are:

kurtosis $_{\text{OLD-Diesel}}$: 2.5416

kurtosis $_{\text{NEW-Diesel}}$: 2.1319

This reduction in kurtosis, accompanied by the probability distributions of the same signals is depicted in the following figure.

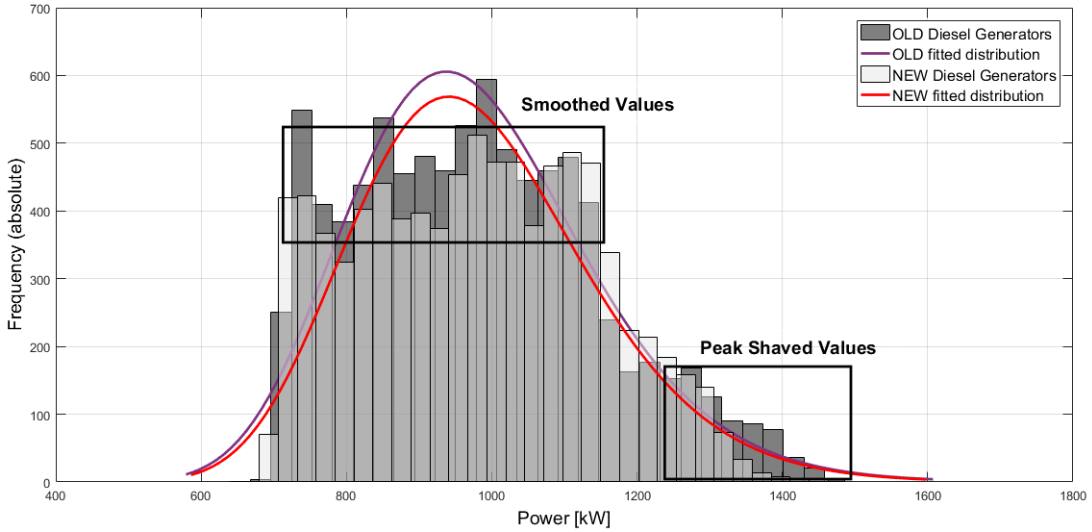

Figure 53: Distribution of OLD and NEW diesel operation

This reduction of the kurtosis implies an improved performance of the power system for the whole year duration. In particular, observing the latter figure, two areas are easily distinguished: The one is related with the peak reduction success level as the frequencies around the peak demand values are considerably decreased, whereas the other area is related with the level of smoothness of the diesel engine operation. The intermediate power demand values with the proposed configuration are more uniformly distributed compared to the frequency distribution of the previous case.

In the next chapter, the results for the BESS and the diesel engines behavior related with the implemented methodology, are presented.

7 Diesel and BESS operation under the proposed EMS

In this chapter, the results for the operation of the Diesel and the BESS are presented. After the simulation of the Apros model was completed, it was possible to investigate the operation of the diesel engines and the battery. The island's existing diesel engines were investigated in terms of unit commitment and loading capabilities while the battery's operation was compared to the ideal trajectory predicted from the developed algorithm.

7.1 Diesel Engine Operation

In order to assess the diesel engine operation as predicted from the simulation of the system, in a more realistic way, the existing and operating diesel engines at the island of Astypalaia were investigated. The island of Astypalaia was decided (relatively to the island of Madeira), because this information was possible to be retrieved more easily and the order of the magnitude of the investigated "synthetic island" was closer to the demand values of Astypalaia. This is better described in section 4.1.1. The diesel engine model used in Astypalaia is the Mitsubishi S16R-PTA with a rated capacity of 1.275 kW and maximum gross delivered power 1.100 kW. The summer maximum achievable delivered power is 1.000 kW. This difference is associated with the higher ambient temperatures observed in the summer time period and the fact that the specific engine model is air-cooled. In order to cover the current demand of Astypalaia, two of the aforementioned engine models are used. The engine mechanical drawing is depicted below.

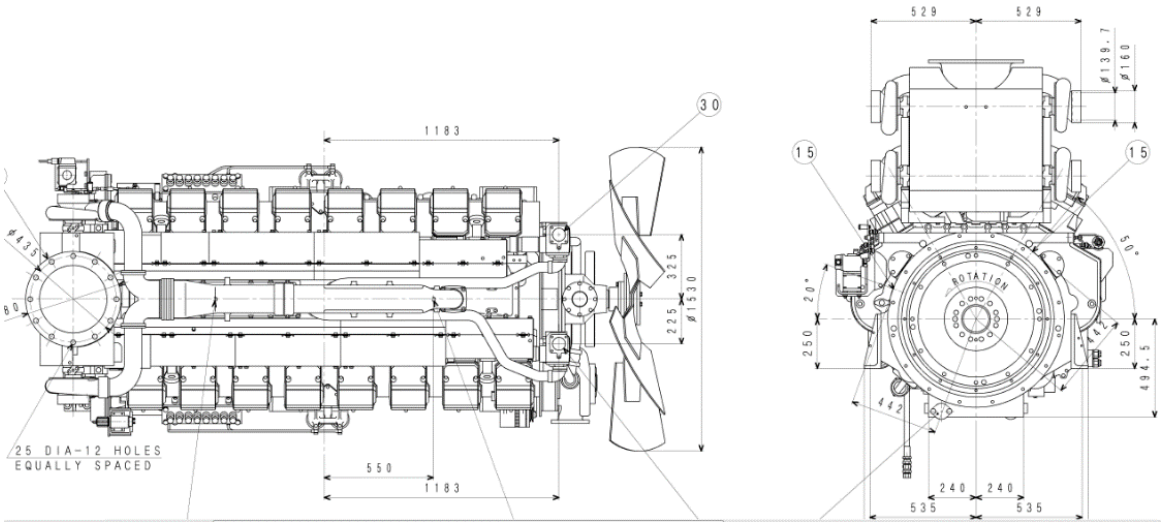

Figure 54: Islands diesel engine drawing

Then, the operation strategy of the diesel generators should be identified. This was due to the fact that there are two main operational strategies that are mostly applied in order to operate a system of diesel generator machines. With the first strategy (load following), a full load operation of as many diesel generators as possible is implied while the peak and valleys are anticipated through spinning reserve diesel generators that are operated in partial load conditions. In the second approach (load sharing), all of the possible diesel generators are operated simultaneously and the total load is divided equally among them. This means that the diesel generators may be operated at

partial load for relatively higher amount of time and especially for the load values which correspond to the switch off and on level of additional generators. This transition region is very important for the power system because the starting up of a unit is a task usually related with higher operational costs emerging from i) higher fuel consumption due to ramping and dynamic effects and ii) higher maintenance cost related with the interrupted operation of the engine. However, there is not a rule of thumb for which strategy should be preferred, as it is highly depended on the size of the power system, the renewable portion of generated power and the load curve pattern. Thus, the strategy to be followed should be evaluated based on the aforementioned attributes and the number and the size of the existing diesel engines. Regarding the strategy adopted by the two diesel generators on the island under investigation, the operational strategy that is followed is depicted in the following figure.

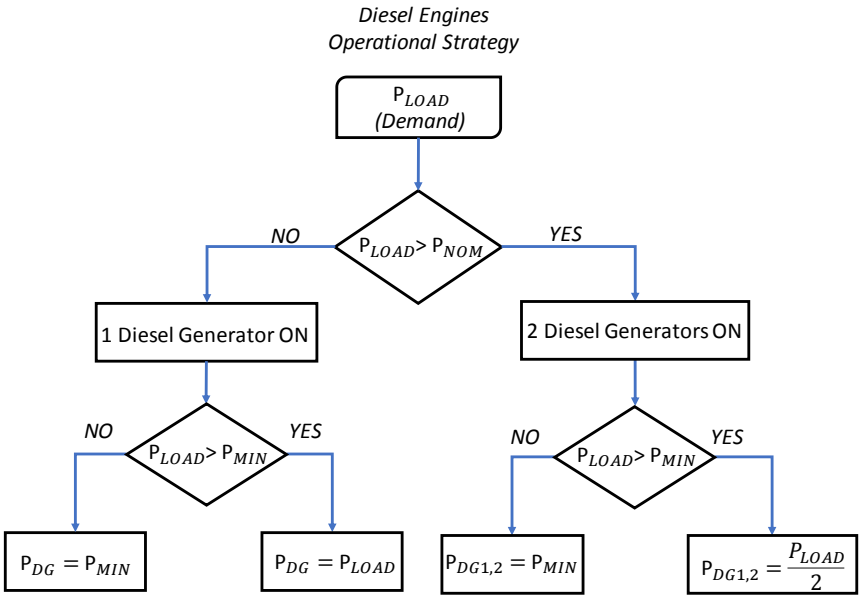

Figure 55: Operational strategy algorithm for the diesel engines of the island

At first, the total demand P_{LOAD} of the next hour is regarded as an input to the algorithm. Then this is compared to the nominal power P_{NOM} in order to evaluate the number of the units that will be active. For values less than the nominal power of a single generator, one diesel engine is operated. Then the demand value to be covered by the engine is compared to the minimum allowed power which is considered at the 75% of the engine's nominal power which was set as 1000 kW. Subsequently, the value of the power that the generator will provide is decided based on this limitation. For the case that the total demand is not possible to be covered by a single generator, both of them are operated with the same logic described above. The total load should be equally divided between the engines so that they are well balanced in terms of loading. However, if the partial loading resulting from the balancing action implies an operating point below the technical minimum, then each of the diesel engines is operated on the technical minimum and the rest of the load is considered as dump load.

It should be stated that the technical minimum and the limits of operation, was set equal to 75% of the nominal load, for efficiency reasons. This value of the technical minimum, has been empirically proved and validated from the real system operators and although the current technical minimum of the diesel engines is 50%, they are

mostly operated over 75% so that the fuel consumption does not reach very high limits. However, in this way the range of flexibility of the units is highly limited and this could negatively affect the dynamic system behavior at changing loads such as the ramping up for the peak demand cover or the PV generation time period where the diesel engines should decrease their power output. In this study, no dynamic model of the diesel fuel consumption was implemented, though this could be a topic for a future study. However, the dynamic operation of a diesel engine, especially for the concept of this study, could show significant results regarding the smoother operation achieved by the developed algorithm, as it is depicted in Figure 50. Thus, the diesel engines were considered as static models, as in the unit commitment problem formulation.

In order to evaluate the fuel consumption regarding the operational strategy described above and depicted in Figure 55 the technical specifications of the engines were retrieved from the manufacturer. The most important attribute of a diesel generator that concerns the fuel consumption is the specific fuel consumption curve. This is basically a representation of the engine's varying efficiency relatively to the loading factor. For calculating this curve, some data points were used from the manufacturer and then a curve fitting for those data was estimated.

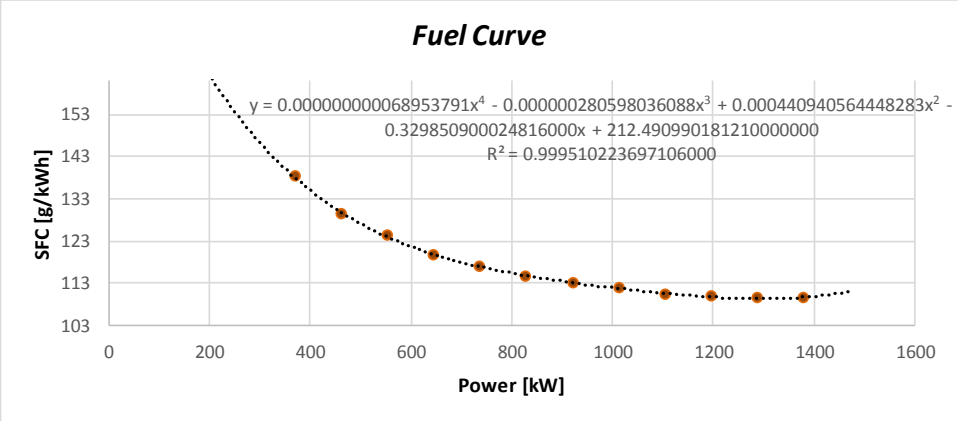

Figure 56: Specific Fuel Curve fitted on manufacturers data

As it can be noticed from the figure above, the specific fuel consumption in terms of fuel mass per energy unit, is higher for lower power delivery of the engine. This is associated with the relatively lower efficiency at lower loading factors compared to the region around the nominal loading. According to [50, 58, 59], the function that describes the fuel consumption of the diesel engine can be represented as a linear function of its power output. Regarding this thesis, the fuel consumption of the diesel engines was calculated using the specific fuel curve depicted in the figure above and the linear interpolation which was implemented to approximate the model described previously. In this way, the equation of the fuel consumption which was derived from data presented in Figure 57 was

$$F\ (t) = f_i \cdot P(t) + f_c \qquad \textit{Equation 76}$$

where F is the fuel consumption at every hour of the year, P is the current power delivery of each diesel engine, f_i and f_c are the constants that are related with the operating fuel consumption per power unit and the fuel used to maintain the engine

spinning respectively. In the figure below, the linear relation of the fuel consumption with the engine loading factor is presented.

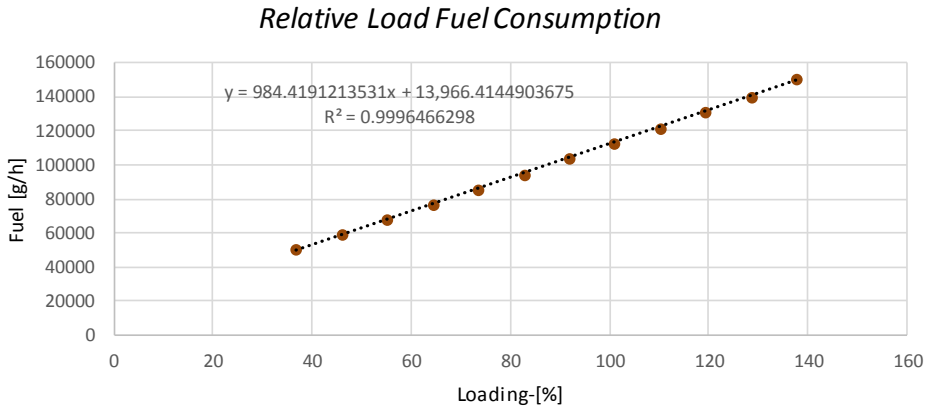

Figure 57: Linear correlation between the fuel consumption and the loading factor

Based on the operational strategy depicted in Figure 55 and the fuel consumption depicted in Figure 57, it was possible to estimate the diesel engine operation for the OLD and NEW cases, as described in 6.2.1. The unit commitment diagram is depicted in the following figure, for the two cases mentioned before.

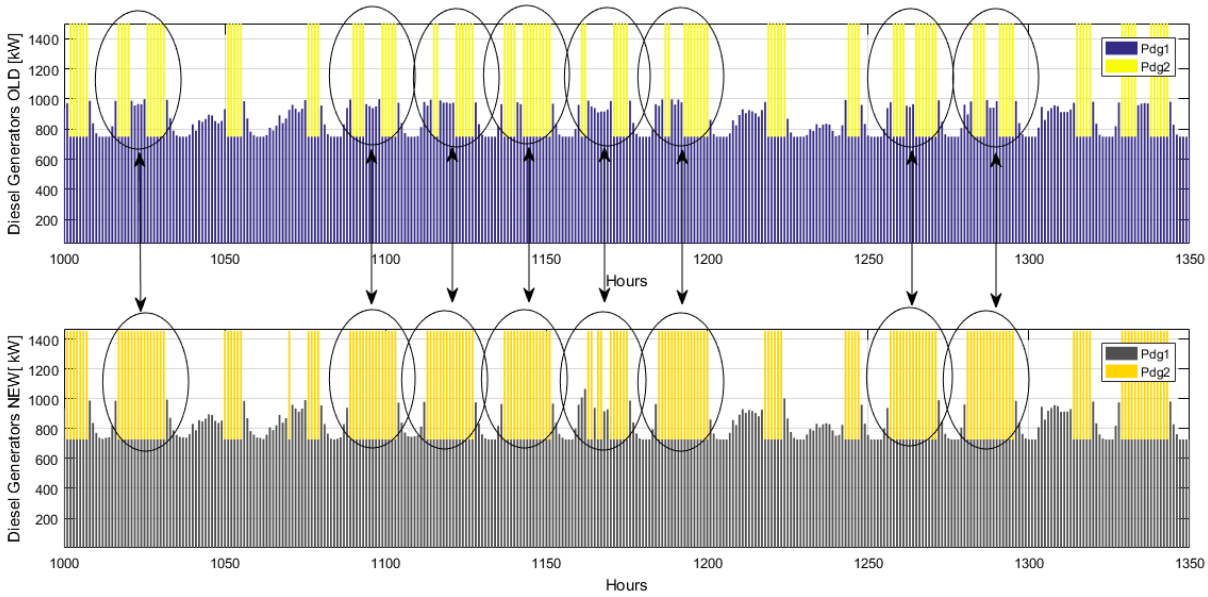

Figure 58: Unit commitment for the diesel operation, under the proposed methodology

In the figure above, P_{dg1} and P_{dg2} are the power produced by the first and the second diesel generator respectively. As it can be noticed, from the corresponding encircled regions, in the NEW case the operation is much smoother compared to the OLD case, where the second unit has to be switched off in the time periods of enhanced PV power production. In turn, this unit should be restarted later to provide additional energy for the peak time periods. This fact is associated with an additional constant cost which is incurred each time that the diesel power generator starts up or shuts down. In addition, this variable operation deteriorates the engine's health, compared to a more scheduled and constant operation, as it is achieved with the proposed method. Regarding the fuel consumption, it was found that the turning point for which the fuel consumption calculated based on Equation 76, is less than the old case is the setting of the new

allowable technical minimum to *0.728*. This conclusion is justified based on the fact that the peak reduction which implies less maximum instantaneous fuel consumption is compensated from the smooth diesel operation which implies higher fuel consumption to preserve. However, the total cost of electricity production is not only related with the fuel cost but also with the higher maintenance cost and the variable operation of the diesel engines of the previous case. The peak fuel reduction is also depicted in the figure below.

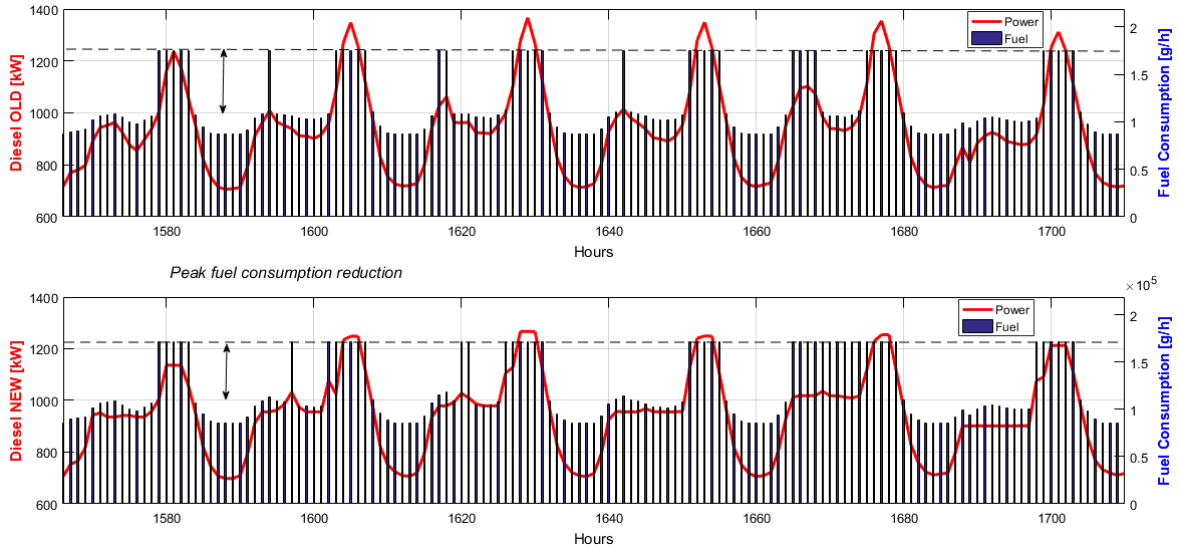

Figure 59: Instantaneous fuel consumption for the OLD and NEW cases

As it can be observed from the figure above, the peak demand reduction is combined with the peak fuel consumption of the diesel engine. However, one fact that affects the fuel consumption and is not predicted from this static analysis, is related with the dynamic phenomena for the loading impulse changes of the diesel engines, which are inevitable when the PV production is maximized. From this perspective, many possible options could be adopted, considering the proposed operation methodology, that will enhance the fuel reduction. This could be a downsizing of the diesel engines or the abolition of one diesel engine. Considering the scenario of one diesel engine operation, the fuel consumption was calculated for the first 4000 hours of one-year operation, in order to assess the winter time period only and it was found that the fuel consumption could be decreased by decreasing the technical minimum based on the following diagram.

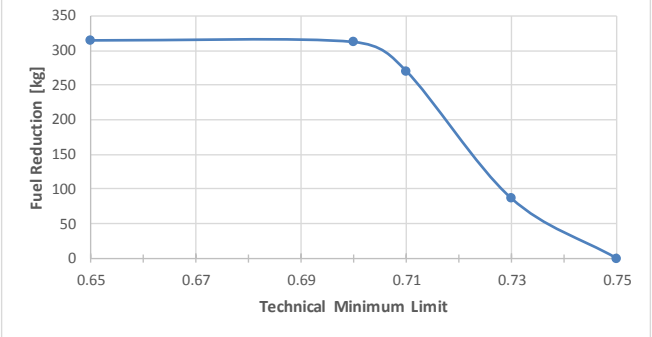

Figure 60: Single diesel generator operation – new technical minimum

7.2 Battery Storage System Operation

The results of the simulation from the battery perspective are presented in this section. The BESS was operated based on the system of switches and the energy management system developed in section 6.1.2, determining the target for the power injections from or to the battery system and the corresponding time periods. From the figure below, it is possible to observe the battery power delivery and state of charge variation patterns for a nine days period.

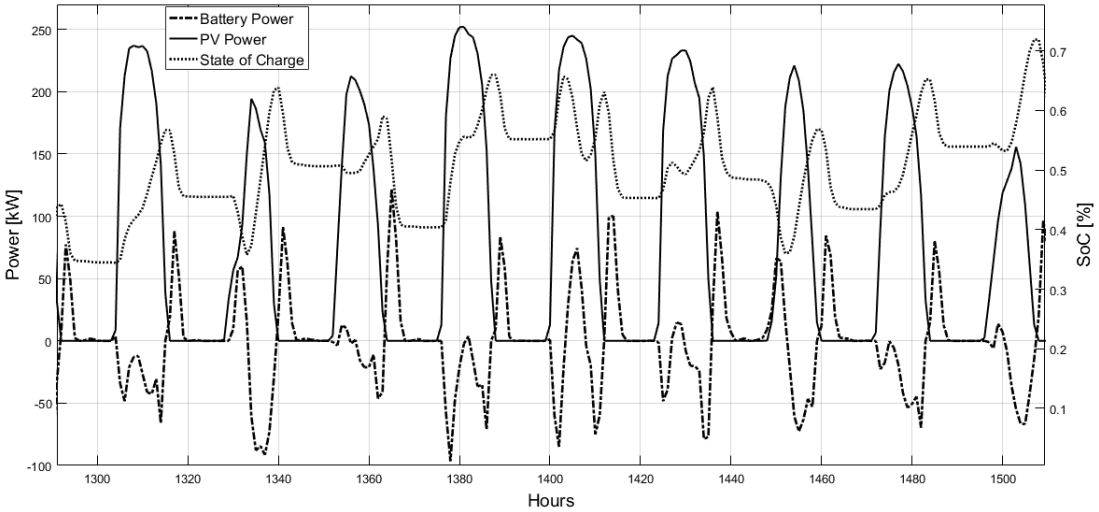

Figure 61: Battery behaviour for 8 days' time period

As it can be noticed from the figure above, the PV power is simultaneously plotted with the main operational attributes of the battery. The state of charge variation follows a constant trend which is described from increasing SOC for the hours of PV production and decreasing or stable SOC for specific time periods right after the PV power generating time periods. This pattern is highly compatible with the logic developed by the algorithm, which implied a charging time period when and only when PV power is available, while the battery system could discharge in different time periods. However, the highest amount of power delivery from the BESS should be right after the last hour of PV production, which is also the case depicted in Figure 61. For a detailed view, the same results are presented for a single day period, in the figure below.

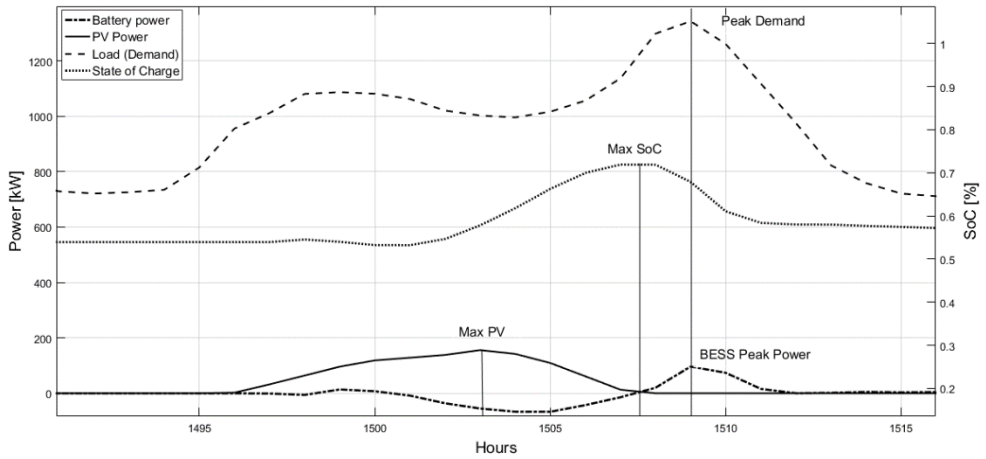

Figure 62: Single day operation BESS results

It is revealed that during the time period of PV production, the BESS stores energy that it is supplied later on during the peak demand. For that reason, the SoC of the BESS is around its daily maximum values right before the peak demand event and subsequently it supplies the daily maximum power when the peak demand event is reached. From the relative position of the vertical lines of Figure 62, it is clear that the maximum PV energy production precedes the maximum value of the battery's SoC, which in turn is followed from the maximum value of the power delivered from the BESS. The latter, is also achieved at the same time of the maximum peak demand value, which is another indication that the peak demand is satisfied from the stored renewable energy.

In order to assess the ability of the developed algorithm (section 4.1), which was implemented via the energy management system in Apros simulation platform (section 6.1.2) to predict a reasonable behavior of the battery system, the scheduled and the resulted battery power trajectories were compared. In Figure 63, the injected and absorbed power flows from or to the battery system are presented. The injected power is regarded as a positive battery power value while the absorbed energy, associated with storage is represented by the negative battery power values. Specifically, in the figure below the two aforementioned trajectories are plotted on the same diagram for the day 63 of the year, which corresponds to a typical winter day. The results concerning the combined power production curve, the energy to be stored and the preplanned system operation for day 63, which were emerged from the developed algorithm, are presented in Figure 32 and Figure 34 respectively. Regarding Figure 63, the red dashed line represents the scheduled trajectory of the battery, which is predicted based on the load forecasting of the next day and the algorithmic procedure for storing enough energy to cover the peak area in a later time period. The black solid line corresponds to the true battery usage after the system was simulated with the real time control and the energy management systems integrated.

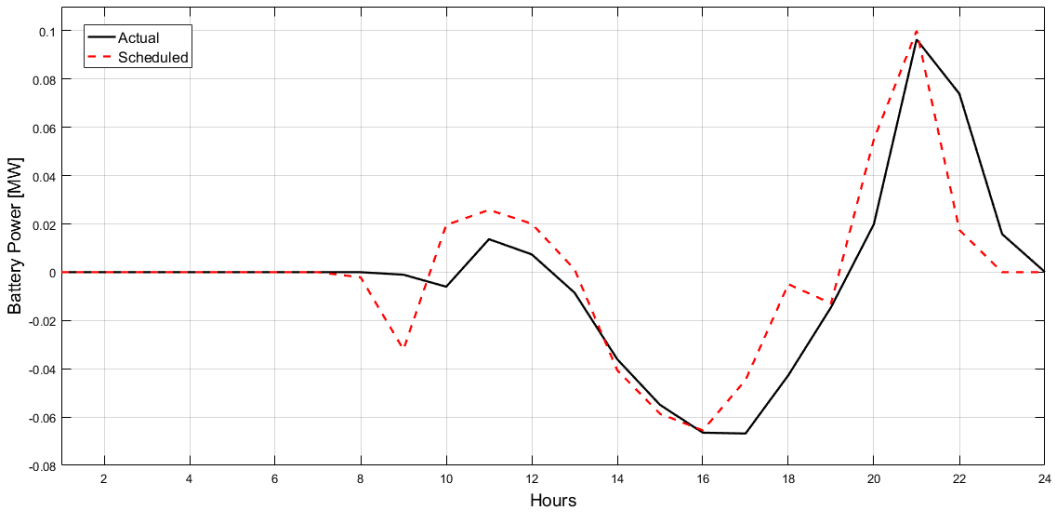

Figure 63: Battery actual vs scheduled power flows for day 63

In the figure above, it can be observed that the scheduled battery profile is similar to the actual profile that was monitored during the system's dynamic simulation. In particular, the two profiles present the same patterns and trends regarding the time periods of charging and discharging the battery system, while a delay associated with the actual case compared to the scheduled can be noticed. This can be attributed to the real time dynamics of the system which are mainly affected from two major aspects. The first is related with the current battery status, concerning the variables operational limits and gradients and the response time of the battery's dynamic behavior. The second aspect is related with the true demand values that are faced from the battery system that can be slightly different from the forecasted values, based on which its operation was planned. However, the overall battery behavior seems to follow the mainstream daily profile which is characterized from storing the artificially generated excess of renewable energy during the sunlight time periods and injecting it back to the grid during the peak demand time periods. In addition, the maximum injected power which can be observed from the battery in Figure 63, coincides with the scheduled peak hour demand. Furthermore, the actual injected power observed from Figure 63, is very close to the scheduled power injection value, which was estimated as the peak reduction level in section 4.1.1, equal to *0.1 MW* of the daily maximum power demand, as the last was predicted from the neural network.

In the following chapter the cumulative conclusions and proposed future work are presented.

8 Conclusions and Future work

8.1 Basic conclusions

In this study, a predictive energy management system (EMS) based on load forecasting was introduced and integrated with the operation of a battery energy storage system (BESS) for peak demand reduction and load smoothening of a South-European islanded power grid. The results of the combined synergy of prediction and a new developed algorithm with real time control of the BESS, revealed that the peak shaving with renewable energy load levelling and smoothening in conjunction with a better diesel generators scheduling, can be achieved.

Specifically, the load forecasting was realized by implementing a single-hidden layer feedforward neural network for day ahead hourly predictions and a good estimation of the next day's load patterns was achieved. The results obtained with the developed artificial neural network (ANN) model were satisfying, despite of the simplicity of its structure and the number of input variables. The training algorithm used in this study, (Levenberg-Marquardt) adaptively varied the parameter updates between the gradient descent and the Gauss-Newton methods, in an effort to find the global optimum in a robust way. In addition, the number of neurons of the developed network was subject to investigation in order to preserve the number of neurons that resulted in the lowest possible error between the model's output and real data. The forecasting quality of the network was identified with the evaluation (calculation) of a commonly used index (metric) in machine learning algorithms, called mean absolute percentage error (MAPE). The training of the developed neural network module was based on the hourly demand values for two consecutive year time periods (2014, 2015) and the model was able to predict the daily load curve of the next day, on an hourly basis, for the test year (2016). In this way, the machine learning and specifically the structure of an ANN was proved as a reliable tool for load forecasting. A basic conclusion that could be derived from the performance of the ANN model, is that a relatively simple structure with small amount of computational resources and required calculations time, should be satisfactory for short term load forecasting.

The forecasted load curve was then used as an input for an optimization algorithm which was also developed under the scope of this thesis. This novel algorithm used as input variables the forecasted load and the PV power generation of the next day, while the peak load reduction could also be determined. The PV power production was estimated based on a well-validated data driven mathematical model and, in this way, it was possible to generate renewable power production time series. The installed capacity of renewable power for the island was estimated to be 300 kW while the peak demand values could reach 1.3-1.5 MW. The developed algorithm was adjusted to counterbalance the high peak demand of the night hours, which was the most common pattern associated with the island's power curve during the winter time period, as it is the case for other similar power systems. This pattern is primarily related with abrupt load changes and steep gradients which are formed due to the deferment of the peak renewable power generation with the peak demand values.

Consequently, the developed algorithm was assigned to search for an appropriate operational level for the diesel generators which could result in load smoothing and peak shaving of the maximum demand values simultaneously. This was achieved with the introduction of an iterative process by which an artificially created excess of renewable energy could be stored in a battery storage system, during the sunlight time periods. This amount of energy, which was expressed as the area under the corresponding power curves, should be requested later from the system to cover the demand associated with the peak load time period. The optimum operating level of the diesel generators that would result in enough energy surplus for storage, was evaluated as the algorithm's output. This iterative procedure would be then terminated only after the surplus energy would be equal to the peak energy demand. After the algorithm was terminated, the diesel and the battery operation setpoints were retrieved and were then used as inputs for the dynamic simulations. The algorithm proved to be stable for the majority of the days that it was executed, achieving an equilibrium between the peak demand and the stored energy. However, during the summer time period, although the results obtained were aligned with the general concept, the method was not efficient as the demand coincided with the peak PV power generation.

Thereafter, a dynamic model of the power system was developed in Apros simulation platform and the system operation was investigated. Although the aforementioned developed algorithm was better suited to a particular winter pattern of the load curve, the system was simulated for a whole year time period and the corresponding results were obtained. The developed model was based on analog and binary signals that represented the power flows and the control actions related with the system's operation. In this way, a centralized energy management system could be integrated into the dynamic simulations which would implement the strategy of the supervisor algorithm, as mentioned before. Nevertheless, the battery model used in this simulation was detailed enough in order to consider the non-linearities of the charging and discharging processes, the capacity losses related to the cycling usage and the aging of the battery and the transient behavior concerning the current flow. For the better representation of the system's dynamics, an appropriate control structure was employed, that implemented the low level real time controls. A cascade feedback control loop was implemented with separate PI controllers that regulated the injected or absorbed battery power by adjusting the current flows and tracking the scheduled setpoints. At the same time, the balance of the system was also regulated by the BESS which would respond to sudden changes in the state of the system, if this was achievable. Otherwise the diesel generators should ensure the balance of the system, by violating their scheduled operation. These issues, that were mostly related with the dynamic behavior of the battery and the forecasting errors associated with the ANN model were compensated by this general setup. Thus, the centralized EMS could supervise the setpoints of the different energy systems of the island, which would then be achieved through specific task dependent controllers.

The system was simulated for a whole year and except from the peak shaving of the load curve by using stored renewable PV energy, a significant reduction in the variability in diesel generators operation was also achieved. This was also highlighted in the corresponding curves that were obtained from the simulation but also from the

reduction of the kurtosis factor, which was used as a signal smoothening factor. The proposed method reinforced the power grid ability to integrate renewable power in a more robust and planned way, leading to predefined zero curtailment and possible cost reduction through fuel savings. This was also depicted though the diesel generators operation that proved to be more stable leading to less start up and ramp up operations for the constantly variable loading conditions. With the implementation of the method proposed in this thesis, the load curve of the islands power system was smoothed while the new maximum demand values were covered by renewable energy instead of conventional. The method could also be implemented in similar power systems that are characterized by peak demand during the night hours and a considerable amount of installed PV power.

8.2 Future work

Considering the proposed simulation framework with the implementation of a predictive energy management system, developed in the framework of this thesis, there are many possible future steps that could improve the method and have a positive impact on the overall procedure.

At first, the neural network's input variables could be investigated by considering many different combinations, including further weather data such as rainfall, wind and cloudiness and special days recognition. Also, the implementation of a NARX (nonlinear autoregressive model with exogenous inputs) could be investigated, instead of the developed feedforward ANN model. Another important factor that could be considered during the forecasting process, could be the development of a classification algorithm for finding special days that present a different profile compared to the standard similar days. In this way, the forecasting module could be improved and a better MAPE could be achieved. The possibility of implementing other machine learning methods for load forecasting could also be investigated. These could be either statistical methods such as support vector regression (SVR) or artificial intelligence methods such as deep neural networks.

Regarding the developed optimization algorithm, the following upgrades could be implemented. Initially, the peak shaving level which is considered as a constant input parameter for the current version of the algorithm, could be subjected to an optimization process, achieving the maximum possible peak shaving for each day of the year. This could be different for each day and it would be mostly influenced by the load and PV power production profiles. Another issue that would greatly update the developed algorithm would be the integration of a pattern recognition algorithm. This would basically identify the load curve profile of the next day and then decide in an automatic way whether the profile is suitable for the current algorithm implementation or not. In case that the identified load profile would be inappropriate, (i.e. summer days' time period), then another technique should be employed that would not abuse the battery operation and store energy unnecessarily. The pattern recognition could be implemented with a symbolic aggregate approximation (SAX) algorithm.

Another issue that could be considered for improvement of the overall methodology, is related to the implementation of PV power production forecasting based on previous data. This could enhance the overall methodology, by eliminating the need for PV

power forecast to be inserted as input time series, while this could be achieved from a similar algorithm, as the developed load forecasting module. In addition, the optimization of the battery size could significantly improve the capital cost of the BESS system and integrate the design with the operation of the system. Also, the fuel consumption of the diesel generators incorporated into a techno economical study, could enlighten the economic feasibility of the proposed configuration, leading to the reduction of the number and capacity of the existing diesel generators. Last but not least, a better tuning of the real time charge controllers or the implementation of advanced control, could slightly improve the systems dynamic behavior, though this is considered as a secondary effect.

References

[1] Das Kumar U., Tey S.K., Seyedmahmoudian M., Mekhilef S., Idris I.Y.M., Van Deventer W., Horan B., Stojcevski A., Forecasting of photovoltaic power generation and model optimization: A review, Renewable and Sustainable Energy Reviews 2018;81:912-928.

[2] Chua H.K., Lim S.Y., Morris S., A novel fuzzy control algorithm for reducing the peak demands using energy storage system, Energy 2017;122:265-273.

[3] Colak I., Kabalci E., Fulli G., Lazarou S., A survey on the contributions of power electronics to smart grid systems, Renewable and Sustainable Energy Reviews 2015;47:562-579

[4] Tsekouras G.J., Kanellos F.D., Kontargyri V.T., Tsirekis C.D., Karanasiou I.S., Elias CH.N., Salis A.D., Kontaxis P.A., Mastorakis N.E., Short term load forecasting in Greek intercontinental power system using ANNs: a study for input variables, Proceedings of the 10th WSEAS International Conference on NEURAL NETWORKS; 2009.

[5] Mordjaoui M., Haddad S., Medoued A., Laouafi A., Electric load forecasting by using dynamic neural network, Int. J. of Hydrogen Energy 2017;42:17655-17663.

[6] Hahn H., Meyer-Nieberg S., Pickl S., Electric load forecasting methods: Tools for decision making, European Journal of Operational Research 2009;199:902-907.

[7] Satish B., Swarup K.S., Srinivas S., Rao Hanumantha A., Effect of temperature on short term load forecasting using an integrated ANN, Electric Power Systems Research 2004;72:95-101.

[8] Brodowski S., Bielecki A., Filocha M., A hybrid system for forecasting 24-h power load profile for Polish electric grid, Applied Soft Computing 2017;58:527-539.

[9] AI-Hamadi H.M., Soliman S.A., Fuzzy short-term electric load forecasting using Kalman filter

[10] Short-term load forecasting based on the Kalman filter and the neural-fuzzy network (ANFIS), IEE Proc.-Gener. Transm. Distrib. 2006;153(2).

[11] Moral-Carcedo J., Perez-Garcia J., Integrating long-term economic scenarios into peak load forecasting: An application to Spain, Energy 2017;140:682-695.

[12] Ghasemi A., Shayeghi H., Moradzadeh M., Nooshyar M., A novel hybrid algorithm for electricity price and load forecasting in smart grids with demand-side management, Applied Energy 2016;177:40-59.

[13] Hossain M., Mekhilef S., Danesh M., Olatomiwa L., Shamshirband S., Application of extreme learning machine for short term output power forecasting of three grid-connected PV systems, Journal of Cleaner Production 2017;167:395-405.

[14] Li J., Ward K.J., Tong J., Collins L., Platt G., Machine learning for solar irradiance forecasting of photovoltaic system, Renewable Energy 2016;90:542-553.

[15] Weniger J., Bergner J., Quaschning V., Integration of PV power and load forecasts into the operation of residential PV battery systems, 4th Solar Integration Workshop.

[16] Bottiger M., Paulitschke M., Bocklisch T., Innovative Reactive Energy Management for a Photovoltaic Battery System, Energy procedia 2016;99:341-349.

[17] Angenendt G., Zurmuhlen S., Mir-Montazeri R., Magnor D., Uwe Sauer D., Enhancing Battery Lifetime in PV Battery Home Storage System Using Forecast Based Operating Strategies, Energy Procedia 2016;99:80-88.

[18] Yoo J., Park B., An K., AI-Ammar E.A., Khan Y., Hur K., Kim J.H., Look-Ahead Energy Management of a Grid-Connected Residential PV System with Energy Storage under Time Based Rate Programs, Energies 2012;5:1116-1134.

[19] Sun C., Sun, F., Moura J.S., Nonlinear predictive energy management of residential buildings with photovoltaics & batteries, Journal of Power Sources 2016;325:723-731.

[20] Arcos-Aviles D., Pascual J., Guinjoan F., Marroyo L., Sanchis P., Marietta M.P., Low complexity energy management strategy for grid profile smoothing of a residential grid- connected microgrid using generation and demand forecasting, Applied Energy 2017;205:69-84.

[21] Sepasi S., Reihani E., Howlader A.M., Roose R.L., Matsuura M.M., Very short-term load forecasting of a distribution system with high PV penetration, Renewable Energy 2017;106:142-148.

[22] Reihani E., Ghorbani R., Load commitment of distribution grid with high penetration of photovoltaics (PV) using hybrid series-parallel prediction algorithm and storage, Electric Power Systems Research 2016;131:224-230.

[23] Reihani E., Motalleb M., Ghorbani R., Saoud S.L., Load peak shaving and power smoothing of a distribution grid with high renewable energy penetration, Renewable Energy 2016;86:1372-1379.

[24] Reihani E. Sepasi S., Roose L.R., Matsuura M., Energy management at the distribution grid using a Battery Energy Storage System (BESS), Electrical Power and Energy systems 2016;77:337-344.

[25] Halfmann F., Alhaider F., Wendiggensen J., Gerhard S. (2017) A Predictive Control Strategy for Battery Energy Storage Systems to combine Peak Shaving with Primary Frequency Control. In: Schulz D. (eds) NEIS Conference 2016. Springer Vieweg, Wiesbaden

[26] Sossan F., Paolone M., Integration and Operation of Utility-Scale Battery Energy Storage Systems: the EPFL's Experience, IFAC-PapersOnline 2016;49:433-438.

[27] Mazzola S., Vergara C., Astolfi M., Li V., Perez-Arriaga I., Macchi E., Assessing the value of forecast-based dispatch in the operation of off-grid rural microgrids, Renewable Energy 2017;108:116-125.

[28] Syed I.M., Raahemifar K., Predictive energy management and control system for PV system connected to power electric grid with periodic load shedding, Solar Energy 2016;136:278-287.

[29] Syed I.M., Raahemifar K., Energy advancement integrated predictive optimization of photovoltaic assisted battery energy storage system for cost optimization, Electric Power systems Research 2016;140:917-924.

[30] Lujano-Rojas J.M., Monteiro C., Dulfo-Lopez R., Bernal-Augustin J.L., Optimum load management strategy for wind/diesel/battery hybrid power Systems, Renewable Energy 2012;44:288-295.

[31] Frédéric Colas, Di Lu, Vladimir Lazarov, Bruno François, Hristiyan Kanchev. Energy management and power planning of a microgrid with a PV-based active generator for Smart Grid Applications. IEEE Transactions on Industrial Electronics, Institute of Electrical and Electronics Engineers, 2011, 58 (10), pp.P. 4583-4592.

[32] Kalkhambkar V., Kumar R., Bhakar R., Energy loss minimization through peak shaving using energy storage, Perspectives in Science 2016;8:162-165.

[33] Prasatsap U., Kiravittaya S., Polprasert J., Determination of Optimal Energy Storage System for Peak Shaving to Reduce Electricity Cost in a University, Energy Procedia 2017;138:967-972.

[34] Hasni, A., Sehli, A., Draoui, B., Bassou, A., Amieur, B., 2012. Estimating global solar radiation using artificial neural network and climate data in the south-western region of Algeria. Energy Procedia. 18, 531-537.

[35] Lippmann, R.P., 1987. An introduction to computing with neural nets. ASSP Mag. IEEE 4, 4e22.

[36] Kung, Y., 1998. Digital Neural Networks. PTR Prentice-Hall.

[37] Celik O., Teke A., Yildirim H. B., The optimized artificial neural network model with Levenberg-Marquardt algorithm for global solar radiation estimation in Eastern Mediterranean Region of Turkey, Journal of Cleaner Production, 2016;116:1-12

[38] Mastorakis N., Bulucea A., Tsekouras G., Computational Problems in Science and Engineering, Springer International Publishing Switzerland 2015

[39] Rojas, R., 1996. Neural Networks. Springer-Verlag, Berlin.

[40] Alam, S., Kaushik, S.C., Garg, S.N., 2009. Assessment of diffuse solar energy under general sky condition using artificial neural network. Appl. Energy 86, 554-564.

[41] Kalogirou, S.A., 2000. Applications of artificial neural-networks for energy systems. Appl. Energy 67, 17-35.

[42] Petrini, M., 2012. Improvements to the back-propagation algorithm. Ann. Univ. Petrosani Econ. 12, 185-192.

[43] Hao Yu and B. M. Wilamowski, Levenberg-Marquardt Training Industrial Electronics Handbook, vol. 5 Intelligent Systems, 2nd Edition, chapter 12, pp. 12-1 to 12-15, CRC Press 2011.

[44] Saha, S., et al. 2011, updated monthly. NCEP Climate Forecast System Version 2 (CFSv2) Selected Hourly Time-Series Products. Research Data Archive at the National Center for Atmospheric Research, Computational and Information Systems Laboratory

[45] S. Haykin. Neural Networks: A Comprehensive Foundation. Prentice Hall, 1994

[46] California Independent System Operator, What the duck curve tells us about managing a green grid,
http://large.stanford.edu/courses/2015/ph240/burnett2/docs/flexible.pdf

[47] Ninad A.Y., Lopes L., A BESS Control System for Reducing FuelConsumption and Maintenance Costs of Diesel Hybrid, 2013, IEEE Mini-Grids with High Penetration of Renewables

[48] Charfi S., Atieh A., Chaabene M., Modeling and cost analysis for different PV/battery/diesel operating options driving a load in Tunisia, Jordan and KSA, Sustainable Cities and Society, 2016;25:49-56

[49] Ammen M.A., Pasupuleti J., Khatib T., Simplified performance models of photovoltaic/diesel generator/battery system considering typical control strategies, Energy Conversion and Management, 2015;99:313-325

[50] Hu Y., Morales J.M., Pineda S., Sanchez J.M., Solana P., Dynamic multi-stage dispatch of isolated wind–diesel power systems, Energy Conversion and Management, 2015;103:605-615

[51] Pfenninger S., Staffell I., Long-term patterns of European PV output using 30 years of validated hourly reanalysis and satellite data, Energy, 2016;114:1251-1265

[52] Huld T., Gottschalg R., Beyer G. H., Topic M., Mapping the performance of PV modules, effects of module type and data averaging, Solar Energy, 2010;84:324-338

[53] Erdinc O., Vural B., Uzunoglu M., A dynamic lithium-ion battery model considering the effects of temperature and capacity fading, 2009 International Conference on Clean Electrical Power, ICCEP 2009. 383 - 386. 10.1109/ICCEP.2009.5212025.

[54] B. Kennedy, D. Patterson and S. Camilleri, "Use of lithium-ion batteries in electric vehicles", Journal of Power Sources, vol. 90, pp. 156–162, 2000.

[55] P. Ramadass, B. Haran, R. White and B. N. Popov, "Mathematical modelling of the capacity fade of Li-ion cells", Journal of Power Sources, vol. 123, pp. 230–240, 2003.

[56] R. Spotnitz, "Simulation of capacity fade in lithium-ion batteries", Journal of Power Sources, vol. 113, pp. 72-80, 2003.

[57] Alobaid F., Mertens N., Starkloff R., Lanz T., Heinze C., Epple B., Progress in dynamic simulation of thermal power plants, Progress in Energy and Combustion Science, 2016;59:79-162

[58] Yap K.W., Karri V., An off-grid hybrid PV/diesel model as a planning and design tool, incorporating dynamic and ANN modelling techniques, Renewable Energy, 2015;78:42-50

[59] Guo L., Wang N., Li X., Wang C., Multi-objective optimal planning of the stand-alone microgrid system based on different benefit subjects, Energy, 2016;116:353-363